

# Network Operation Strategies for Efficient Localization and Navigation

*This paper provides network operation strategies, including node prioritization, node activation, and node deployment to improve the localization performance and prolong the network lifetime.*

By MOE Z. WIN<sup>ID</sup>, Fellow IEEE, WENHAN DAI<sup>ID</sup>, Student Member IEEE, YUAN SHEN<sup>ID</sup>, Member IEEE, GEORGE CHRISIKOS, Fellow IEEE, AND H. VINCENT POOR<sup>ID</sup>, Fellow IEEE

**ABSTRACT** | Reliable and accurate position information is of great importance for many mass-market and emerging applications. Network localization and navigation (NLN) is a promising paradigm to provide such information ubiquitously, where a network of nodes is used to aid in localizing its members. This paper explores various network operation strategies, which play an essential role in NLN as they determine the network lifetime and localization accuracy. Efficient network operation requires several functionalities, including node prioritization, node activation, and node deployment. The roles of these functionalities are described and different techniques for implementing respective functionalities via algorithmic modules are introduced. Some important concepts such as cooperative operation, robustness guarantee, and distributed design in the development of the network operation strategies are also introduced. Finally, numerical results are provided to demon-

strate the localization performance improvement attributed to the optimized network operation strategies.

**KEYWORDS** | Deployment; localization; navigation; optimization; resource allocation; scheduling; wireless network

## I. INTRODUCTION

Location awareness using wireless signals is critical for many mobile applications [1]–[6], including autonomous driving [7]–[9], assisted living [10]–[12], Internet-of-Things [13]–[16], crowdsensing [17]–[20], medical services [21]–[23], as well as search-and-rescue operations [24]–[26]. In outdoor scenarios, global navigation satellite systems (GNSSs) can provide meter-level localization accuracy around the earth through a constellation of satellites [27]–[31]. However, the effectiveness of GNSS is limited in challenging propagation environments, such as inside buildings and in urban canyons, due to signal degradation or blockage by obstacles [32]. To complement GNSS in these challenging propagation environments, wireless localization networks have been developed in the past decades for providing high-accuracy location awareness [33]–[39].

In a typical wireless localization network, there are two types of nodes, referred to as anchors and agents [40]–[42]. Anchors have perfectly known positions, whereas agents have unknown positions. For example, anchor nodes may consist of WiFi access points or cellular base stations, and agent nodes may consist of user smartphones or sensors. The goal of the localization network is to determine the position of agents using inter-node and intra-node measurements [43]–[49]. Inter-node measurements refer to measurements between nodes, e.g., ranging with ultrasound or radio-frequency

---

Manuscript received September 7, 2017; revised April 8, 2018; accepted April 9, 2018. Date of current version July 25, 2018. This work was supported in part by the U.S. Office of Naval Research under Grant N00014-16-1-2141; in part by the U.S. National Science Foundation under Grants CNS-1702808 and ECCS-1647198, and in part by the MIT Institute for Soldier Nanotechnologies. (Corresponding author: Moe Z. Win.)

**M. Z. Win** is with the Laboratory for Information and Decision Systems, Massachusetts Institute of Technology, Cambridge, MA 02139 USA (e-mail: win@mit.edu).

**W. Dai** is with the Wireless Information and Network Sciences Laboratory, Massachusetts Institute of Technology, Cambridge, MA 02139 USA (e-mail: whdai@mit.edu).

**Y. Shen** was with the Wireless Information and Network Sciences Laboratory, Massachusetts Institute of Technology, Cambridge, MA 02139 USA, and is now with the Department of Electronic Engineering, Tsinghua University and Beijing National Research Center for Information Science and Technology, Beijing 100084, China (e-mail: shenyuan\_ee@tsinghua.edu.cn).

**G. Chrisikos** is with Qualcomm Inc., San Diego, CA 92121 USA (e-mail: gchrisikos@ieee.org).

**H. V. Poor** is with the Department of Electrical Engineering, Princeton University, Princeton, NJ 08544 USA (e-mail: poor@princeton.edu).

---

Digital Object Identifier 10.1109/JPROC.2018.2835314

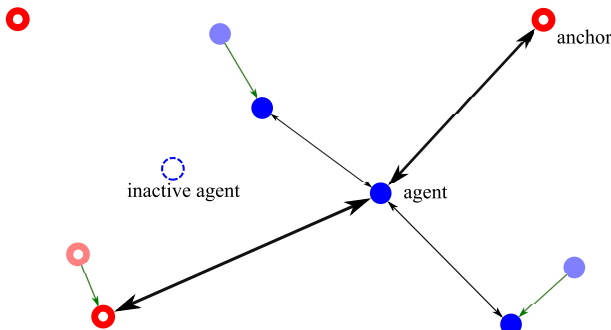


**Fig. 1.** Illustration of node prioritization, node activation, and node deployment actions. Black arrows denote the inter-node measurements, and the thickness of an arrow represents the amount of resources allocated to that measurement according to the node prioritization module; the blue hollow circle denotes the inactive agent, which does not transmit wireless signals as dictated by the node activation module; green arrows denote the movement of nodes, determined by the node deployment module from the original position (faded circle) to the required position (bright circle).

signals [50]–[57]. Intra-node measurements refer to those measured with respect to a single node. Typical examples include data from an inertial measurement unit (IMU) that obtains the agents' angular velocity and acceleration [58]–[61]. Among the studies on localization and navigation, those using cooperative techniques have attracted increasing research interest [62]–[67]. Cooperative techniques exploit inter-node measurements among agents and can significantly improve the localization performance [68]–[71], obviating the use of high-density anchor deployments. Recently, a general paradigm called network localization and navigation (NLN), which incorporates spatiotemporal cooperation, has been established for position inference [72]–[75].

The performance of NLN depends on various factors, such as the transmitting energy, signal bandwidth, network geometry, and the propagation conditions [72]–[76]. These factors are generally functions of the *network operation* strategy, which determines the allocation of transmitting resources, the activation of transmitting nodes, and the deployment of agents and anchors. Network operation plays a critical role in NLN since it not only affects the network lifetime, but also determines the localization accuracy [77]–[81]. For example, range measurements between two nodes with poor channel conditions consume significant amounts of energy, thereby reducing nodes' lifetime (e.g., the battery life of sensors) while providing little localization accuracy improvement. Another example of the network operation strategy is that placing all anchors together in a small region will likely lead to low localization accuracies of the agents because the ranging information from different anchors is along almost the same direction.

Network operation strategies for efficient localization and navigation can be categorized into several functionalities, including node prioritization, node activation, and node deployment. Fig. 1 illustrates the actuation

of these functionalities in a typical NLN system. The roles of these functionalities can be described in the context of algorithmic modules as follows.

- Node prioritization module—This module implements node prioritization strategies for allocating transmitting resources (such as power, bandwidth, and time) to achieve the best trade-off between resource consumption and localization accuracy [82]–[86]. For a particular agent, the output of this module is the amount of transmitting resources for the measurements made between the agent and its neighboring nodes [87]–[90].
- Node activation module—This module implements node activation strategies for determining the nodes that are allowed to make inter-node measurements so that the localization accuracy of the entire network is maximized [91]–[95]. For a particular network, the output of this module is the particular set of nodes to be used for making inter-node measurements with their neighbors [96]–[100]. For a selected node, it may make measurements with one or more of its neighbors.
- Node deployment module—This module implements node deployment strategies for determining the positions of new nodes in the network so that the localization accuracy of certain existing nodes can be maximally improved [101]–[106]. For a particular network, the output of this module is the destination positions of the new nodes [107]–[116].

Network operation strategies are implemented in some recently developed localization systems [117]. As a matter of comparison, there are extensive studies on *data* network operation strategies, which aim to maximize a communication performance metric, such as the capacity and throughput, by for example resource allocation [118]–[121], scheduling [122]–[126], and node deployment [127]–[129]. Yet these techniques are inefficient or even infeasible for network operation in localization, because of the significant difference in the performance metrics between localization and data networks. Rather than optimizing the capacity or throughput, the major goal of the network operation in localization networks is to improve the accuracy. Hence, new techniques are required to account for the structure of the localization metric.

One critical concept used in the study of NLN is the Fisher information matrix (FIM) [72]–[74]. It characterizes the amount of information that the measurements carry about the agents' positions. Prevailing studies on network operation for localization generally adopt certain functions of the FIM (or its equivalent form, such as the inverse of the covariance matrix) as the performance metrics to be used [130]–[135]. The most commonly used metric is the Cramér–Rao lower bound (CRLB), which is a function of the inverted FIM [136]–[138]. Other metrics used include the determinant of the FIM [139] and the smallest eigenvalue of the FIM [140]–[142]. As the FIM plays such an important role, it is prudent to determine

the structure of the FIM and exploit amenable properties of its structure for the design of network operation techniques.

Various methodologies are described in the literature to design the network operation strategies for NLN. The typical methods are as follows.

- Node prioritization strategies typically formulate and solve optimization problems to obtain trade-offs between localization accuracy and resource constraints [82]–[84], [142]–[145]. For example, in [142] and [143], the node prioritization problem was obtained by conic programs in non-cooperative networks. In a recent study [145], a computational geometry method was used to solve node prioritization problems. This method enables the derivation of an important sparsity property for node prioritization.
- Node activation strategies typically minimize or stabilize the long-term position error in a greedy manner [92]–[96]. For example, in [96], opportunistic strategies were developed to minimize the trace of error covariance matrices; moreover, the error evolution of these opportunistic strategies was determined for different network settings (e.g., agent trajectories, anchor deployments, measurement models, and multiple-access protocols) in comparison with random strategies.
- Node deployment strategies typically optimize the position error over the geometry of the nodes in a localization network [105]–[116]. For example, in [108], iterative approaches are proposed to place anchors for minimizing the CRLB of agents' position errors; in [116], second-order cone program (SOCP)-based strategies are developed to place new agents for minimizing the squared position error bound (SPEB) of an existing agent and the performance gap between the proposed and optimal strategies is determined.

This paper provides a tutorial on network operation strategies for efficient NLN. The emphasis will be on the optimization of the localization performance through node prioritization, node activation, and node deployment. The main body of the paper consists of the following five parts.

- We present a general framework for the network operation including the system model and the performance metric. We also introduce several important notions of the network operation, such as cooperation, robustness, and distributed design.
- We present node prioritization strategies for non-cooperative and cooperative networks. Conic programming-based approaches and computational geometry-based approaches are used to determine node prioritization strategies.
- We present node activation strategies for cooperative networks. Opportunistic activation and probabilistic activation strategies are presented and the error evolution corresponding to these two strategies is shown.

- We present node deployment strategies for both non-cooperative and cooperative networks. An iterative approach and a conic programming-based approach are used to determine node deployment strategies.
- We show how the network operation strategies can significantly improve the localization performance through numerical examples.

The subsequent sections are organized as follows. Section II presents the preliminaries of the network operation in NLN. Sections III and IV present node prioritization strategies for non-cooperative and cooperative networks, respectively. Section V presents the design and analysis of node activation strategies. Section VI presents node deployment strategies for non-cooperative and cooperative networks. Section VII presents numerical results to demonstrate the benefits of optimization in network operation. The last section draws conclusions.

*Notation:* Random variables are displayed in sans serif, upright fonts, and their realizations in serif, italic fonts. Vectors and matrices are denoted by bold lowercase and uppercase letters, respectively. For example, a random variable and its realization are denoted by  $x$  and  $\bar{x}$ ; a random vector and its realization are denoted by  $\mathbf{x}$  and  $\bar{\mathbf{x}}$ ; a random matrix and its realization are denoted by  $\mathbf{X}$  and  $\bar{\mathbf{X}}$ , respectively. Sets and random sets are denoted by upright sans serif and calligraphic font, respectively. For example, a random set and its realization are denoted by  $\mathcal{X}$  and  $\bar{\mathcal{X}}$ , respectively. The  $m$ -by- $n$  matrix of zeros (resp. ones) is denoted by  $\mathbf{0}_{m \times n}$  (resp.  $\mathbf{1}_{m \times n}$ ); when  $n = 1$ , the  $m$ -dimensional vector of zeros (resp. ones) is simply denoted by  $\mathbf{0}_m$  (resp.  $\mathbf{1}_m$ ). The  $m$ -by- $m$  identity matrix is denoted by  $\mathbf{I}_m$ : the subscript is removed when the dimension of the matrix is clear from the context.  $\mathbb{H}_c\{\mathcal{A}\}$  denotes the convex hull of  $\mathcal{A}$ .  $\text{diag}\{x_1, x_2, \dots, x_n\}$  denotes an  $n \times n$  diagonal matrix with diagonal elements  $x_1, x_2, \dots, x_n$ .  $\mathbf{A} \succcurlyeq 0$  denotes that the matrix  $\mathbf{A}$  is positive semi-definite.  $\text{tr}\{\cdot\}$  is the trace of a square matrix;  $[x]_n$  denotes the  $n$ th element of the vector  $\mathbf{x}$ .  $[\mathbf{A}]_{n,m}$  is the element at the  $n$ th row and  $m$ th column of the matrix  $\mathbf{A}$ ;  $\mathbf{x} \sim \mathcal{N}(\mu, \Sigma)$  denotes that the random vector  $\mathbf{x}$  follows the Gaussian distribution with mean  $\mu$  and covariance matrix  $\Sigma$ .  $\mathcal{A}^c$  denotes the complement of a set  $\mathcal{A}$ . Define the unit vectors  $u(\phi) := [\cos \phi \ \sin \phi]^T$ . The notation  $\mathbf{x}_{k_1:k_2}$  is used for concatenating the set of vectors  $\{x_{k_1}, x_{k_1+1}, \dots, x_{k_2}\}$  and similarly  $\mathbf{x}_{k_1:k_2}^{(t_1:t_2)}$  for  $\{x_{k_1:k_2}^{(t_1)}, x_{k_1:k_2}^{(t_1+1)}, \dots, x_{k_1:k_2}^{(t_2)}\}$ , for  $k_1 \leq k_2$ ,  $t_1 \leq t_2$ . We denote by  $\otimes$  the Kronecker product and by  $E_{i,j}^N$  an  $N \times N$  matrix with all zeros except for a 1 on the  $i$ th row and  $j$ th column. The function  $\mathbb{1}_{\mathcal{S}}(x)$  is an indicator function defined to be 1 if  $x \in \mathcal{S}$ , and 0 otherwise. Finally, the notation for important quantities and optimization problems that is used throughout the paper is summarized in Tables 1 and 2, respectively.

## II. PRELIMINARIES

This section presents the system model in an NLN scenario, explains basic concepts, and introduces the performance metric of the network operation.

**TABLE 1** Notation for Important Quantities

Notation	Definition	Notation	Definition
$\mathcal{N}_a$	Index set of agents with cardinality $N_a$	$\mathcal{N}_b$	Index set of anchors with cardinality $N_b$
$\mathbf{p}_k$	Position of node $k$	$\phi_{kj}$	Angle of the vector from node $k$ to node $j$
$d_{kj}$	Distance between nodes $k$ and node $j$	$\mathbf{r}_{kj}(t)$	Waveform received at agent $k$ from node $j$
$s_j(t)$	Transmitting waveform of node $j$	$t_n$	The $n$ th time instant
$\mathbf{z}_k^{(n)}$	Vector of intra-node measurements of agent $k$ at time $n$	$\mathbf{w}_k^{(n)}$	Gaussian noise for intra-node measurement of agent $k$ at $t_n$
$\sigma_m$	Standard deviation of the Gaussian noise $\mathbf{w}_k^{(n)}$	$\mathbf{p}$	A vector that consists of all the parameters of interest
$\hat{\mathbf{p}}$	Unbiased estimator of $\mathbf{p}$	$J_e(\mathbf{p})$	EFIM for $\mathbf{p}$
$J_e^A(\mathbf{p}_k)$	Position information between agent $k$ and the anchors	$C_{kj}$	Ranging information between agent $k$ and agent $j$
$\lambda_{kj}$	RII between node $k$ and node $j$	$J_r(\phi)$	RDM with the angle $\phi$
$\mathcal{P}(\mathbf{p})$	nSPEB	$\hat{\mathbf{p}}_k$	Unbiased estimator of $\mathbf{p}_k$
$J_e(\mathbf{p}_k)$	EFIM for $\mathbf{p}_k$	$\mathcal{P}(\mathbf{p}_k)$	iSPEB for agent $k$
$\mathbf{T}^{(n)}$	Error increase matrix at $t_n$	$S^{(n)}$	Information from spatial cooperation at $t_n$
$\mathbf{p}^{(N)}$	Positions of $N_a$ agents at time $t_N$	$\hat{\mathbf{p}}^{(N)}$	Unbiased estimator of $\mathbf{p}^{(N)}$
$J_e(\mathbf{p}^{(N)})$	EFIM for $\mathbf{p}^{(N)}$	$\mathcal{P}(\mathbf{p}^{(N)})$	nSPEB at time $t_N$ for $N_a$ agents
$x_{kj}$	Amount of resources for the measurement from node $k$ to node $j$	$\xi_{kj}$	Quality of the measurement from node $k$ to node $j$
$\mathbf{x}$	Vector consisting of all agents' NPVs	$\mathbf{x}_k$	NPV for node $k$
$\mathcal{P}(\mathbf{p}_k; \mathbf{x}_k)$	iSPEB as a function of $\mathbf{x}_k$	$\mathcal{P}(\mathbf{p}; \mathbf{x})$	nSPEB as a function of $\mathbf{x}$

## A. System Models

Consider a wireless localization network with  $N_b$  anchors and  $N_a$  agents. The sets of agents and anchors are denoted by  $\mathcal{N}_a = \{1, 2, \dots, N_a\}$  and  $\mathcal{N}_b = \{N_a + 1, N_a + 2, \dots, N_a + N_b\}$ , respectively. The position of node  $k$  is denoted by  $\mathbf{p}_k$ ,  $k \in \mathcal{N}_b \cup \mathcal{N}_a$ . The angle and distance from node  $k$  to node  $j$  are denoted by  $\phi_{kj}$  and  $d_{kj}$ , respectively.

We first consider inter-node measurements, which can be obtained from received waveforms. The equivalent narrowband waveform received at node  $j$  from node  $k$  is modeled as

$$\mathbf{r}_{kj}(t) = \frac{\sqrt{E_{kj}}}{d_{kj}^\gamma} \alpha_{kj} s_j(t - \tau_{kj}) + \mathbf{z}_{kj}(t) \quad (1)$$

where  $E_{kj}$  is the transmitting energy,  $\gamma$  is the amplitude loss exponent,  $\{s_j(t)\}_{j \in \mathcal{N}_b \cup \mathcal{N}_a}$  is a set of transmitting waveforms,  $\alpha_{kj}$  and  $\tau_{kj}$  are the amplitude gain and propagation delay, respectively, and  $\mathbf{z}_{kj}(t)$  represents the observation noise, modeled as additive white complex Gaussian processes.<sup>1</sup> The relationship between  $\tau_{kj}$  and the node relative position is given by

$$\tau_{kj} = \frac{1}{c} \| \mathbf{p}_k - \mathbf{p}_j \|$$

where  $c$  is the propagation speed of the signal.

In the dynamic scenarios, we consider intra-node measurements of agents themselves in addition to the inter-node measurements. Both the measurements and

inference processes are made at discrete instants  $t_n$  where  $n = 1, 2, \dots, N$ . The intra-node measurement  $\mathbf{z}_k^{(n)}$  of agent  $k$  at time  $t_n$  typically consists of acceleration and angular velocity, which can be obtained from the IMU. For ease of exposition in this paper, the model for intra-node measurements is considered to be the displacement corrupted by additive Gaussian noise, i.e.,

$$\mathbf{z}_k^{(n)} = \mathbf{p}_k^{(n)} - \mathbf{p}_k^{(n-1)} + \mathbf{w}_k^{(n)} \quad (2)$$

where  $\mathbf{p}_k^{(n)}$  denotes the position of agent  $k$  at time  $t_n$  and  $\mathbf{w}_k^{(n)}$  is modeled as  $\mathcal{N}(\mathbf{0}, \sigma_m^2 \mathbf{I})$ , in which  $\sigma_m$  is a known positive real number.

## B. Network Operation

To further understand the role of the network operation strategies, we present the architecture of a localization and navigation system in Fig. 2, highlighting the various functionalities considered in this paper. The system consists of three different layers: the measurement layer, the localization layer, and the operation layer. The measurement layer performs raw inter- and intra-node measurements, extracts information regarding the agents' positions and channel qualities, and outputs this information to the localization layer and the operation layer. The localization layer aggregates the information from the measurement layer, estimates the positions of the agents, and outputs these position estimates to the operation layer. Based on the input from the measurement layer and the localization layer, the operation layer produces the decisions for node prioritization, node activation, and node deployment. The decisions for node prioritization and node activation will serve as the input to the measurement layer to control the set of active agents and determine the allocation of transmitting resources, and the decision for node

<sup>1</sup>Note that although we use a single-path channel model for the inter-node measurements and time-of-arrival as the signal metric, the results of this paper can be easily extended to other models, e.g., multipath channel models and ranging models with additive noise, and other signal metrics, e.g., time-difference-of-arrival [83], [143]. Moreover, we focus on line-of-sight scenarios, whereas the strategies proposed in this paper can also be applied to non-line-of-sight scenarios with slight modification.

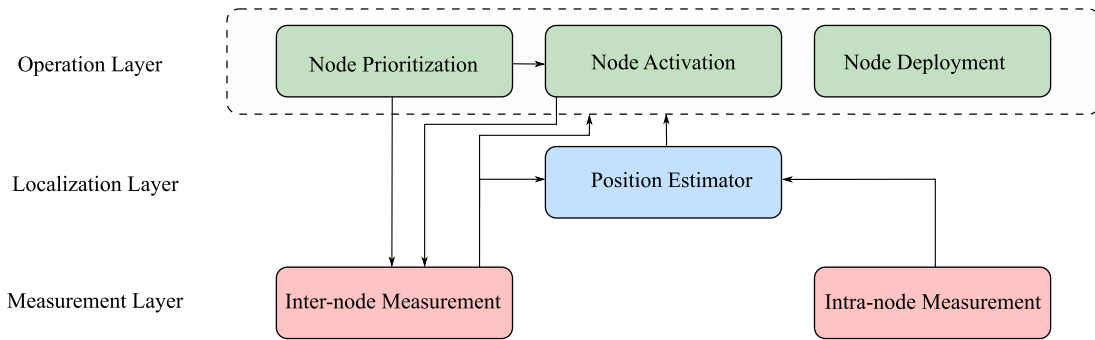


**Fig. 2.** Architecture of the considered network-based localization and navigation system.

deployment will be used to guide certain agents to appointed regions.

There are several important concepts relating to the network operation strategies in NLN, which are described as follows.

- Centralized versus distributed—With centralized network operation, there is a central controller that collects information from all the nodes in the network and produces the operation decisions for all the agents. With distributed network operation, there is no central controller; instead, each agent produces its own operation decision based on the information collected locally. Generally speaking, centralized strategies give better performance, but are usually not scalable with the size of the network.
- Cooperative versus non-cooperative—With non-cooperative NLN, agents do not make measurements amongst each other, whereas with cooperative NLN, agents assist each other in estimating their positions. Cooperation among agents can offer increased localization accuracy and circumvent the need for high-transmitting power anchors and high-density anchor deployments. However, the design of network operation strategies in a cooperative setting is generally more complicated.
- Robust versus non-robust—The design of network operation strategies often requires the knowledge of certain parameters, such as inter-node angles and distances, but perfect knowledge of these parameters is usually unavailable. Non-robust approaches use the estimated values of these parameters as input to the operation layer without accounting for their uncertainty, whereas robust approaches aim to design strategies that guarantee the localization performance subject to parameter uncertainty. Generally, non-robust approaches improve average performance if the uncertainty is small, while robust approaches result in better worst-case performance.
- Two-dimensional (2-D) versus three-dimensional (3-D)—The performance metrics that arise in these two scenarios have different structures. Generally speaking, the network operation strategies in

3-D networks are more challenging than their 2-D counterparts due in part to the more complicated expression of the metric.<sup>2</sup> In this paper, we will focus on 2-D localization, whereas most results are also applicable to 3-D localization.

### C. Performance Metrics

The localization accuracy can be quantified in terms of the mean squared error (MSE) of a position estimator. Let  $\mathbf{p}$  denote the vector that consists of all the parameters of interest. We first consider static scenarios where there is no temporal cooperation, in which case

$$\mathbf{p} = \begin{bmatrix} \mathbf{p}_1^T & \mathbf{p}_2^T & \dots & \mathbf{p}_{N_a}^T \end{bmatrix}^T.$$

Let  $\hat{\mathbf{p}}$  denote an unbiased estimator of  $\mathbf{p}$  based on the inter-node measurement  $\{\mathbf{r}_{kj}(t)\}_{k \in \mathcal{N}_a, j \in \mathcal{N}_a \cup \mathcal{N}_b \setminus \{k\}}$  in (1). From the information inequality [73], the MSE matrix of  $\mathbf{p}$  satisfies

$$\mathbb{E}\{(\hat{\mathbf{p}} - \mathbf{p})(\hat{\mathbf{p}} - \mathbf{p})^T\} \succcurlyeq \mathbf{J}_e^{-1}(\mathbf{p}) \quad (3)$$

where  $\mathbf{J}_e(\mathbf{p})$  is the equivalent Fisher information matrix (EFIM) for  $\mathbf{p}$ , structured as (4), shown at the top of the next page. In  $\mathbf{J}_e(\mathbf{p})$ ,  $\mathbf{J}_e^A(\mathbf{p}_k)$  and  $\mathbf{C}_{kj}$  can be expressed as follows<sup>3</sup>:

$$\mathbf{J}_e^A(\mathbf{p}_k) = \sum_{j \in \mathcal{N}_b} \lambda_{kj} \mathbf{J}_r(\phi_{kj}) \quad (5)$$

and

$$\mathbf{C}_{kj} = \mathbf{C}_{jk} = (\lambda_{kj} + \lambda_{jk}) \mathbf{J}_r(\phi_{kj}) \quad k, j \in \mathcal{N}_a$$

where the matrix  $\mathbf{J}_r(\phi)$  is referred to as the rang direction matrix (RDM) and  $\lambda_{kj}$  is referred to as the ranging information intensity (RII) between node  $k$  and  $j$  [72], given

<sup>2</sup>Specifically, the evaluation of the performance metric involves the inversion of a  $3 \times 3$  matrix. Due to the complicated expression after this inversion, it is challenging to obtain some of the amenable properties, e.g., the second-order cone structure in (20), in 3-D localization networks.

<sup>3</sup>We consider synchronous networks in this section, whereas the discussion of asynchronous networks is in Section III-A.

$$\mathbf{J}_e(\mathbf{p}) = \begin{bmatrix} \mathbf{J}_e^A(\mathbf{p}_1) + \sum_{j \in \mathcal{N}_a \setminus \{1\}} C_{1,j} & -C_{1,2} & \dots & -C_{1,N_a} \\ -C_{2,1} & \mathbf{J}_e^A(\mathbf{p}_2) + \sum_{j \in \mathcal{N}_a \setminus \{2\}} C_{2,j} & & -C_{2,N_a} \\ \vdots & & \ddots & \\ -C_{N_a,1} & -C_{N_a,2} & \dots & \mathbf{J}_e^A(\mathbf{p}_{N_a}) + \sum_{j \in \mathcal{N}_a \setminus \{N_a\}} C_{N_a,j} \end{bmatrix} \quad (4)$$


---

by

$$\begin{aligned} \mathbf{J}_r(\phi_{kj}) &= \begin{bmatrix} \cos^2 \phi_{kj} & \cos \phi_{kj} \sin \phi_{kj} \\ \cos \phi_{kj} \sin \phi_{kj} & \sin^2 \phi_{kj} \end{bmatrix} \\ \lambda_{kj} &= \frac{8\pi^2 \beta_0^2 E_{kj}}{c^2} (1 - \chi_{kj}) \frac{\alpha_{kj}^2}{N_0} \quad k \in \mathcal{N}_a, j \in \mathcal{N}_a \cup \mathcal{N}_b \end{aligned} \quad (6)$$

in which  $\beta_0$  is the effective bandwidth of the transmitted signal, and  $\chi_{kj} \in [0, 1]$  is the path-overlap coefficient characterizing the effect of multipath propagation. Note that the EFIM (4) consists of blocks that represent localization information from the anchors and agent cooperation. In particular,  $\mathbf{J}_e^A(\mathbf{p}_k)$  describes the information about agent  $k$  obtained from the measurements between the anchors and agent  $k$ ; and  $C_{k,j}$  describes the range information (RI) obtained from the measurement between agent  $k$  and agent  $j$ . The RII characterizes the quality of the measurement between two nodes, which is affected by a number of different factors such as the power and bandwidth of the transmitting signal as well as multipath effects [72].

As a result of (3), the MSE of the position estimator for all agents  $\hat{\mathbf{p}}$  is lower bounded by

$$\mathbb{E}\{\|\hat{\mathbf{p}} - \mathbf{p}\|^2\} \geq \text{tr}\{\mathbf{J}_e^{-1}(\mathbf{p})\} =: \mathcal{P}(\mathbf{p}).$$

Let  $\hat{\mathbf{p}}_k$  denote an unbiased estimator of  $\mathbf{p}_k$  based on the measurements  $\{\mathbf{r}_{kj}(t)\}_{k \in \mathcal{N}_a, j \in \mathcal{N}_a \cup \mathcal{N}_b \setminus \{k\}}$ . As a result of (3), we have

$$\mathbb{E}\{(\hat{\mathbf{p}}_k - \mathbf{p}_k)(\hat{\mathbf{p}}_k - \mathbf{p}_k)^T\} \succcurlyeq [\mathbf{J}_e^{-1}(\mathbf{p})]_{p_k}$$

where  $[\mathbf{J}_e^{-1}(\mathbf{p})]_{p_k}$  denotes a  $2 \times 2$  matrix corresponding to the  $k$ th diagonal block of  $\mathbf{J}_e^{-1}(\mathbf{p})$ . We can then introduce the EFIM for  $\mathbf{p}_k$  as

$$\mathbf{J}_e(\mathbf{p}_k) := \left\{ [\mathbf{J}_e^{-1}(\mathbf{p})]_{p_k} \right\}^{-1}. \quad (7)$$

The MSE of the estimator  $\hat{\mathbf{p}}_k$  is then lower bounded by

$$\mathbb{E}\{\|\hat{\mathbf{p}}_k - \mathbf{p}_k\|^2\} \geq \text{tr}\{\mathbf{J}_e^{-1}(\mathbf{p}_k)\} =: \mathcal{P}(\mathbf{p}_k).$$

Note that in a non-cooperative setting,  $C_{kj} = \mathbf{0}$  for all  $k, j \in \mathcal{N}_a$ , and the EFIM  $\mathbf{J}_e(\mathbf{p})$  degenerates to a block-diagonal matrix. Consequently,  $\mathbf{J}_e(\mathbf{p}_k)$  degenerates to  $\mathbf{J}_e^A(\mathbf{p}_k)$ . In this paper, we will adopt  $\mathcal{P}(\mathbf{p})$  and  $\mathcal{P}(\mathbf{p}_k)$  as the performance metrics, referred to as the network squared position error bound (nSPEB) and the individual squared position error bound (iSPEB), respectively.

In dynamic scenarios, we have to consider the agent positions at different time instances to develop the network operation strategies. In these scenarios, the parameter of interest can be written as  $\mathbf{p} = \mathbf{p}_{1:N_a}^{(1:N)}$ . The EFIM for the entire network over time  $t_1$  to  $t_N$  can be derived as<sup>4</sup> [74]

$$\begin{aligned} \mathbf{J}_e(\mathbf{p}) &= \sum_{n=1}^N \mathbf{E}_{n,n}^N \otimes (\mathbf{S}^{(n)} + \mathbf{T}^{(n)} + \mathbf{T}^{(n+1)}) \\ &\quad - \sum_{n=1}^N (\mathbf{E}_{n,n+1}^N + \mathbf{E}_{n+1,n}^N) \otimes \mathbf{T}^{(n)} \end{aligned} \quad (8)$$

where

$$\begin{aligned} \mathbf{S}^{(n)} &= \sum_{k \in \mathcal{N}_a} \sum_{j \in \mathcal{N}_a \cup \mathcal{N}_b \setminus \{k\}} \mathbf{E}_{k,k}^{N_a} \otimes \mathbf{S}_{kj}^{(n)} \\ &\quad - \sum_{k \in \mathcal{N}_a} \sum_{j \in \mathcal{N}_a \setminus \{k\}} \mathbf{E}_{k,j}^{N_a} \otimes \mathbf{S}_{kj}^{(n)} \end{aligned} \quad (9)$$

in which  $\mathbf{S}_{kj}^{(n)} = \lambda_{kj}^{(n)} \mathbf{J}_r(\phi_{kj}^{(n)})$  with  $\lambda_{kj}^{(n)}$  and  $\phi_{kj}^{(n)}$  characterizing the RII and the angle between node  $k$  and  $j$  at time  $t_n$ , respectively, and  $\mathbf{T}^{(n)} = \sum_{k \in \mathcal{N}_a} \mathbf{E}_{k,k}^{N_a} \otimes \mathbf{T}_k^{(n)}$  with

$$\mathbf{T}_k^{(n)} = \sigma_m^{-2} \mathbf{I}_2.$$

Let  $\hat{\mathbf{p}}^{(N)} := \hat{\mathbf{p}}_{1:N_a}^{(N)}$  denote an unbiased estimator of  $\mathbf{p}^{(N)} := \mathbf{p}_{1:N_a}^{(N)}$ . From the information inequality, the MSE of  $\mathbf{p}^{(N)}$  satisfies

$$\mathbb{E}\{(\hat{\mathbf{p}}^{(N)} - \mathbf{p}^{(N)})(\hat{\mathbf{p}}^{(N)} - \mathbf{p}^{(N)})^T\} \succcurlyeq [\mathbf{J}_e^{-1}(\mathbf{p})]_{p^{(N)}}^{-1}. \quad (10)$$

Then the corresponding nSPEB at instant  $t_N$  can be written as

$$\mathcal{P}(\mathbf{p}^{(N)}) := \text{tr}\{\mathbf{J}_e^{-1}(\mathbf{p}^{(N)})\} \quad (11)$$

where  $\mathbf{J}_e(\mathbf{p}^{(N)}) := [\mathbf{J}_e^{-1}(\mathbf{p})]_{p^{(N)}}^{-1}$ . We can then introduce the EFIM for  $\mathbf{p}_k$  at time  $t_N$  as

$$\mathbf{J}_e(\mathbf{p}_k^{(N)}) = \left\{ [\mathbf{J}_e^{-1}(\mathbf{p}^{(N)})]_{p_k} \right\}^{-1}.$$

The MSE of the estimator  $\hat{\mathbf{p}}_k^{(N)}$  is then lower bounded by

$$\mathbb{E}\{\|\hat{\mathbf{p}}_k^{(N)} - \mathbf{p}_k^{(N)}\|^2\} \geq \text{tr}\{\mathbf{J}_e^{-1}(\mathbf{p}_k^{(N)})\} =: \mathcal{P}(\mathbf{p}_k^{(N)}) \quad (12)$$

where  $\mathcal{P}(\mathbf{p}_k^{(N)})$  denotes the iSPEB at instant  $t_N$ .

<sup>4</sup>For notational convenience, we let  $\mathbf{T}^{(1)} = \mathbf{T}^{(N+1)} = \mathbf{0}$ .

**TABLE 2** Notation for Important Optimization Problems

Notation	Definition
$\mathcal{P}_c$	Centralized node prioritization problems for non-cooperative localization
$\mathcal{P}_k$	Distributed node prioritization problems for agent $k$ for non-cooperative localization
$\mathcal{P}_{R,k}$	Robust node prioritization problem for agent $k$
$\mathcal{P}_{R,k}^M$ and $\underline{\mathcal{P}}_{R,k}^M$	Relaxation problems of $\mathcal{P}_{R,k}$
$\mathcal{P}_{C-c}$	Centralized node prioritization problems for cooperative localization
$\mathcal{P}_{C,k}$	Distributed node prioritization problems for agent $k$ for cooperative localization
$\mathcal{P}_{C,k}^{\text{Anc}}$ and $\mathcal{P}_{C,k}^{\text{Agt}}$	Node prioritization problem for agent $k$ in the infrastructure and cooperative phase, respectively
$\mathcal{P}^S$	Problem for optimizing the access probability
$\mathcal{D}$ and $\mathcal{D}_C$	Node deployment problems for agents for non-cooperative and cooperative localization, respectively
$\mathcal{D}_{SP}$ and $\mathcal{D}_{C-SP}$	Node deployment problems for an agent in a single position for non-cooperative and cooperative localization, respectively

The nSPEB and iSPEB characterize the lower bounds for the mean squared position errors. These bounds are asymptotically achievable by the maximum likelihood estimators in high signal-to-noise ratio regimes (over approximately 15 dB [41]). Since high accuracy localization and navigation networks typically operate in such regimes, the nSPEB and iSPEB can be used as the performance metric for the design of network operation strategies for a broad range of applications.

### III. NODE PRIORITIZATION FOR NON-COOPERATIVE LOCALIZATION

This section presents the node prioritization strategies for non-cooperative static networks.

#### A. Problem Formulation

We first formulate the node prioritization problem, aiming to achieve the optimal tradeoff between localization accuracy and resource consumption. We rewrite  $\lambda_{kj}$  in (6) as

$$\lambda_{kj} = x_{kj} \xi_{kj} \quad (13)$$

where  $x_{kj}$  denotes the amount of resources consumed by node  $k$  for the inter-node measurement between node  $k$  and  $j$  and  $\xi_{kj}$  denotes the quality of that measurement. Note that (13) is general enough to accommodate various node prioritization problems based on the type of resources manifested in  $x_{kj}$  and  $\xi_{kj}$ . One example is node prioritization based on transmitting power, where  $x_{kj} = E_{kj}$  and

$$\xi_{kj} = \frac{8\pi^2\beta_0^2}{c^2} (1 - \chi_{kj}) \frac{\alpha_{kj}^2}{N_0}.$$

We first consider the non-robust formulation, where parameters  $\xi_{kj}$  and  $\phi_{kj}$  are estimated values used as the input to the node prioritization module. Let  $\mathbf{x}_k$  denote the node prioritization vector (NPV) for node  $k$ . In non-cooperative networks, agents make measurements only with anchors, and therefore,  $\mathbf{x}_k \in \mathbb{R}^{N_b}$ . We can write  $\mathbf{x}_k$  as

$$\mathbf{x}_k = [x_{k(N_a+1)} \ x_{k(N_a+2)} \ \dots \ x_{k(N_a+N_b)}]^T.$$

Let  $\mathbf{x}$  denote the vector that consists of all the agents' NPVs

$$\mathbf{x} = [\mathbf{x}_1^T \ \mathbf{x}_2^T \ \dots \ \mathbf{x}_{N_a}^T]^T.$$

To emphasize its dependence on NPVs, we rewrite the nSPEB and iSPEB as  $\mathcal{P}(\mathbf{p}; \mathbf{x})$  and  $\mathcal{P}(\mathbf{p}_k; \mathbf{x}_k)$ . Note that  $\mathcal{P}(\mathbf{p}; \mathbf{x}) = \sum_{k \in \mathcal{N}_a} \mathcal{P}(\mathbf{p}_k; \mathbf{x}_k)$  and in the non-cooperative setting

$$\mathcal{P}(\mathbf{p}_k; \mathbf{x}_k) = \text{tr} \left\{ \left( \sum_{j \in \mathcal{N}_b} x_{kj} \xi_{kj} \mathbf{J}_e(\phi_{kj}) \right)^{-1} \right\}.$$

The centralized node prioritization problem can be written as

$$\mathcal{P}_c : \underset{\mathbf{x}}{\text{minimize}} \quad \mathcal{P}(\mathbf{p}; \mathbf{x}) \quad (14)$$

$$\text{subject to} \quad \mathbf{x} \succcurlyeq \mathbf{0} \quad (14)$$

$$c_l(\mathbf{x}) \leq 0, \quad l = 1, 2, \dots, L_c \quad (15)$$

and the distributed node prioritization problem for agent  $k$  can be written as

$$\mathcal{P}_k : \underset{\mathbf{x}_k}{\text{minimize}} \quad \mathcal{P}(\mathbf{p}_k; \mathbf{x}_k) \quad (16)$$

$$\text{subject to} \quad \mathbf{x}_k \succcurlyeq \mathbf{0} \quad (16)$$

$$c_{k,l}(\mathbf{x}_k) \leq 0, \quad l = 1, 2, \dots, L_k \quad (17)$$

where (14) and (16) denote the nonnegativity constraints on the amounts of resources; and  $\{c_l(\cdot)\}$  in (15) and  $\{c_{k,l}(\cdot)\}$  in (17) denote  $L_c$  and  $L_k$  linear constraints on the NPVs for  $\mathcal{P}_c$  and  $\mathcal{P}_k$ , respectively. Examples of these linear constraints include the total resource constraints of the network and of the individual agent  $k$ , i.e.,  $c_l(\mathbf{x}) = \mathbf{1}^T \mathbf{x} - C_{\text{tot}}$  and  $c_{k,l}(\mathbf{x}_k) = \mathbf{1}^T \mathbf{x}_k - C_{k,\text{tot}}$ , where  $C_{\text{tot}}$  and  $C_{k,\text{tot}}$  are some positive constants.

*Remark 1:* In non-cooperative networks,  $\mathcal{P}(\mathbf{p}_k; \mathbf{x}_k) = \text{tr} \{ (\mathbf{J}_e^A(\mathbf{p}_k))^{-1} \}$ . Since evaluating  $\mathbf{J}_e^A(\mathbf{p}_k)$  involves only local parameters, i.e.,  $\{\phi_{kj}\}_{j \in \mathcal{N}_b}$  and  $\{\xi_{kj}\}_{j \in \mathcal{N}_b}$ , the formulation of  $\mathcal{P}_k$  does not require the parameters of the entire network and the solution of  $\mathcal{P}_k$  naturally gives rise to distributed implementation. This does not hold for the node prioritization problems in cooperative networks, as will be shown in Section IV.

*Remark 2:* The methods developed in this paper are also applicable to other formulations of the node prioritization problem (e.g., minimizing the total resource consumption subject to a given localization performance requirement).

In particular, one can consider a *broadcast* setting, in which only anchors are required to transmit signals, and each of the agents can use the received waveform for ranging. In this setting, the NPV  $\mathbf{x}_b \in \mathbb{R}^{N_b}$  and its  $k$ th element  $x_k$  refers to the amount of resources for the wireless signals broadcast by anchor  $k$ . The RII can then be written as

$$\lambda_{kj} = x_k \xi_{kj} \mathbb{1}_{\mathcal{N}_b}(k) \mathbb{1}_{\mathcal{N}_a}(j). \quad (18)$$

Here, it is more reasonable to select nSPEB  $\mathcal{P}(\mathbf{p}; \mathbf{x}_b)$  as the performance metric and the optimization problem is then

$$\begin{aligned} & \underset{\mathbf{x}}{\text{minimize}} \quad \mathcal{P}(\mathbf{p}; \mathbf{x}_b) \\ & \text{subject to} \quad \mathbf{x}_b \succcurlyeq \mathbf{0} \\ & \quad c_l(\mathbf{x}_b) \leq 0, \quad l = 1, 2, \dots, L_c. \end{aligned}$$

This problem has a similar structure to  $\mathcal{P}_c$  and  $\mathcal{P}_k$ , but it optimizes the resources broadcast by anchors, whereas  $\mathcal{P}_c$  and  $\mathcal{P}_k$  optimize the resources used in point-to-point measurements. The techniques that will be introduced in Section III-B can be easily used for this optimization problem in the broadcast setting because it has a structure similar to  $\mathcal{P}_c$  and  $\mathcal{P}_k$ .

The considered problems  $\mathcal{P}_c$  and  $\mathcal{P}_k$  can address the synchronous case as well as the asynchronous case with only a slight modification. In particular, consider that anchors and agents are not synchronized. A feasible localization method in this case uses round-trip ranging: node  $k$  initiates by transmitting a wireless signal to node  $j$ , and node  $j$  responds by transmitting a wireless signal back to node  $k$ ; the range  $d_{kj}$  is inferred at node  $k$  from the round trip time. Let  $\lambda_{jk}$  and  $x_{jk}$  denote the RII and the resource of the response signal sent from node  $j$  to node  $k$ , respectively. The matrix  $\mathbf{J}_e^A(\mathbf{p}_k)$  can then be expressed as

$$\begin{aligned} \mathbf{J}_e^A(\mathbf{p}_k) &= \sum_{j \in \mathcal{N}_b} \frac{4\lambda_{kj}\lambda_{jk}}{\lambda_{kj} + \lambda_{jk}} \mathbf{J}_r(\phi_{kj}) \\ &= \sum_{j \in \mathcal{N}_b} \frac{4x_{kj}x_{jk}}{x_{kj} + x_{jk}} \xi_{kj} \mathbf{J}_r(\phi_{kj}) \end{aligned}$$

where the second equality is because of the channel reciprocity, i.e.,  $\xi_{kj} = \xi_{jk}$ . In practice, there are two common scenarios.

- Highly asymmetric networks—In certain networks (e.g., cellular networks), the transmitting resources (e.g., transmitting power) from anchors (e.g., base stations) are significantly larger than those from agents (e.g., mobile users) and cannot be controlled by the agents. In this scenario, the node prioritization problem is to optimize over  $\{x_{kj}\}_{j \in \mathcal{N}_b}$  for each agent  $k$  with the assumption that  $x_{jk} \gg x_{kj}$ ,  $j \in \mathcal{N}_b$ . The matrix  $\mathbf{J}_e^A(\mathbf{p}_k)$  can be approximated as

$$\mathbf{J}_e^A(\mathbf{p}_k) \approx \sum_{j \in \mathcal{N}_b} 4x_{kj}\xi_{kj} \mathbf{J}_r(\phi_{kj})$$

and has the same structure as (5) with  $\lambda_{kj}$  given in (13).

- Proportional amount of response resources—In certain scenarios, the amounts of resources for the response signals are proportional to those for the initiating signals, i.e.,  $x_{jk} = \eta x_{kj}$ , where  $\eta \in \mathbb{R}^+$  does not depend on  $k$  or  $j$ .<sup>5</sup> With this resource allocation method, the node prioritization problem is to optimize over  $\{x_{kj}\}_{j \in \mathcal{N}_b}$  for each agent  $k$  with the assumption that  $x_{jk} = \eta x_{kj}$ ,  $j \in \mathcal{N}_b$ . The matrix  $\mathbf{J}_e^A(\mathbf{p}_k)$  becomes

$$\mathbf{J}_e^A(\mathbf{p}_k) = \sum_{j \in \mathcal{N}_b} \frac{4\eta}{1 + \eta} x_{kj} \xi_{kj} \mathbf{J}_r(\phi_{kj})$$

and has the same structure as (5) with  $\lambda_{kj}$  given in (13).

For readers who are interested in the node prioritization strategies in asynchronous networks, see [88]–[90] for a more detailed discussion.

## B. Conic Programming-Based Approaches

We next provide solutions to the node prioritization problems  $\mathcal{P}_c$  and  $\mathcal{P}_k$  with conic programming-based approaches. Note that if there is only one agent in the network,  $\mathcal{P}_c$  degenerates to  $\mathcal{P}_k$ . Therefore,  $\mathcal{P}_k$  can be seen as a special case of  $\mathcal{P}_c$ , and we will focus our attention on  $\mathcal{P}_c$  in the following.

*Proposition 1 (Convexity):* The nSPEB  $\mathcal{P}(\mathbf{p}; \mathbf{x})$  in non-cooperative networks is convex in  $\mathbf{x} \succcurlyeq \mathbf{0}$ .

There are many ways to prove Proposition 1, where the details can be found in [142]–[144]. One way is to take the second derivative of  $\mathcal{P}(\mathbf{p}; \mathbf{x})$  with respect to  $\mathbf{x}$  and show that the Hessian matrix is positive semidefinite [144].

Proposition 1 shows that the objective function of  $\mathcal{P}_c$  is convex in  $\mathbf{x}$ . Thus, together with the fact that  $\mathcal{P}$  has convex constraints, Proposition 1 implies that  $\mathcal{P}_c$  is a convex program [146]–[148]. Consequently, the optimal solution can be obtained numerically by standard convex optimization algorithms [146].

Conic optimization is a special type of convex optimization, and it includes the most well-known classes of convex optimization problems such as semidefinite programs (SDPs) and SOCPs. We next show that  $\mathcal{P}_c$  can be converted to an SDP, which is a more favorable formulation than the general convex formulation. Recall that the nSPEB can be written as

$$\mathcal{P}(\mathbf{p}; \mathbf{x}) = \text{tr}\{\mathbf{J}_e(\mathbf{p})^{-1}\} = \sum_{k \in \mathcal{N}_b} \text{tr}\{\mathbf{J}_e^A(\mathbf{p}_k)^{-1}\}.$$

Let us consider an auxiliary matrix  $\mathbf{M}_k$  with the following constraint:

$$\mathbf{M}_k \succcurlyeq (\mathbf{J}_e^A(\mathbf{p}_k))^{-1}.$$

Due to the fact that  $\mathbf{J}_e^A(\mathbf{p}_k) \succcurlyeq \mathbf{0}$ , the constraint above can be equivalently transformed to the semidefiniteness of a matrix that involves  $\mathbf{M}_k$  and  $\mathbf{x}_k$ , as shown in the following

<sup>5</sup>This allocation for the response signals is shown to be optimal in the scenario with certain resource constraints [142], and it has been implemented in practice [117].

proposition. A detailed proof of Proposition 2 can be found in [142].

*Proposition 2 (SDP):* The problem  $\mathcal{P}_c$  is equivalent to the SDP

$$\begin{aligned} & \underset{\mathbf{x}, \{\mathbf{M}_k\}_{k \in \mathcal{N}_b}}{\text{minimize}} \quad \sum_{k \in \mathcal{N}_a} \text{tr}\{\mathbf{M}_k\} \\ & \text{subject to} \quad \begin{bmatrix} \mathbf{M}_k & \mathbf{I} \\ \mathbf{I} & \sum_{j \in \mathcal{N}_b} x_{kj} \xi_{kj} \mathbf{J}_r(\phi_{kj}) \end{bmatrix} \succcurlyeq 0, \quad \forall k \in \mathcal{N}_a \end{aligned} \quad (14) - (15)$$

Furthermore, the problem  $\mathcal{P}_c$  can also be converted to an SOCP problem, which is an even more favorable formulation than the SDP formulation. To see how we can achieve this, we first transform  $\mathcal{P}_c$  to the following problem:

$$\begin{aligned} & \underset{\mathbf{x}, \{\varrho_k\}_{k \in \mathcal{N}_b}}{\text{minimize}} \quad \sum_{k \in \mathcal{N}_b} \varrho_k \\ & \text{subject to} \quad \mathcal{P}(\mathbf{p}_k; \mathbf{x}_k) \leq \varrho_k, \quad \forall k \in \mathcal{N}_a \end{aligned} \quad (14) - (15)$$

To transform the constraint  $\mathcal{P}(\mathbf{p}_k; \mathbf{x}_k) \leq \varrho_k$  to a desired form, we next explicitly rewrite the iSPEB as follows:

$$\mathcal{P}(\mathbf{p}_k; \mathbf{x}_k) = \frac{4 \cdot \mathbf{1}^T \mathbf{R}_k \mathbf{x}_k}{\mathbf{x}_k^T \mathbf{R}_k^T (\mathbf{1} \mathbf{1}^T - \mathbf{c}_k \mathbf{c}_k^T - \mathbf{s}_k \mathbf{s}_k^T) \mathbf{R}_k \mathbf{x}_k} \quad (19)$$

where

$$\mathbf{R}_k = \text{diag}\{\xi_{k(N_a+1)}, \xi_{k(N_a+2)}, \dots, \xi_{k(N_a+N_b)}\}$$

and

$$\begin{aligned} \mathbf{c}_k &= [\cos 2\phi_{k(N_a+1)} \cos 2\phi_{k(N_a+2)} \dots \cos 2\phi_{k(N_a+N_b)}]^T \\ \mathbf{s}_k &= [\sin 2\phi_{k(N_a+1)} \sin 2\phi_{k(N_a+2)} \dots \sin 2\phi_{k(N_a+N_b)}]^T. \end{aligned}$$

The constraint  $\mathcal{P}(\mathbf{p}_k; \mathbf{x}_k) \leq \varrho_k$  can then be transformed into

$$\left\| [\mathbf{c}_k^T \mathbf{y}_k \quad \mathbf{s}_k^T \mathbf{y}_k \quad 2t_k]^T \right\| \leq \mathbf{1}^T \mathbf{y}_k - 2t_k \quad (20)$$

where  $\mathbf{y}_k = \mathbf{R}_k \mathbf{x}_k$  and  $t_k = 1/\varrho_k$ . The constraint  $t_k = 1/\varrho_k$  can be replaced with the following constraint without changing the optimal solution:

$$\left\| [t_k \quad \varrho_k \quad \sqrt{2}]^T \right\| \leq t_k + \varrho_k.$$

We then have the following proposition. A detailed proof of Proposition 3 can be found in [143].

*Proposition 3 (SOCP):* The problem  $\mathcal{P}_c$  is equivalent to the SOCP

$$\begin{aligned} & \underset{\mathbf{x}, \{t_k, \varrho_k\}_{k \in \mathcal{N}_a}}{\text{minimize}} \quad \sum_{k \in \mathcal{N}_a} \varrho_k \\ & \text{subject to} \quad \|\mathbf{A}_k \mathbf{R}_k \mathbf{x}_k + \mathbf{b}_k\| \leq \mathbf{1}^T \mathbf{R}_k \mathbf{x}_k - 2t_k, \quad \forall k \in \mathcal{N}_a \\ & \quad \left\| [t_k \quad \varrho_k \quad \sqrt{2}]^T \right\| \leq t_k + \varrho_k, \quad \forall k \in \mathcal{N}_a \end{aligned} \quad (14) - (15)$$

where  $\mathbf{A}_k = [\mathbf{c}_k \quad \mathbf{s}_k \quad \mathbf{0}]^T$  and  $\mathbf{b}_k = [0 \quad 0 \quad 2t_k]^T$ .

*Remark 3:* Regarding the computational complexity, the worst-case running time of both the SDP- and SOCP-based approaches is  $O(N_b^{3.5})$  for the single-agent case [149].

### C. Computational Geometry-Based Approaches

While conic programming-based approaches can provide solutions with amenable complexity, those solutions are  $\epsilon$ -approximate numerical ones and limited insight into the problem can be gained from the numerical solutions. We next present another type of approach, which not only provides exact solutions to the problem, but also reveals the essence of node prioritization problems.

In this section, we consider that the NPVs are subject to nonnegative constraints, i.e., (14) and (16), and the total resource constraints, i.e., (15) with  $L_c = 1$  and  $c_1(\mathbf{x}) = \mathbf{1}^T \mathbf{x} - 1$ , and (17) with  $L_k = 1$  and  $c_{k,1} = \mathbf{1}^T \mathbf{x}_k - 1$ . This is a common scenario in the design and implementation of a localization and navigation system. For example, the amount of available time for ranging with different anchors is subject to a total time constraint.

We next formulate a geometric framework, under which we can obtain solutions of  $\mathcal{P}_k$ , and then adopt these solutions to solve  $\mathcal{P}_c$ .

*1) Geometric Framework:* Inspired by the structure in (19), we introduce an affine transformation that maps an NPV to a point in 3-D space

$$\mathbf{z}_k = \mathbf{C}_k \mathbf{x}_k \quad (21)$$

where  $\mathbf{C}_k = [\mathbf{c}_k \quad \mathbf{s}_k \quad \mathbf{1}]^T \mathbf{R}_k$ . With this transformation, the iSPEB can be written as

$$Q(\mathbf{z}_k) := \frac{4[\mathbf{z}_k]_3}{[\mathbf{z}_k]_3^2 - [\mathbf{z}_k]_1^2 - [\mathbf{z}_k]_2^2} = \mathcal{P}(\mathbf{p}_k; \mathbf{x}_k).$$

This leads to the following geometric interpretation of the iSPEB. Given an NPV  $\mathbf{x}_k$ , the point  $\mathbf{z}_k = \mathbf{C}_k \mathbf{x}_k$  lies on a hyperboloid, given by

$$(z_3 - 2\eta^{-1})^2 - z_1^2 - z_2^2 - 4\eta^{-2} = 0 \quad (22)$$

where  $z_1$ ,  $z_2$ , and  $z_3$  are variables and  $\eta = \mathcal{P}(\mathbf{p}_k; \mathbf{x}_k)$ .

Denote the feasible NPV set of  $\mathcal{P}_k$  and its image set under the transformation (21), respectively, by

$$\mathcal{X}_k = \{\mathbf{x}_k \in \mathbb{R}^{N_b} : \mathbf{1}^T \mathbf{x}_k = 1, \mathbf{0} \preccurlyeq \mathbf{x}_k\}$$

and

$$\mathcal{Z}_k = \{\mathbf{z}_k \in \mathbb{R}^{N_b} : \mathbf{z}_k = \mathbf{C}_k \mathbf{x}_k, \mathbf{x}_k \in \mathcal{X}_k\}.$$

Note that each element  $\mathbf{x}_k \in \mathcal{X}_k$  can be written as a convex combination of elements in  $\mathcal{E} := \{e_1, e_2, \dots, e_{N_b}\}$ , where  $e_k$  is a unit vector with the  $k$ th element being 1 and all other elements being 0's. Hence, the image set  $\mathcal{Z}_k$  is a convex polyhedron, given by  $\mathbb{H}_c\{\mathbf{C}_k e : e \in \mathcal{E}\}$ . This implies that for  $\mathbf{x}_k \in \mathcal{X}_k$  with the corresponding iSPEB  $\mathcal{P}(\mathbf{p}_k; \mathbf{x}_k)$ ,  $\mathbf{C}_k \mathbf{x}_k$  is in the intersection of  $\mathcal{Z}_k$  and the

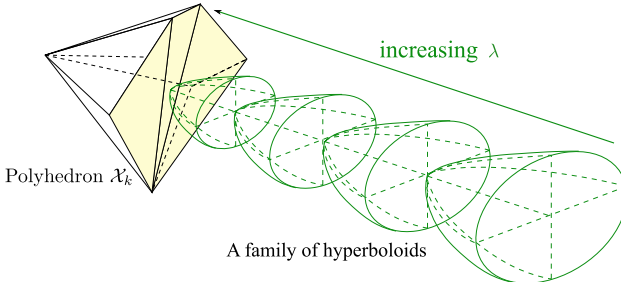


**Fig. 3.** Illustration of solving  $\mathcal{P}_{G,k}$ : the polyhedron corresponds to the image of the feasible set; a hyperboloid consists of the points that correspond to a particular value of the iSPEB. The optimal solution corresponds to a point on the surface of the polyhedron.

hyperboloid in (22). Such a geometric interpretation can be used to transform  $\mathcal{P}_k$  to a geometric problem. Consider the following problem:

$$\begin{aligned} \mathcal{P}_{G,k} : & \underset{\eta}{\text{minimize}} && \eta \\ & \text{subject to} && \mathcal{Z}_k \cap \mathcal{H}(\eta) \neq \emptyset \\ & && \eta > 0 \end{aligned}$$

where

$$\mathcal{H}(\eta) = \{z = [z_1 \ z_2 \ z_3]^T : z_1, z_2 \text{ and } z_3 \text{ satisfy (22)}\}.$$

The following proposition connects the optimal solution of  $\mathcal{P}_k$  and that of  $\mathcal{P}_{G,k}$ .

*Proposition 4* [145]: For  $x_k \in \mathcal{X}_k$ , if  $C_k x_k^* \in \mathcal{H}(\eta^*)$ , where  $\eta^*$  is the optimal solution for  $\mathcal{P}_{G,k}$ , then  $x_k^*$  is an optimal solution for  $\mathcal{P}_k$ .

Let  $\eta^*$  denote the optimal solution of  $\mathcal{P}_{G,k}$ . Proposition 4 provides a way to solve  $\mathcal{P}_k$  using  $\eta^*$ : we can find a point  $z_k^* \in \mathcal{Z}_k \cap \mathcal{H}(\eta^*)$  and determine a vector in  $\mathcal{X}_k$  that is an inverse image of  $z_k^*$  under the transformation (21).<sup>6</sup> Such a vector is then an optimal solution for  $\mathcal{P}_k$ .

2) Solving  $\mathcal{P}_{G,k}$  and  $\mathcal{P}_k$ : The process of solving  $\mathcal{P}_{G,k}$  is illustrated in Fig. 3.  $\mathcal{X}_k$  is a fixed polyhedron, whereas  $\mathcal{H}(\eta)$  is a family of hyperboloids parameterized by  $\eta$ . As  $\eta$  increases, the hyperboloid  $\mathcal{H}(\eta)$  gradually approaches  $\mathcal{X}_k$ . If  $\mathcal{H}(\eta)$  and  $\mathcal{X}_k$  are disjoint, then  $\eta$  is too small to be feasible; if  $\mathcal{H}(\eta)$  and  $\mathcal{X}_k$  intersect, then  $\eta$  is too large to be optimal. Hence, the optimal solution  $\eta^*$  corresponds to the scenario where  $\mathcal{X}_k$  is tangent to  $\mathcal{H}(\eta^*)$ . This implies that the  $\mathcal{Z}_k \cap \mathcal{H}(\eta^*)$  contains only one point, and this point lies on the surface of  $\mathcal{Z}_k$ . For brevity, we consider only the scenario where  $z_k^*$  is an interior point of some triangle on the surface of  $\mathcal{X}_k$ . Other scenarios are discussed in [145]. The answers to the following two questions are sufficient for solving  $\mathcal{P}_{G,k}$ :

- How can  $z_k^*$  be determined if it is known to lie on a triangle  $\mathcal{T}$ ?
- On which triangle does  $z_k^*$  lie?

<sup>6</sup>How to find the inverse image of  $z_k^*$  in  $\mathcal{X}_k$  will be given in the explanation of Theorem 1.

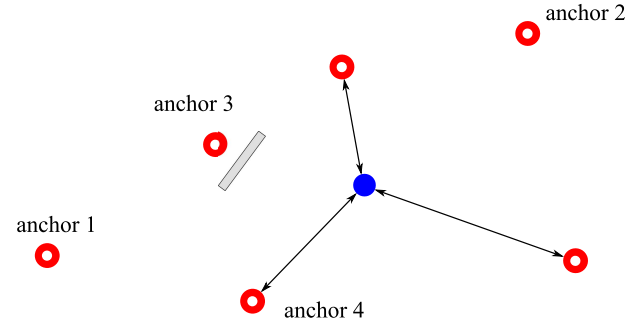


**Fig. 4.** Illustration of the sparsity: resources can be optimally allocated to only three anchors. Most anchors will not be used due to less favorable channel qualities or poorer network geometry.

For the first question, note that the normal vectors of  $\mathcal{T}$  and  $\mathcal{H}(\eta^*)$  are aligned at  $z_k^*$  as  $\mathcal{T}$  is tangent to  $\mathcal{H}(\eta^*)$  at  $z_k^*$ . This gives us an equation involving  $z_k^*$  and solving this equation gives the position of  $z_k^*$ . For the second question, we can adopt a seemingly brute-force method: search over every triangle on the surface of  $\mathcal{Z}_k$  and select the triangle with the minimum  $\eta$ . Details can be found in [145]. The computational complexity of this geometric method largely depends on the complexity associated with generating a convex hull of  $N_b$  given points in 3-D space [150], [151] and is  $O(N_b \log N_b)$ , which is more efficient than the conic programming-based approaches.

The observation that the unique point in  $\mathcal{Z}_k \cap \mathcal{H}(\eta^*)$  lies on the surface of  $\mathcal{H}(\eta^*)$  not only provides a way to solve  $\mathcal{P}_{G,k}$ , but also leads to the following theorem.

*Theorem 1 (Sparsity)* There exists an optimal NPV  $x_k^*$  for  $\mathcal{P}_k$  such that  $\|x_k^*\|_0 \leq 3$ .

This theorem has an intuitive explanation: the unique element of  $\mathcal{Z}_k \cap \mathcal{H}(\eta^*)$  lies on the surface of  $\mathcal{H}(\eta^*)$  and is therefore inside a triangle. Consequently, this element can be written as a convex combination of the triangle's three vertices. In this convex combination, replacing the three vertices with their inverse images in  $\mathcal{X}_k$  gives the desired  $x_k^*$ .

Theorem 1 shows that the total transmitting resources can be allocated to only three anchors without loss of optimality in 2-D networks. This implies that most anchors are not used due to less-favorable channel qualities or poorer network geometry. For example in Fig. 4, anchor 1 is not used since it is farthest from the agent and therefore the corresponding ranging quality is poorest. Hence, the same amount of resources allocated to other anchors contribute more in reducing the iSPEB. Furthermore, allocating resources to anchor 2 is not as efficient as allocating resources to anchor 4 as they both provide information along a similar direction but anchor 4 is closer to the agent.

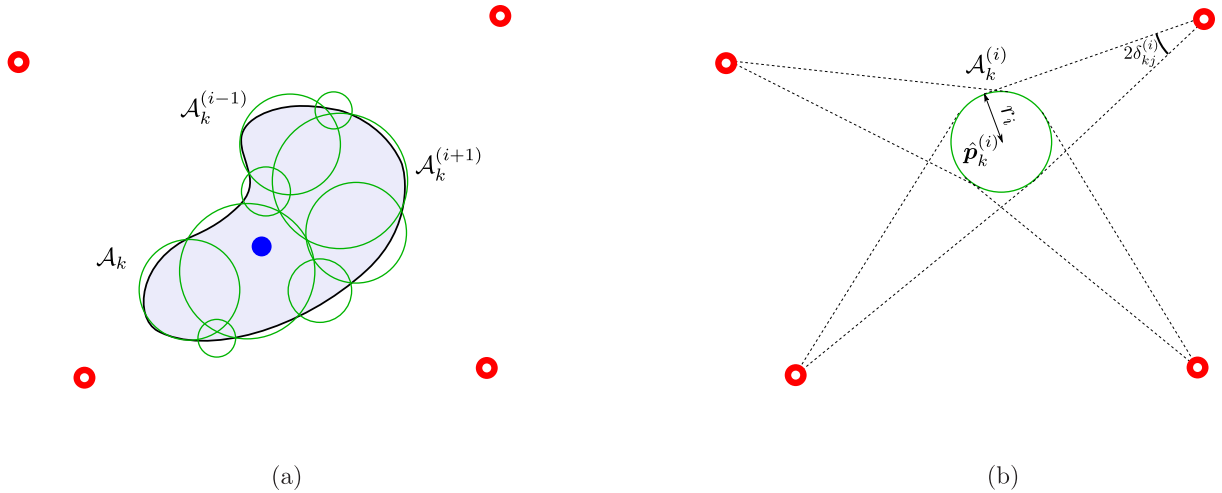


**Fig. 5.** Illustration of the robust formulation: (a) Irregular uncertainty area; (b) Circular uncertainty area.

3) Solving  $\mathcal{P}_c$ : We next show how to use the solution of  $\mathcal{P}_k$  to solve  $\mathcal{P}_c$ . First rewrite  $\mathcal{P}_c$  as

$$\begin{aligned} & \text{minimize}_{\{\mathbf{x}_k\}_{k \in \mathcal{N}_a}, \{\mu_k\}_{k \in \mathcal{N}_a}} \sum_{k \in \mathcal{N}_a} \mathcal{P}(\mathbf{p}_k; \mathbf{x}_k) \\ & \text{subject to} \quad \mathbf{1}^T \mathbf{x}_k \leq \mu_k, \quad k \in \mathcal{N}_a \\ & \quad \sum_{k \in \mathcal{N}_a} \mu_k \leq 1 \\ & \quad \mathbf{x}_k \succcurlyeq \mathbf{0}, \quad \mu_k \geq 0, \quad k \in \mathcal{N}_a. \end{aligned}$$

Note that  $\mathbf{x}_k$  contributes only one summand in the objective function, i.e.,  $\mathcal{P}(\mathbf{p}_k; \mathbf{x}_k)$ , and its constraint does not involve  $\mathbf{x}_j$ ,  $j \neq k$  if  $\mu_k$  is determined. Therefore, this optimization problem can be transformed to the following problem:

$$\begin{aligned} & \text{minimize}_{\{\mu_k\}_{k \in \mathcal{N}_a}} \sum_{k \in \mathcal{N}_a} f_k(\mu_k) \\ & \text{subject to} \quad \sum_{k \in \mathcal{N}_a} \mu_k \leq 1 \\ & \quad \mu_k \geq 0, \quad k \in \mathcal{N}_a \end{aligned}$$

where

$$f_k(\mu_k) = \min_{\mathbf{x}_k: \mathbf{1}^T \mathbf{x}_k \leq \mu_k, \mathbf{x}_k \succcurlyeq \mathbf{0}} \mathcal{P}(\mathbf{p}_k; \mathbf{x}_k).$$

Let  $\mathbf{x}_k^*$  denote the optimal solution of  $\mathcal{P}_k$  with constraints  $\mathbf{x}_k \succcurlyeq \mathbf{0}$  and  $\mathbf{1}^T \mathbf{x}_k \leq 1$  and  $\eta_k^* = \mathcal{P}(\mathbf{p}_k; \mathbf{x}_k^*)$ . Note that  $J_e^A(\mathbf{p}_k)$  is linear in  $\mathbf{x}_k$  and  $\mathcal{P}(\mathbf{p}_k; \mathbf{x}_k) = \text{tr}\left\{[J_e^A(\mathbf{p}_k)]^{-1}\right\}$ , and therefore  $f_k(\mu_k)$  is inversely proportional to  $\mu_k$ , which gives  $f_k(\mu_k) = \eta_k^*/\mu_k$ . Hence

$$\sum_{k \in \mathcal{N}_a} f_k(\mu_k) = \sum_{k \in \mathcal{N}_a} \eta_k^*/\mu_k \geq \left( \sum_{k \in \mathcal{N}_a} \sqrt{\eta_k^*} \right)^2 \quad (23)$$

where the equality in (23) is achieved when

$$\mu_k = \frac{\sqrt{\eta_k^*}}{\sum_{k \in \mathcal{N}_a} \sqrt{\eta_k^*}} := \mu_k^*. \quad (24)$$

The solution of  $\mathcal{P}_c$  can be obtained in two steps: first, obtain  $\mathbf{x}_k^*$  and  $\eta_k^*$  by solving  $\mathcal{P}_k$ ; second, obtain the

optimal  $\mu_k^*$  based on (24). The optimal solution of  $\mathcal{P}_c$  is then  $\tilde{\mathbf{x}}_k = \mu_k^* \mathbf{x}_k^*, k \in \mathcal{N}_a$ .

#### D. Robust Node Prioritization

The solutions in Sections III-C and III-B require the knowledge of network parameters such as  $\xi_{kj}$  and  $\phi_{kj}$ . Perfect knowledge of these parameters is usually not available. Since these estimated values are subject to uncertainty, directly using them in the algorithms may yield unreliable solutions. Hence, we will next develop robust methods to cope with the parameter uncertainty. For brevity, we only discuss the distributed setting in this section and the proposed approaches can be adapted to the centralized setting.

Consider the unknown position of agent  $k$  in an area  $\mathcal{A}_k$ , and the goal of robust node prioritization is to minimize the largest iSPEB for agent  $k$  over all of possible positions in such an area. The worst-case iSPEB due to the parameter uncertainty is

$$\mathcal{P}_R(\mathcal{A}_k, \mathbf{x}_k) := \max_{\mathbf{p}_k \in \mathcal{A}_k} \mathcal{P}(\mathbf{p}_k; \mathbf{x}_k).$$

The iSPEB  $\mathcal{P}_R(\mathcal{A}_k, \mathbf{x}_k)$  depends on the shape of  $\mathcal{A}_k$  through the uncertainty of  $\xi_{kj}$  and  $\phi_{kj}$ ,  $j \in \mathcal{N}_b$ . Note that the area  $\mathcal{A}_k$  can be highly irregular and the maximization over  $\mathbf{p}_k$  is intractable. To address this issue, we consider a finite cover of  $\mathcal{A}_k$ , denoted by  $\{\mathcal{A}_k^{(i)}\}_{i \in \mathcal{I}_k}$ , where  $\mathcal{A}_k^{(i)}$  is a circle with center  $\hat{\mathbf{p}}_k^{(i)}$  and radius  $r_i$ , and  $\mathcal{I}_k$  is the index set of these covering circles (see Fig. 5). For the agent's position  $\mathbf{p}_k \in \mathcal{A}_k^{(i)}$ , one can see that the actual network parameters belong to the linear sets

$$\phi_{kj} \in \left[ \hat{\phi}_{kj}^{(i)} - \delta_{kj}^{(i)}, \hat{\phi}_{kj}^{(i)} + \delta_{kj}^{(i)} \right] := \Phi_{kj}^{(i)}$$

$$\xi_{kj} \in \left[ \underline{\xi}_{kj}^{(i)}, \bar{\xi}_{kj}^{(i)} \right] := \Xi_{kj}^{(i)}$$

where  $\delta_{kj}^{(i)} = \arcsin(r_i/\|\hat{\mathbf{p}}_k^{(i)} - \mathbf{p}_j\|)$  and  $\underline{\xi}_{kj}^{(i)}$  and  $\bar{\xi}_{kj}^{(i)}$  are known scalars representing the upper and lower bounds of  $\xi_{kj}$ . Consequently, the worst-case iSPEB can be

bounded by

$$\mathcal{P}_R(\mathcal{A}_k, \mathbf{x}_k) \leq \max_{i \in \mathcal{I}_k} \mathcal{P}_R^{(i)}(\mathcal{A}_k, \mathbf{x}_k)$$

where

$$\mathcal{P}_R^{(i)}(\mathcal{A}_k, \mathbf{x}_k) := \max_{\phi_{kj} \in \Phi_{kj}^{(i)}, \xi_{kj} \in \Xi_{kj}^{(i)}} \mathcal{P}(\mathbf{p}_k; \mathbf{x}_k). \quad (25)$$

We can then formulate the robust node prioritization problem as

$$\begin{aligned} \mathcal{P}_{R,k} : & \underset{\mathbf{x}_k}{\text{minimize}} \quad \max_{i \in \mathcal{I}_k} \mathcal{P}_R^{(i)}(\mathcal{A}_k, \mathbf{x}_k) \\ & \text{subject to} \quad (16) - (17) \end{aligned}$$

which can be equivalently transformed into

$$\begin{aligned} & \underset{\mathbf{x}_k, t}{\text{minimize}} \quad t \\ & \text{subject to} \quad \mathcal{P}_R^{(i)}(\mathcal{A}_k, \mathbf{x}_k) \leq t, \quad \forall i \in \mathcal{I}_k \\ & \quad (16) - (17). \end{aligned} \quad (26)$$

We need to convert  $\mathcal{P}_R^{(i)}(\mathcal{A}_k, \mathbf{x}_k)$  into an expression amenable to efficient optimization. Note that in (25), the maximization over  $\xi_{kj}$  is achieved at  $\xi_{kj} = \underline{\xi}_{kj}^{(i)}$  since the iSPEB  $\mathcal{P}(\mathbf{p}_k; \mathbf{x}_k)$  is a monotonically decreasing function in  $\xi_{kj}$ . However, maximization over  $\phi_{kj}$  is nontrivial. We next provide upper bounds on  $\mathcal{P}_R^{(i)}(\mathcal{A}_k, \mathbf{x}_k)$  that lead to conic programming solutions.

*Proposition 5 ([142])* The maximum iSPEB over the actual angle  $\phi_{kj}$  is upper bounded by

$$\mathcal{P}_R^{(i)}(\mathcal{A}_k, \mathbf{x}_k) \leq \text{tr} \left\{ \left( \sum_{j \in \mathcal{N}_b} x_{kj} \underline{\xi}_{kj}^{(i)} \mathbf{Q}_r(\hat{\phi}_{kj}^{(i)}, \delta_{kj}^{(i)}) \right)^{-1} \right\} \quad (27)$$

provided that  $\sum_{j \in \mathcal{N}_b} x_{kj} \underline{\xi}_{kj}^{(i)} \mathbf{Q}_r(\hat{\phi}_{kj}^{(i)}, \delta_{kj}^{(i)}) \succcurlyeq 0$ , where

$$\mathbf{Q}_r(\hat{\phi}_{kj}^{(i)}, \delta_{kj}^{(i)}) = \mathbf{J}_r(\hat{\phi}_{kj}^{(i)}) - \sin \delta_{kj}^{(i)} \mathbf{I}.$$

Proposition 5 can be proved by noting that if  $\phi_{kj} \in \Phi_{kj}^{(i)}$ ,

$$\mathbf{J}_r(\phi_{kj}) \succcurlyeq \mathbf{Q}_r(\hat{\phi}_{kj}^{(i)}, \delta_{kj}^{(i)})$$

and thus

$$\mathbf{J}_e^A(\mathbf{p}_k) = \sum_{j \in \mathcal{N}_b} x_{kj} \xi_{kj} \mathbf{J}_r(\varphi_{kj}) \succcurlyeq \sum_{j \in \mathcal{N}_b} x_{kj} \underline{\xi}_{kj}^{(i)} \mathbf{Q}_r(\hat{\phi}_{kj}^{(i)}, \delta_{kj}^{(i)}).$$

This together with the monotonicity of  $\text{tr}\{\cdot\}^{-1}\}$  completes the proof. Replacing  $\mathcal{P}_R^{(i)}(\mathcal{A}_k, \mathbf{x}_k)$  in (26) with its upper bound in (27) and adopting a similar transformation as in Proposition 2, we can relax the robust node prioritization problem  $\mathcal{P}_{R,k}$  into the following SDP:

$$\begin{aligned} & \underset{\mathbf{x}, \{\mathbf{M}_i\}_{i \in \mathcal{I}_k}}{\text{minimize}} \quad t \\ & \text{subject to} \quad \text{tr}\{\mathbf{M}_i\} \leq t, \quad i \in \mathcal{I}_k \\ & \quad \left[ \begin{array}{cc} \mathbf{M}_i & \mathbf{I} \\ \mathbf{I} & \sum_{j \in \mathcal{N}_b} x_{kj} \underline{\xi}_{kj}^{(i)} \mathbf{Q}_r(\hat{\phi}_{kj}^{(i)}, \delta_{kj}^{(i)}) \end{array} \right] \succcurlyeq 0, \\ & \quad i \in \mathcal{I}_k \\ & \quad (16) - (17). \end{aligned}$$

The above SDP can cope with small uncertainty in the parameters. However, the performance loss from the relaxation is difficult to quantify since the optimal solution of the robust formulation remains unknown. To address this issue, we look for new bounds of the worst-case iSPEB. We denote  $\mathcal{M} = \{0, 1, \dots, M-1\}$ , where  $M \in \mathbb{Z}$ .

*Proposition 6 ([143])* For any given NPV  $\mathbf{x}_k$  such that  $\mathcal{P}_R^{(i)}(\mathcal{A}_k; \mathbf{x}_k) < \infty$ , if

$$M \geq \frac{\pi}{2} \sqrt{\mathcal{P}_R^{(i)}(\mathcal{A}_k, \mathbf{x}_k) \cdot \mathbf{1}^T \underline{\mathbf{R}}_k^{(i)} \mathbf{x}_k}$$

where  $\underline{\mathbf{R}}_k^{(i)} = \text{diag}\{\underline{\xi}_{k(N_a+1)}^{(i)}, \underline{\xi}_{k(N_a+2)}^{(i)}, \dots, \underline{\xi}_{k(N_a+N_b)}^{(i)}\}$ , then  $\mathcal{P}_R^{(i)}(\mathcal{A}_k, \mathbf{x}_k)$  is bounded below and above, respectively, by

$$\underline{\mathcal{P}}_M^{(i)}(\mathcal{A}_k; \mathbf{x}_k) = \max_{m \in \mathcal{M}} \frac{4 \cdot \mathbf{1}^T \underline{\mathbf{R}}_k^{(i)} \mathbf{x}_k}{(\mathbf{1}^T \underline{\mathbf{R}}_k^{(i)} \mathbf{x}_k)^2 - (\mathbf{h}_{k,m}^{(i)\top} \underline{\mathbf{R}}_k^{(i)} \mathbf{x}_k)^2} \quad (28)$$

$$\overline{\mathcal{P}}_M^{(i)}(\mathcal{A}_k; \mathbf{x}_k) = \max_{m \in \mathcal{M}} \frac{4 \cdot \mathbf{1}^T \underline{\mathbf{R}}_k^{(i)} \mathbf{x}_k}{(\mathbf{1}^T \underline{\mathbf{R}}_k^{(i)} \mathbf{x}_k)^2 - (\mathbf{g}_{k,m}^{(i)\top} \underline{\mathbf{R}}_k^{(i)} \mathbf{x}_k)^2} \quad (29)$$

where  $\mathbf{h}_{k,m}^{(i)}, \mathbf{g}_{k,m}^{(i)} \in \mathbb{R}^{N_b}$ , in which their  $j$ th elements are given by

$$\left[ \mathbf{h}_{k,m}^{(i)} \right]_j = \max_{|\epsilon| \leq 2\underline{\xi}_{kj}^{(i)}} \cos(2\hat{\phi}_{kj}^{(i)} - \vartheta_m + \epsilon)$$

$$\left[ \mathbf{g}_{k,m}^{(i)} \right]_j = \frac{1}{\cos(\pi/M)} \cdot \left[ \mathbf{h}_{k,m}^{(i)} \right]_j$$

with  $\vartheta_m = (2m+1)\pi/M$  for  $m \in \mathcal{M}$ .

Unlike Proposition 5, Proposition 6 provides both lower and upper bounds for  $\mathcal{P}_R^{(i)}(\mathcal{A}_k, \mathbf{x}_k)$ . We can replace  $\mathcal{P}_R^{(i)}(\mathcal{A}_k, \mathbf{x}_k)$  in (26) by the lower and upper bounds (28) and (29), leading to the relaxed problems  $\underline{\mathcal{P}}_{R,k}^M$  and  $\overline{\mathcal{P}}_{R,k}^M$ , respectively.  $\overline{\mathcal{P}}_{R,k}^M$  is more desirable since it guarantees the worst-case performance, whereas the lower bound is useful to bound the performance loss of such relaxation. Note that the relaxed constraint  $\overline{\mathcal{P}}_M^{(i)}(\mathcal{A}_k; \mathbf{x}_k) \leq t$  can be transformed into  $M$  second-order cone forms of  $\mathbf{x}_k$ . Consequently,  $\overline{\mathcal{P}}_{R,k}^M$  can be transformed into an SOCP as follows:

$$\begin{aligned} & \underset{\mathbf{x}_k, y}{\text{minimize}} \quad -y \\ & \text{subject to} \quad \left\| \mathbf{A}_{k,m}^{(i)} \underline{\mathbf{R}}_k^{(i)} \mathbf{x}_k + \mathbf{b}_k \right\| \leq \mathbf{1}^T \underline{\mathbf{R}}_k^{(i)} \mathbf{x}_k - 2y, \\ & \quad \forall m \in \mathcal{M}, \quad \forall i \in \mathcal{I}_k \\ & \quad (16) - (17) \end{aligned}$$

where  $\mathbf{A}_{k,m}^{(i)} = [\mathbf{g}_{k,m}^{(i)} \quad \mathbf{0}]^T$  and  $\mathbf{b}_k = [0 \quad 2y]^T$ .

The next proposition shows that the solution of the relaxed problem  $\overline{\mathcal{P}}_{R,k}^M$  converges to that of the original problem  $\mathcal{P}_{R,k}$  as  $M$  increases.

*Proposition 7 [143]* Let  $\mathbf{x}_k^*$  and  $\overline{\mathbf{x}}_k^M$  be the optimal solutions of  $\mathcal{P}_{R,k}$  and  $\overline{\mathcal{P}}_{R,k}^M$ , respectively. Then

$$\frac{\mathcal{P}_R^{(i)}(\mathcal{A}_k; \overline{\mathbf{x}}_k^M)}{1 + C_M} \leq \mathcal{P}_R^{(i)}(\mathcal{A}_k; \mathbf{x}_k^*) \leq \mathcal{P}_R^{(i)}(\mathcal{A}_k; \overline{\mathbf{x}}_k^M)$$

where

$$C_M = \max_{i \in \mathcal{I}_k} \frac{\sin^2(\pi/M)[B_i(\mathbf{x}_k^*) - 1]}{1 - \sin^2(\pi/M)B_i(\mathbf{x}_k^*)}$$

in which

$$B_i(\mathbf{x}_k) = \frac{1}{4} \mathcal{P}_{\mathbf{R}}^{(i)}(\mathcal{A}_k, \mathbf{x}_k) \cdot \mathbf{1}^T \underline{\mathbf{R}}_k^{(i)} \mathbf{x}_k.$$

Moreover,  $C_M$  converges to zero at the rate of  $O(M^{-2})$ .

Proposition 7 implies that the optimal solution of  $\overline{\mathcal{P}}_{\mathbf{R},k}^M$  can approximate  $\mathcal{P}_{\mathbf{R},k}$  with a small value of  $M$  due to the fast convergence rate  $O(M^{-2})$ . Consequently, the performance of the proposed SOCP algorithms can achieve near-optimal performance with negligible increase in computational complexity.

#### IV. NODE PRIORITIZATION FOR COOPERATIVE LOCALIZATION

This section presents the node prioritization strategies for cooperative networks in static scenarios. In this section, we consider only the non-robust formulation for brevity. The techniques developed in Section III-D can be adopted to address the robust formulation as shown in [84] and [85].

##### A. Problem Formulation

Similarly to Section III-A, we rewrite  $\lambda_{kj}$  as in (13). In cooperative networks, agents make measurements only with anchors and agents, and therefore, the NPV for node  $k$   $\mathbf{x}_k \in \mathbb{R}^{N_a+N_b-1}$  can be written as

$$\mathbf{x}_k = [x_{k1} \ x_{k2} \ \dots \ x_{k(k-1)} \ x_{k(k+1)} \ \dots \ x_{k(N_b+N_a)}]^T$$

and the NPV for all the agents  $\mathbf{x}$  can be written as

$$\mathbf{x} = [x_1^T \ x_2^T \ \dots \ x_{N_a}^T]^T.$$

For the centralized and distributed settings, the node prioritization problem can then be written, respectively, as

$$\begin{aligned} \mathcal{P}_{C-c} : & \underset{\mathbf{x}}{\text{minimize}} \quad \mathcal{P}(\mathbf{p}; \mathbf{x}) \\ & \text{subject to} \quad (14) - (15) \end{aligned}$$

and

$$\begin{aligned} \mathcal{P}_{C,k} : & \underset{\mathbf{x}_k}{\text{minimize}} \quad \mathcal{P}(\mathbf{p}_k; \mathbf{x}_k) \\ & \text{subject to} \quad (16) - (17) \end{aligned}$$

where  $\mathcal{P}_{C-c}$  denotes the cooperative centralized node prioritization problem and  $\mathcal{P}_{C,k}$  denotes the cooperative distributed node prioritization problem for agent  $k$ . Unlike the node prioritization in non-cooperative networks, the performance metrics  $\mathcal{P}(\mathbf{p}; \mathbf{x})$  and  $\mathcal{P}(\mathbf{p}_k; \mathbf{x}_k)$  incorporate range information from agents in addition to that from anchors. As we will see in the following sections, such additional information makes the node prioritization problem more complicated.

##### B. Centralized Setting

We next provide solutions to the cooperative node prioritization problem  $\mathcal{P}_{C-c}$  in the centralized setting.

*Proposition 8:* The nSPEB  $\mathcal{P}(\mathbf{p}; \mathbf{x})$  in cooperative networks is convex in  $\mathbf{x} \succcurlyeq \mathbf{0}$ .

Proposition 8 can be proved in a similar way as Proposition 1. As the result of convexity, the optimal solution for  $\mathcal{P}_{C-c}$  can be obtained numerically by standard convex optimization algorithms [146].

We next show that  $\mathcal{P}_{C-c}$  can be converted to an SDP. Note that

$$\mathbf{J}_e(\mathbf{p}; \mathbf{x}) = \sum_{k \in \mathcal{N}_a} \sum_{j \in \mathcal{N}_a \cup \mathcal{N}_b \setminus \{k\}} x_{kj} \xi_{kj} \mathbf{V}_{kj}$$

where

$$\mathbf{V}_{kj} = \begin{cases} \mathbf{E}_{k,k}^{N_a} \otimes \mathbf{J}_r(\phi_{kj}), & j \in \mathcal{N}_b \\ (\mathbf{E}_{k,k}^{N_a} + \mathbf{E}_{j,j}^{N_a} - \mathbf{E}_{k,j}^{N_a} - \mathbf{E}_{j,k}^{N_a}) \otimes \mathbf{J}_r(\phi_{kj}), & j \in \mathcal{N}_a. \end{cases}$$

Since  $\mathbf{J}_e(\mathbf{p}; \mathbf{x})$  is linear in  $\mathbf{x}$ , we can use the same technique as used in Section III-B to prove that  $\mathcal{P}_{C-c}$  is equivalent to the SDP

$$\begin{aligned} & \underset{\mathbf{x}, M}{\text{minimize}} \quad \sum_{k \in \mathcal{N}_a} \text{tr}\{M\} \\ & \text{subject to} \quad \left[ \begin{array}{c|c} M & \mathbf{I} \\ \mathbf{I} & \sum_{k \in \mathcal{N}_a} \sum_{j \in \mathcal{N}_a \cup \mathcal{N}_b \setminus \{k\}} x_{kj} \xi_{kj} \mathbf{V}_{kj} \end{array} \right] \succcurlyeq 0 \\ & \quad (14) - (15). \end{aligned}$$

Unfortunately, the techniques of transforming node prioritization problems further into SOCPs in non-cooperative networks cannot be applied here because the off-diagonal blocks  $-C_{j,k}$  in (4) make the expression of inverted EFIM  $\mathbf{J}_e^{-1}(\mathbf{p}; \mathbf{x})$  complicated [152], and thus it cannot be written as the sum of fractional forms as in (19).

##### C. Distributed Setting

The optimal solutions of the problem  $\mathcal{P}_{C,k}$ 's cannot be obtained in a distributed manner because the iSPEB  $\mathcal{P}(\mathbf{p}_k; \mathbf{x}_k) = \text{tr}\{\mathbf{J}_e^{-1}(\mathbf{p}; \mathbf{x})\}_{p_k}\}$  depends on the angles and qualities of all the inter-node measurements of the entire network as well as the node prioritization decisions (i.e., the NPV) of other agents. To address this issue, we derive an upper bound for  $\mathcal{P}(\mathbf{p}_k; \mathbf{x}_k)$  that is amenable for distributed implementation.

Consider an auxiliary matrix  $\mathbf{J}_e^L(\mathbf{p}; \mathbf{x})$  representing the measurements between agents and anchors as well as measurements made from agent 1 to other agents

$$\mathbf{J}_e^L(\mathbf{p}; \mathbf{x}) = \sum_{k \in \mathcal{N}_a} \sum_{j \in \mathcal{N}_b} x_{kj} \xi_{kj} \mathbf{V}_{kj} + \sum_{j \in \mathcal{N}_a \setminus \{1\}} x_{1j} \xi_{1j} \mathbf{V}_{1j}. \quad (30)$$

Note that

$$\mathbf{J}_e(\mathbf{p}; \mathbf{x}) - \mathbf{J}_e^L(\mathbf{p}; \mathbf{x}) = \sum_{k \in \mathcal{N}_a \setminus \{1\}} \sum_{j \in \mathcal{N}_a \setminus \{k\}} x_{kj} \xi_{kj} \mathbf{V}_{kj} \succcurlyeq 0$$

where the inequality is due to the fact that each summand is positive semidefinite. Based on  $\mathbf{J}_e^L(\mathbf{p}; \mathbf{x})$ , a lower bound for the EFIM of agent 1 is shown to be

$$\begin{aligned} & \left\{ \left[ (\mathbf{J}_e^L(\mathbf{p}; \mathbf{x}))^{-1} \right]_{\mathbf{p}_1} \right\}^{-1} \\ &= \mathbf{J}_e^A(\mathbf{p}_1) + \sum_{j \in \mathcal{N}_a \setminus \{1\}} \frac{x_{1j}\xi_{1j}\mathbf{J}_r(\phi_{1j})}{1 + x_{1j}\xi_{1j}\Delta_{1j}} := \mathbf{J}_e^L(\mathbf{p}_1; \mathbf{x}_1) \end{aligned}$$

where

$$\Delta_{1j} = \text{tr}\{\mathbf{J}_r(\phi_{1j})(\mathbf{J}_e^A(\mathbf{p}_j))^{-1}\} \quad (31)$$

represents the position uncertainty of agent  $j$  along the direction between agent 1 and agent  $j$  [85]. Consequently

$$\begin{aligned} \mathcal{P}(\mathbf{p}_1; \mathbf{x}_1) &= \text{tr}\left\{ \left[ (\mathbf{J}_e(\mathbf{p}; \mathbf{x}))^{-1} \right]_{\mathbf{p}_1} \right\} \\ &\leq \text{tr}\left\{ \left[ (\mathbf{J}_e^L(\mathbf{p}; \mathbf{x}))^{-1} \right]_{\mathbf{p}_1} \right\} \\ &= \text{tr}\left\{ (\mathbf{J}_e^L(\mathbf{p}_1; \mathbf{x}_1))^{-1} \right\}. \end{aligned} \quad (32)$$

Similarly, we can obtain  $\mathbf{J}_e^L(\mathbf{p}_k; \mathbf{x}_k)$  as the lower bound for the EFIM of agent  $k$  in cooperative networks. Note that if  $\Delta_{kj}$  is available to agent  $k$ , then  $\mathbf{J}_e^L(\mathbf{p}_k; \mathbf{x}_k)$  depends only on the local network parameters and on the node prioritization decision of agent  $k$ , facilitating the design of distributed node prioritization strategies.

Using the upper bound in (32) as the optimization objective for agent 1 requires obtaining  $\Delta_{1j}$ . Obtaining  $\Delta_{1j}$  in turn requires the node prioritization decision of agent  $j$ . To circumvent this difficulty, the original problem can be transformed into a sequential two-phase optimization problem. Specifically, each agent  $k$  produces its node prioritization decision through the following two phases:

- infrastructure phase—produce the node prioritization decision to allocate resources for the measurements between agent  $k$  and the anchors;
- cooperation phase—produce the node prioritization decision to allocate resources for the measurements between agent  $k$  and its neighboring agents, which have obtained their position knowledge in the infrastructure phase.

Note that in the infrastructure phase, each agent  $k$  minimizes  $\text{tr}\{(\mathbf{J}_e^A(\mathbf{p}_k))^{-1}\}$  without requiring the node prioritization decisions of other agents; and in the cooperation phase, each agent  $k$  minimizes  $\text{tr}\{(\mathbf{J}_e^L(\mathbf{p}_k; \mathbf{x}_k))^{-1}\}$  with  $\Delta_{kj}$  based on  $\mathbf{J}_e^A(\mathbf{p}_j)$  ( $j \in \mathcal{N}_a \setminus \{k\}$ ) from the infrastructure phase.

In the infrastructure phase, each agent  $k$  minimizes  $\text{tr}\{(\mathbf{J}_e^A(\mathbf{p}_k; \mathbf{x}_k))^{-1}\}$  with respect to NPV  $x_k$  with  $x_{kj} = 0$  for all  $j \in \mathcal{N}_a$ , i.e.,

$$\mathcal{P}_{C,k}^{\text{Anc}} : \underset{\mathbf{x}_k}{\text{minimize}} \quad \text{tr}\{(\mathbf{J}_e^A(\mathbf{p}_k; \mathbf{x}_k))^{-1}\}$$

subject to  $x_{kj} = 0, \forall j \in \mathcal{N}_a$

$$(16) - (17).$$

Note that  $\mathcal{P}_{C,k}^{\text{Anc}}$  is equivalent to  $\mathcal{P}_k$  and can be solved via the techniques in Section III.

Using the solution of  $\mathcal{P}_{C,k}^{\text{Anc}}$  in the infrastructure phase, each agent  $j$  broadcasts  $\mathbf{J}_e^A(\mathbf{p}_j)$  to its neighboring agents and agent  $k$  computes  $\Delta_{kj}$ . The node prioritization problem for agent  $k$  in the cooperation phase is then formulated using the upper bound (32) as relaxed performance metrics

$$\mathcal{P}_{C,k}^{\text{Agt}} : \underset{\mathbf{x}_k}{\text{minimize}} \quad \text{tr}\{(\mathbf{J}_e^L(\mathbf{p}_k; \mathbf{x}_k))^{-1}\}$$

subject to (16) – (17).

We next show that  $\mathcal{P}_{C,k}^{\text{Agt}}$  can be converted to an SOCP. We rewrite  $\mathbf{J}_e^L(\mathbf{p}_k; \mathbf{x}_k)$  as

$$\mathbf{J}_e^L(\mathbf{p}_k; \mathbf{x}_k) = \mathbf{J}_e^A(\mathbf{p}_k) + \sum_{j \in \mathcal{N}_a \setminus \{k\}} \xi_{kj} q_{kj} \mathbf{J}_r(\phi_{kj})$$

where

$$q_{kj} = \frac{x_{kj}}{1 + x_{kj}\xi_{kj}\Delta_{kj}}.$$

Since  $\text{tr}\{(\mathbf{J}_e^L(\mathbf{p}_k; \mathbf{x}_k))^{-1}\}$  is an increasing function of  $q_{kj}$ ,  $\mathcal{P}_{C,k}^{\text{Agt}}$  is equivalent to the following program:

$$\begin{aligned} & \underset{\mathbf{x}_k, \{q_{kj}\}_{j \in \mathcal{N}_a \setminus \{k\}}}{\text{minimize}} \quad \text{tr}\left\{ \left( \mathbf{J}_e^A(\mathbf{p}_k) + \sum_{j \in \mathcal{N}_a \setminus \{1\}} \xi_{kj} q_{kj} \mathbf{J}_r(\phi_{kj}) \right)^{-1} \right\} \\ & \text{subject to} \quad 0 \leq q_{kj}, \forall j \in \mathcal{N}_a \setminus \{k\} \\ & \quad q_{kj} \leq \frac{x_{kj}}{1 + x_{kj}\xi_{kj}\Delta_{kj}}, \forall j \in \mathcal{N}_a \setminus \{k\} \quad (33) \\ & \quad (16) - (17). \end{aligned}$$

The objective function has a similar structure to (19). Therefore, it can be shown that we can transform the objective function to a linear objective function and an SOCP constraint by following steps similar to those in Section III-B [85]. Consequently,  $\mathcal{P}_{C,k}^{\text{Agt}}$  can be transformed into

$$\begin{aligned} & \underset{\mathbf{x}_k, \{q_{kj}\}_{j \in \mathcal{N}_a \setminus \{k\}}}{\text{minimize}} \quad -t \\ & \text{subject to} \quad 0 \leq q_{kj}, \quad \forall j \in \mathcal{N}_a \setminus \{k\} \\ & \quad \left\| \begin{bmatrix} \sqrt{2} & 1 - q_{kj}\xi_{kj}\Delta_{kj} & 1 + q_{kj}\xi_{kj}\Delta_{kj} \end{bmatrix}^T \right\| \\ & \quad \leq 2 + (x_{kj} - q_{kj})\xi_{kj}\Delta_{kj}, \quad \forall j \in \mathcal{N}_a \setminus \{k\} \\ & \quad \left\| \tilde{\mathbf{A}}_k \tilde{\mathbf{R}}_k \mathbf{q}_k + \tilde{\mathbf{b}}_k \right\| \leq \mathbf{1}^T \tilde{\mathbf{R}}_k \mathbf{q}_k - 2t \\ & \quad (16) - (17) \end{aligned}$$

where  $\tilde{\mathbf{A}}_k = [\tilde{\mathbf{c}}_k \ \tilde{\mathbf{s}}_k \ \mathbf{0}]^T$  and  $\tilde{\mathbf{b}}_k = [0 \ 0 \ 2t]^T$ , in which

$$\begin{aligned} \mathbf{q}_k &= [q_{k(N_a+1)} \ q_{k(N_a+2)} \ \dots \ q_{k(k-1)} \ q_{k(k+1)} \ \dots \\ &\quad q_{k(N_a+N_b)} \ 1 \ 1]^T \\ \tilde{\mathbf{R}}_k &= \text{diag}\{\xi_{k(N_a+1)}, \xi_{k(N_a+2)}, \dots, \xi_{k(k-1)}, \xi_{k(k+1)}, \dots, \\ &\quad \xi_{k(N_a+N_b)}, \nu_k^{(1)}, \nu_k^{(2)}\} \\ \tilde{\mathbf{c}}_k &= [\cos 2\phi_{k(N_a+1)} \ \cos 2\phi_{k(N_a+2)} \ \dots \ \cos 2\phi_{k(k-1)} \\ &\quad \cos 2\phi_{k(k+1)} \ \dots \ \cos 2\phi_{k(N_a+N_b)} \ \cos 2\theta_k \ - \cos 2\theta_k]^T \end{aligned}$$

$$\tilde{\mathbf{s}}_k = [\sin 2\phi_{k(N_a+1)} \ \sin 2\phi_{k(N_a+2)} \ \dots \ \sin 2\phi_{k(k-1)} \\ \sin 2\phi_{k(k+1)} \dots \sin 2\phi_{k(N_a+N_b)} \ \sin 2\theta_k \ -\sin 2\theta_k]^T$$

with  $\nu_k^{(1)}, \nu_k^{(2)} \geq 0$  being the eigenvalues of  $\mathbf{J}_e^A(\mathbf{p}_k)$  and  $\mathbf{u}(\theta_k)$  and  $\mathbf{u}(\theta_k + \pi/2)$  being the corresponding eigenvectors, i.e.,  $\mathbf{J}_e^A(\mathbf{p}_k) = \nu_k^{(1)} \mathbf{J}_r(\theta_k) + \nu_k^{(2)} \mathbf{J}_r(\theta_k + \pi/2)$ .

The detailed distributed cooperative node prioritization strategy is described in Algorithm 1. In Algorithm 1, each agent requires only local network parameters and little information from its neighbors, which makes the algorithm amenable for distributed implementation.

---

**Algorithm 1:** Distributed Cooperative Node Prioritization [84]

---

- Input:**  $\phi_{kj}$  and  $\xi_{kj}$ ,  $k \in \mathcal{N}_a$ ,  $j \in \mathcal{N}_b \cup \mathcal{N}_a \setminus \{k\}$   
**Output:**  $\mathbf{x}_k$ ,  $k \in \mathcal{N}_a$
- 1: For  $k \in \mathcal{N}_a$ , agent  $k$  solves  $\mathcal{P}_{C,k}^{\text{Anc}}$  in the infrastructure phase;
  - 2: For  $k \in \mathcal{N}_a$ , agent  $k$  broadcasts  $\mathbf{J}_e^A(\mathbf{p}_k)$  to its neighboring agents;
  - 3: For  $k \in \mathcal{N}_a$ , agent  $k$  solves  $\mathcal{P}_{C,k}^{\text{Agt}}$  in the cooperation phase;
  - 4: For  $k \in \mathcal{N}_a$ , agent  $k$  outputs  $\mathbf{x}_k$ ;
- 

## V. NODE ACTIVATION

This section presents the node activation strategies for cooperative dynamic networks. For the sake of collision avoidance in implementation, only one node is activated at each time slot to make inter-node measurements, and the node then allocates its resource for performing measurements with different neighbors based on the node prioritization strategies discussed in Section IV. We will also consider a simpler case for which the node merely selects one neighbor for the inter-node measurement.

### A. Activation Formulation

In the dynamic scenario, recall the EFIM  $\mathbf{J}_e(\mathbf{p}^{(n)})$  given in (10) for all the node positions at time  $t_n$ . For ease of discussion, we define the error matrix at time  $t_n$  as  $\mathbf{Q}^{(n)} = (\mathbf{J}_e(\mathbf{p}^{(n)}))^{-1}$ , and  $\{\mathbf{Q}^{(n)}\}_{n \geq 1}$  denotes an evolution of the error matrix over time.

With node activation, at each instant  $t_n$ , one node  $k_n$  is selected to make inter-node measurements with its neighbors and a fraction of resources is used for each neighbor through for instance spectrum sharing. In this case, the error evolution  $\{\mathbf{Q}^{(n)}\}_{n \geq 1}$  can be written as

$$\mathbf{Q}^{(n+1)} = \mathbf{Q}^{(n)} - \boldsymbol{\Gamma}_{k_n}^{(n)} + \mathbf{T}^{(n)} \quad (34)$$

where  $\boldsymbol{\Gamma}_{k_n}^{(n)}$  is the error reduction matrix corresponding to the inter-node measurements between nodes  $k_n$  and its neighbors, and  $\mathbf{T}^{(n)}$  is the error increase matrix given in (8) due to the uncertainty in the intra-node measurements. Moreover, let  $\mathcal{N}_k^{(n)}$  be the set of neighbors of node  $k$

at time  $t_n$ , and then the error reduction matrix can be derived as

$$\boldsymbol{\Gamma}_k^{(n)} = \mathbf{Q}^{(n)} - \left( (\mathbf{Q}^{(n)})^{-1} + \sum_{j \in \mathcal{N}_k^{(n)}} \lambda_{kj}^{(n)} \mathbf{a}_{kj}^{(n)} \mathbf{a}_{kj}^{(n)T} \right)^{-1} \quad (35)$$

where  $\lambda_{kj}^{(n)}$  is the RII of the inter-node measurement between node  $k$  and node  $j$  [72], and

$$\mathbf{a}_{kj}^{(n)} = \begin{cases} \mathbf{e}_k \otimes \mathbf{u}(\phi_{kj}^{(n)}), & k \in \mathcal{N}_a, j \in \mathcal{N}_b \\ (\mathbf{e}_k - \mathbf{e}_j) \otimes \mathbf{u}(\phi_{kj}^{(n)}), & k, j \in \mathcal{N}_a. \end{cases} \quad (36)$$

*Remark 4:* The evolution of the error matrix (34) implies that a high accuracy in the inter-node measurements (i.e., large  $\lambda_{kj}^{(n)}$ ) or intra-node measurements (i.e., small  $\sigma_m^2$ ) translates to large  $\boldsymbol{\Gamma}_k^{(n)}$  or small  $\mathbf{T}^{(n)}$ , both leading to high localization accuracy (i.e., small  $\mathbf{Q}^{(n+1)}$ ). Moreover, the values of RII  $\lambda_{kj}^{(n)}$ 's for  $j \in \mathcal{N}_k^{(n)}$  are subject to the total resource constraint, and node prioritization can be applied to optimize the resource allocation.

The error evolution in (34) depends on the activation strategy via the selected node  $k_n$  together with the node prioritization (or simply neighbor selection) strategy as well as the error increase due to the nodes' mobility at each instant. Comparing this with data networks, we can view  $\mathbf{Q}^{(n)}$ ,  $\boldsymbol{\Gamma}^{(n)}$ , and  $\mathbf{T}^{(n)}$  as the *queue length*, *service*, and the *packet arrival*, respectively. In contrast to queueing dynamics where the service rates are commonly independent of the queue lengths and network geometry, the error reduction matrices in NLN are nonlinear functions of the *queue length*  $\mathbf{Q}^{(n)}$  and of the relative node positions, which are characterized by  $\phi_{kj}^{(n)}$ 's and  $\lambda_{kj}^{(n)}$ 's.

Node activation strategies for NLN are typically designed to coordinate the inter-node measurements, with a goal of minimizing a performance metric such as the nSPEB  $\text{tr}\{\mathbf{Q}^{(n)}\}$  at each time  $t_n$ , or the time-averaged nSPEB over the first  $n$  instants, given by

$$q_n := \frac{1}{n} \sum_{n'=1}^n \text{tr}\{\mathbf{Q}^{(n')}\}. \quad (37)$$

We next adopt the former as the performance metric for designing node activation strategies.

**Opportunistic activation:** The opportunistic activation algorithm is one-step optimal and it can be described as follows: it selects the best agent for inter-node measurements with its neighbors, i.e.,

$$k_n = \arg \max_{k \in \mathcal{N}_a} \text{tr}\{\boldsymbol{\Gamma}_k^{(n)}\} \quad (38)$$

where for a given selection of agent  $k$ , the values of RII  $\lambda_{kj}^{(n)}$ 's for  $j \in \mathcal{N}_k^{(n)}$  are determined by the node prioritization problem  $\mathcal{P}_k$  in Section III-A.

We introduce a special case of the opportunistic node activation strategy, in which only a single neighbor  $j_n$  of node  $k_n$  is selected for an inter-node measurement. In this case, the entire resources are dedicated for the

link  $(k_n, j_n)$  and  $\lambda_{k_n, j}^{(n)} = 0$  for all  $j \in \mathcal{N}_{k_n}^{(n)} \setminus \{j_n\}$ . Consequently, the error reduction matrix in (35) can be simplified as

$$\boldsymbol{\Gamma}_k^{(n)}|_{(k,j)} = \frac{\mathbf{Q}^{(n)} \mathbf{a}_{kj}^{(n)} \mathbf{a}_{kj}^{(n)\top} \mathbf{Q}^{(n)}}{\lambda_{kj}^{(n)-1} + \mathbf{a}_{kj}^{(n)\top} \mathbf{Q}^{(n)} \mathbf{a}_{kj}^{(n)}}$$

where  $|_{(k,j)}$  denotes the selection of a single link  $(k, j)$  for the inter-node measurement. In this case, the opportunistic activation in (38) reduces to single-neighbor selection, which selects the optimal pair for an inter-node measurement in terms of the error reduction, i.e.,

$$(k_n, j_n) = \arg \max_{(k,j) \in \mathcal{M}^{(n)}} \text{tr}\{\boldsymbol{\Gamma}_k^{(n)}|_{(k,j)}\} \quad (39)$$

where  $\mathcal{M}^{(n)}$  denotes the set of all possible measurement pairs at time  $t_n$ .

The activation strategy with single-neighbor selection will yield a suboptimal performance compared to that with node prioritization, as the latter has more freedom for resource utilization. Nevertheless, single-neighbor selection highlights the simplicity in implementation as it eliminates the calculation of node prioritization in the process.

Note that the opportunistic activation algorithm requires perfect knowledge of network parameters such as angles and qualities of all the inter-node measurements as well as a centralized controller. First, such perfect knowledge is not available in practice and the activation algorithm can only use estimates of these parameters, leading to suboptimal performance. Second, the centralized controller would need to collect all the information about network parameters incurring high communication overhead, which is inefficient in medium- to large-scale networks. To reduce the communication overhead, we introduce an alternative algorithm called probabilistic activation.

**Probabilistic activation:** The probabilistic activation algorithm selects an agent randomly according to a certain (possibly optimized) access probability given by  $\{p_1^{(n)}, p_2^{(n)}, \dots, p_{N_a}^{(n)}\}$  with  $p_i^{(n)} \geq 0$  for all  $i \in \mathcal{N}_a$  and the normalization constraint  $\sum_{i=1}^{N_a} p_i^{(n)} = 1$ .<sup>7</sup> The selected node then performs inter-node measurements using resources allocated according to the solution of node prioritization problems or according to the single-neighbor selection in (39). Thus, the communication overhead among the agents is much lower than in opportunistic activation, and therefore such an activation algorithm is better suited for distributed implementation. In Section V-B, we will discuss how to design  $p_i^{(n)}$ .

## B. Activation in Distributed Networks

We now further analyze the performance of the opportunistic and probabilistic activation in distributed settings. In these settings, the exact error evolution  $\{\mathbf{Q}^{(n)}\}$  in (34)

<sup>7</sup>Note that (uniformly) random activation is a special case of probabilistic activation with  $p_i^{(n)} = 1/N_a$  for all  $i \in \mathcal{N}_a$ .

is not available to the agents, and each agent can only keep a record of its own error evolution, as an *approximation* for the error evolution of the entire network. Therefore, in the distributed setting, the error evolution of agent  $k \in \mathcal{N}_a$  is given by

$$\tilde{\mathbf{Q}}_k^{(n+1)} = \tilde{\mathbf{Q}}_k^{(n)} - \tilde{\boldsymbol{\Gamma}}_k^{(n)} + \mathbf{T}_k^{(n)} \quad (40)$$

with  $\tilde{\mathbf{Q}}_k^{(1)} = [\mathbf{Q}^{(1)}]_k$  denoting the submatrix of  $\mathbf{Q}^{(1)}$  corresponding to agent  $k$ . In the above equation

$$\tilde{\boldsymbol{\Gamma}}_k^{(n)} = \begin{cases} \tilde{\mathbf{Q}}_k^{(n)} - \left( (\tilde{\mathbf{Q}}_k^{(n)})^{-1} + \sum_{j \in \mathcal{N}_k^{(n)}} \zeta_{kj}^{(n)} \lambda_{kj}^{(n)} \mathbf{J}_r(\phi_{kj}^{(n)}) \right)^{-1}, & k \text{ is activated} \\ \tilde{\mathbf{Q}}_k^{(n)} - ((\tilde{\mathbf{Q}}_k^{(n)})^{-1} + \zeta_{kj}^{(n)} \lambda_{kj}^{(n)} \mathbf{J}_r(\phi_{kj}^{(n)}))^{-1}, & j \in \mathcal{N}_k^{(n)} \text{ is activated} \\ 0, & \text{otherwise} \end{cases} \quad (41)$$

in which  $\zeta_{kj}^{(n)} \in (0, 1]$  is a coefficient determined by  $\tilde{\mathbf{Q}}_j^{(n)}$  and  $\lambda_{kj}^{(n)}$ 's [73]. This coefficient characterizes the effectiveness of RII due to the position uncertainty associated with each agent, and as a special case  $\zeta_{kj}^{(n)} = 1$  if node  $j$  is an anchor.

The opportunistic activation then selects the best agent according to (38), where for each potential agent  $k$  the calculation of  $\tilde{\boldsymbol{\Gamma}}_k^{(n)}$  uses the estimated value of the parameters and the RII  $\lambda_{kj}^{(n)}$ 's as determined by the node prioritization strategy. On the other hand, the probabilistic activation selects the node according to the designated access probability.

For the neighbor selection case, i.e., where only pair  $(k, j)$  is selected for measurements, the error reduction matrix reduces to

$$\tilde{\boldsymbol{\Gamma}}_k^{(n)}|_{(k,j)} = \begin{cases} \frac{\tilde{\mathbf{Q}}_k^{(n)} \mathbf{u}(\phi_{kj}^{(n)}) \mathbf{u}^T(\phi_{kj}^{(n)}) \tilde{\mathbf{Q}}_k^{(n)}}{\lambda_{kj}^{(n)-1} + \mathbf{u}^T(\phi_{kj}^{(n)}) \tilde{\mathbf{Q}}_k^{(n)} \mathbf{u}(\phi_{kj}^{(n)})}, & k \text{ is activated with } j \in \mathcal{N}_b \\ \frac{\tilde{\mathbf{Q}}_k^{(n)} \mathbf{u}(\phi_{kj}^{(n)}) \mathbf{u}^T(\phi_{kj}^{(n)}) \tilde{\mathbf{Q}}_k^{(n)}}{\lambda_{kj}^{(n)-1} + \mathbf{u}^T(\phi_{kj}^{(n)}) (\tilde{\mathbf{Q}}_k^{(n)} + \tilde{\mathbf{Q}}_j^{(n)}) \mathbf{u}(\phi_{kj}^{(n)})}, & k \text{ is activated with } j \in \mathcal{N}_a \setminus \{k\} \\ 0, & k \text{ is not activated.} \end{cases} \quad (42)$$

**1) Performance Analysis:** Based on the error evolution in distributed networks, we next analyze the performance of opportunistic and probabilistic activation. In particular, we consider that the anchors' positions follow a homogeneous Poisson point process (PPP) with density  $\mu_b$  [153]–[157], and let  $p_b = 1 - \exp(-\pi \mu_b R^2)$  be the probability that there exists at least one anchor in the neighborhood of a given agent, where  $R$  is the communication radius of an agent. The performance metric to be analyzed is  $q_n$ , i.e., the time-averaged nSPEB over the first  $n$  instants.

*Proposition 9 ([96])* Under mild conditions, for both opportunistic and probabilistic node activation strategies, the time-averaged nSPEB is bounded from above as

$$q_n \leq \frac{N_a}{p_b} \left( \rho_n + \sqrt{\rho_n^2 + 4 p_b \lambda_{\min}^{-1} \rho_n} \right)$$

where  $\lambda_{\min}$  is the lower bound for the RII of the inter-node measurements between two nodes in the communication range, and

$$\rho_n = 2 N_a \sigma_m^2 + \frac{1}{n} \mathbb{E}\{\text{tr}\{\mathbf{Q}^{(1)}\}\}.$$

Moreover, as  $n \rightarrow \infty$ , the upper bound can be simplified as

$$\limsup_{n \rightarrow \infty} q_n \leq \frac{2 N_a^2}{p_b} \left( \sigma_m^2 + \sigma_m \sqrt{\sigma_m^2 + \frac{2}{N_a} p_b \lambda_{\min}^{-1}} \right).$$

The proposition provides important insights into the activation problem in view of the upper bound. First, the upper bound increases with the intra-node measurement error  $\sigma_m$ , and decreases with the RII  $\lambda_{\min}$ . This agrees with our intuition that good quality of intra-node and inter-node measurements decreases the nSPEB. Second, the upper bound decreases with increasing  $p_b$ , or equivalently with  $\mu_b$ , that is, the nSPEB decreases with increasing anchor density. This also agrees with our intuition that agents are more likely to access to anchors, which have perfect position knowledge. Third, the time-averaged nSPEB is upper bounded as  $O(N_a^2)$ . In fact, when the maximum number of neighbors for each agent is fixed, it can also be shown that the lower bound for the time-averaged nSPEB is also  $\Omega(N_a^2)$  [96], which leads to the conclusion that  $q_n$  is on the order of  $\Theta(N_a^2)$ . Finally, we comment that the claims from Proposition 9 hold for node activation with or without the node prioritization process.

*2) Probabilistic Activation Design:* We next design the access probability  $\{p_1^{(n)}, p_2^{(n)}, \dots, p_{N_a}^{(n)}\}$  for probabilistic activation using the upper bound for the time-averaged nSPEB  $q_n$ . In the distributed setting, denote the time-averaged iSPEB for agent  $k$  as

$$q_{n,k} := \frac{1}{n} \sum_{n'=1}^n \text{tr}\{\tilde{\mathbf{Q}}_k^{(n')}\}. \quad (43)$$

Then, with the given access probabilities, the upper bound for agent  $k$ 's time-averaged iSPEB can be obtained as

$$\begin{aligned} q_{n,k} &\leq \frac{1}{p_b \tilde{p}_k} \left( \rho_{n,k} + \sqrt{\rho_{n,k}^2 + 4 p_b \lambda_{\min}^{-1} \rho_{n,k} \tilde{p}_k} \right) \\ &=: g_k(\{p_i^{(n)}\}_{i \in \mathcal{N}_a}) \end{aligned} \quad (44)$$

where  $\tilde{p}_k := p_k^{(n)} \prod_{j \in \mathcal{N}_a \setminus \{k\}} (1 - p_j^{(n)})$  and  $\rho_{n,k} := \sigma_m^2 + \text{tr}\{\mathbf{Q}_k^{(1)}\}/n$ . As a consequence, the nSPEB can be upper bounded as

$$q_n \leq \sum_{k \in \mathcal{N}_a} q_{n,k} = \sum_{k \in \mathcal{N}_a} g_k(\{p_i^{(n)}\}_{i \in \mathcal{N}_a}). \quad (45)$$

The right-hand side of (45) is in a closed form and can be used as the objective function for optimizing the access

probability as

$$\begin{aligned} \mathcal{P}^S : \quad &\underset{\{p_i^{(n)}\}_{i \in \mathcal{N}_a}}{\text{minimize}} \quad \sum_{k \in \mathcal{N}_a} g_k(\{p_i^{(n)}\}_{i \in \mathcal{N}_a}) \\ &\text{subject to} \quad \sum_{i \in \mathcal{N}_a} p_i^{(n)} = 1 \\ &\quad p_i^{(n)} \geq 0, \quad \forall i \in \mathcal{N}_a. \end{aligned} \quad (46)$$

An optimal solution to the above optimization problem can be found by generalized geometric programming, which can be efficiently solved via interior point methods.

The probabilistic activation algorithm can be described in Algorithm 2. Agents take turns to be the designated agent, which optimizes the access probabilities at the beginning of each instant. In particular, the designated agent collects  $\rho_{n,k}$  from each of its neighboring agents; after the designated agent obtains the solution of the access probabilities, it broadcasts the probabilities to the other agents. All the agents then access the channels according to  $\{p_i^{(n)*}\}_{i \in \mathcal{N}_a}$  for the next  $N$  time slots. The parameter  $N$  induces a trade-off between the performance and complexity, where a larger  $N$  requires less communication and computation overheads at the expense of performance loss due to outdated input of the problem  $\mathcal{P}^S$ .

---

#### Algorithm 2: Distributed Probabilistic Node Activation

**Input:**  $\phi_{kj}^{(n)}$  and  $\lambda_{kj}^{(n)}$ ,  $k \in \mathcal{N}_a$ ,  $j \in \mathcal{N}_b \cup \mathcal{N}_a \setminus \{k\}$

**Output:** Optimal access probability  $\{p_i^{(n)*}\}_{i \in \mathcal{N}_a}$

- 1: Let agent  $k^*$  be the designated agent (which rotates among the  $N_a$  agents);
  - 2: At the beginning of time  $t_n$ , each agent  $k$  calculates  $\rho_{n,k}$  for  $k \in \mathcal{N}_a$ , and then agent  $k^*$  collects  $\rho_{n,k}$  from its neighbors;
  - 3: Agent  $k^*$  obtains an optimal solution  $\{p_i^{(n)*}\}_{i \in \mathcal{N}_a}$  by solving  $\mathcal{P}^S$ ;
  - 4: Agent  $k^*$  sends  $p_i^{(n)*}$  to agent  $i \in \mathcal{N}_a \setminus \{k^*\}$ ;
  - 5: Agent  $k$  accesses the channel with probability  $p_k^{(n)*}$  for  $k \in \mathcal{N}_a$  in the following  $N$  time slots.
- 

## VI. NODE DEPLOYMENT

This section presents the node deployment strategies for both non-cooperative and cooperative networks.

### A. Problem Formulation

We now formulate the node deployment problem, aiming to place nodes for increasing the localization accuracy associated with a certain set of nodes. We first consider the non-cooperative case, where anchors are deployed to minimize the average iSPEB for the agent within a certain region or along a preplanned path. In particular, let  $\mathcal{R}^a$  denote the region or the preplanned path in which the agent may lie, and the average iSPEB for the agent positions in  $\mathcal{R}^a$  is

$$\mathcal{P}^a(\mathcal{R}^a) := \int_{\mathbf{q} \in \mathcal{R}^a} \mathcal{P}(\mathbf{q}) f(\mathbf{q}) d\mathbf{q}$$

where  $f(q)$  is the weight function of the agent's position. The optimization problem can be formulated as follows:

$$\begin{aligned} \mathcal{Q} : & \underset{\{\mathbf{p}_k\}_{k \in \mathcal{N}_b}}{\text{minimize}} \quad \mathcal{P}^a(\mathcal{R}^a) \\ & \text{subject to} \quad \mathbf{p}_k \in \mathcal{R}^d, \quad k \in \mathcal{N}_b \end{aligned} \quad (47)$$

where  $\mathcal{R}^d$  denotes the feasible region for deploying nodes.

In the cooperative case, a set of nodes needs to be deployed to increase the localization accuracy associated with a set of agents. The nodes to be deployed are designated as *assisting nodes*, whereas the agents that need to increase localization accuracy are designated as *target agents*. Following the definition of  $\mathcal{P}^a(\mathcal{R}^a)$ , we introduce  $\mathcal{P}_k^a(\mathcal{R}_k^a)$  as

$$\mathcal{P}_k^a(\mathcal{R}_k^a) := \int_{q \in \mathcal{R}_k^a} \mathcal{P}(q) f_k(q) dq$$

where  $\mathcal{R}_k^a$  denotes the region or path in which a target agent  $k$  may lie, and  $f_k(q)$  denotes the weight function of target agent  $k$ 's position. The optimization problem can then be formulated as follows:

$$\begin{aligned} \mathcal{Q}_C : & \underset{\{\mathbf{p}_j\}_{j \in \mathcal{S}_1}}{\text{minimize}} \quad \sum_{k \in \mathcal{S}_2} \mathcal{P}_k^a(\mathcal{R}_k^a) \\ & \text{subject to} \quad \mathbf{p}_j \in \mathcal{R}^d, \quad j \in \mathcal{S}_1 \end{aligned} \quad (48)$$

where  $\mathcal{S}_1$  denotes the set of assisting nodes,  $\mathcal{S}_2 = \mathcal{N}_a \setminus \mathcal{S}_1$  denotes the set of target agents, and  $C$  denotes the cooperative deployment problems.

## B. Non-cooperative Case

We first consider a special case of  $\mathcal{Q}$ , where  $f(q) = \delta(q - \mathbf{p}_1)$ . This corresponds to the case where the agent is in a single position  $\mathbf{p}_1$ . In this case, the performance metric  $\mathcal{P}^a(\mathcal{R}^a) = \mathcal{P}(\mathbf{p}_1)$  and the node deployment problem becomes

$$\begin{aligned} \mathcal{Q}_{SP} : & \underset{\{\mathbf{p}_k\}_{k \in \mathcal{N}_b}}{\text{minimize}} \quad \mathcal{P}(\mathbf{p}_1) \\ & \text{subject to} \quad \mathbf{p}_k \in \mathcal{R}^d, \quad k \in \mathcal{N}_b \end{aligned} \quad (49)$$

where  $SP$  denotes the deployment problem for the agent in a single position.

The solution of this problem largely depends on  $\mathcal{R}^d$ . For simplicity, we consider that each anchor can be deployed on the boundary of a convex region and the agent is inside this region. The anchors' positions can then be parametrized by angles  $\phi_{1j}$ ,  $j \in \mathcal{N}_b$  (see Fig. 6). The problem  $\mathcal{Q}_{SP}$  then becomes

$$\begin{aligned} & \underset{\{\phi_{1j}\}_{j \in \mathcal{N}_b}}{\text{minimize}} \quad \mathcal{P}(\mathbf{p}_1) \\ & \text{subject to} \quad 0 \leq \phi_{1j} < 2\pi, \quad j \in \mathcal{N}_b. \end{aligned}$$

We further assume that  $\lambda_{1j}$  in (6) is a constant function of  $\phi_{1j}$ , i.e.,  $\lambda_{1j}$  does not change with  $\phi_{1j}$ . This assumption will be relaxed later. For notational convenience, in this section, we let  $\nu_k = \lambda_{1(k+N_a)}$  and  $\psi_k = \phi_{1(k+N_a)}$ . Without

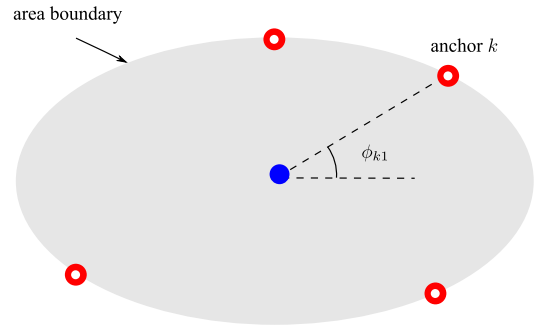


**Fig. 6.** Anchors are deployed on the boundary of a convex region. The position of an anchor can be parametrized by the angle from itself to the agent.

loss of generality, we assume that  $\nu_1 \geq \nu_2 \geq \dots \geq \nu_{N_b}$ . Similarly to (19), we can rewrite the performance metric  $\mathcal{P}(\mathbf{p}_1)$  defined in (5) as follows:

$$\mathcal{P}(\mathbf{p}_1) = \frac{4 \sum_{k=1}^{N_b} \nu_k}{\left( \sum_{k=1}^{N_b} \nu_k \right)^2 - \|\boldsymbol{\nu}_0\|^2} \quad (50)$$

where

$$\boldsymbol{\nu}_0 = \sum_{k=1}^{N_b} \nu_k [\cos 2\psi_k \sin 2\psi_k]^T.$$

Note that, by assumption,  $\nu_k$  is a constant and does not depend on  $\psi_k$ . Therefore, changing the positions  $\mathbf{p}_k$  does not change  $\sum_{k=1}^{N_b} \nu_k$ . As a consequence, the expression in (50) implies that minimizing  $\mathcal{P}(\mathbf{p}_1)$  is equivalent to minimizing  $\|\boldsymbol{\nu}_0\|$ . Fig. 7 illustrates the way of generating  $\boldsymbol{\nu}_0$ . In particular,  $-\boldsymbol{\nu}_0$  and  $\{\nu_k [\cos 2\psi_k \sin 2\psi_k]^T\}_{k=1}^{N_b}$  form a closed polygon (not necessarily convex). We have the following claims.

- If  $\nu_1 > \sum_{k=2}^{N_b} \nu_k$ , we can deploy the anchors such that  $\psi_1 - \psi_k = \pi/2 + m\pi$ , where  $k = 2, 3, \dots, N_b$  and  $m \in \mathbb{Z}$ . In this case,  $\|\boldsymbol{\nu}_0\| = \nu_1 - \sum_{k=2}^{N_b} \nu_k$ .
- If  $\nu_1 \leq \sum_{k=2}^{N_b} \nu_k$ , we can deploy the anchors such that  $\{\nu_k [\cos 2\psi_k \sin 2\psi_k]^T\}_{k=1}^{N_b}$  forms a closed polygon. In this case,  $\|\boldsymbol{\nu}_0\| = 0$ . One way to generate such a closed polygon is to use the Huffman Tree algorithm [109].

The method above gives a simple way to determine the optimal solution for  $\mathcal{Q}_{SP}$  with constant RII. However, constant RII may sometimes be an impractical assumption since at certain angles, there may be obstacles such as walls that block the line of sight (LOS) between the agent and potential anchors. To account for such a scenario, we now consider that  $\nu_k$  is a piecewise constant function of the angle  $\psi_k$ . In particular, consider discretizing the angles in to  $I$  sets, denoted by  $\mathcal{V}_i = [\underline{\vartheta}_i, \bar{\vartheta}_i)$ ,  $i = 1, 2, \dots, I$ . Without loss of generality, we assume  $\underline{\vartheta}_1 = 0$  and  $\bar{\vartheta}_I = 2\pi$ . The RII  $\nu_k$  takes a constant value  $\mu_i$  for all  $\psi_k \in \mathcal{V}_i$ .

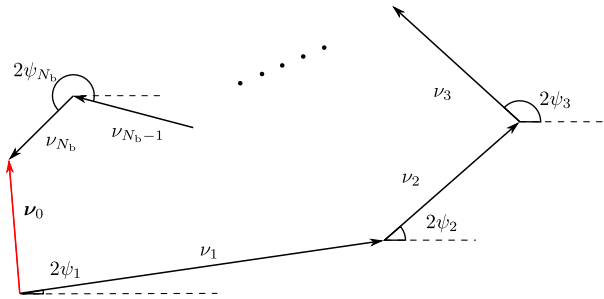


**Fig. 7.** Illustration of  $\nu_0$ : the summation of the vectors with length  $\nu_k$  and angle  $2\psi_k$ .

We next describe a coordinate descent method in Algorithm 3 that can produce node deployment decisions numerically for scenarios in which  $\nu_k$  depends on  $\psi_k$ . In fact, the performance metric iSPEB is reduced in each iteration by minimizing over one variable while fixing the other ones. The efficiency of this algorithm largely depends on the complexity of the minimization in line 3. Thus, we focus on finding the optimal solution to the minimization problem in line 3. The next proposition narrows down the search for the optimal solution to a finite number of points.

---

**Algorithm 3:** Relocate [108]

**Input:**  $\mathcal{V}_i = [\underline{\vartheta}_i, \bar{\vartheta}_i)$  and  $\mu_i, i = 1, 2, \dots, I$   
**Output:** The optimal angle vector

- 1: Randomly initialize  $\psi = [\psi_1 \psi_2 \dots \psi_{N_b}]^T$ ,  $m = 1$ ;
  - 2: **while**  $\psi$  has not converged do
  - 3:   Find the angle  $\psi_m^*$  that minimizes the iSPEB  $\mathcal{P}(\mathbf{p}_1)$  over  $\psi_m$  while fixing  $\psi_k, k \neq m$ ;
  - 4:    $\psi_m \leftarrow \psi_m^*$ ;
  - 5:    $m \leftarrow \text{mod}(m + 1, N_b)$ ;
  - 6: **end while**
- 

*Proposition 10:* The minimal  $\psi_m^*$  in line 3 of Algorithm 3 is in the following set  $\{\psi_m^1, \psi_m^2\} \cup \{\underline{\vartheta}_i, \bar{\vartheta}_i, i = 1, 2, \dots, I\}$ , where

$$\begin{aligned}\psi_m^1 &= \frac{1}{2} \arctan \frac{\sum_{k \neq m} \nu_k \sin 2\psi_k}{\sum_{k \neq m} \nu_k \cos 2\psi_k} \\ \psi_m^2 &= \frac{1}{2} \arctan \frac{\sum_{k \neq m} \nu_k \sin 2\psi_k}{\sum_{k \neq m} \nu_k \cos 2\psi_k} + \frac{\pi}{2}.\end{aligned}$$

*Proof:* The minimum of iSPEB is achieved either when  $\psi_m$  is on the boundary, i.e.,  $\psi_m \in \{\underline{\vartheta}_i, \bar{\vartheta}_i, i = 1, 2, \dots, I\}$ , or  $\psi_m$  is an interior point in some interval  $\mathcal{V}_i$ . In the latter case, the RII  $\mu_m$  is constant when  $\psi_m$  is in a small neighborhood of  $\psi_m^*$ . In this neighborhood, minimizing iSPEB is equivalent to minimizing  $\|\nu_0\|$ . The partial derivative of  $\|\nu_0\|$  with respect to  $\psi_m$  at  $\psi_m^*$  should be zero since  $\psi_m$  is

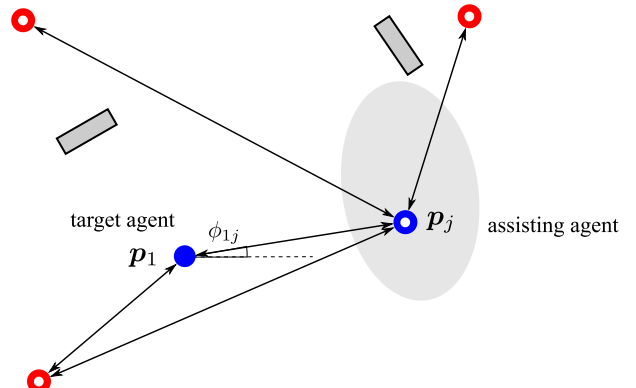


**Fig. 8.** Illustration of  $\mathcal{Q}_{C-SP}$ : assisting agents are deployed to increase the localization accuracy of the other agent.

an interior point. Hence

$$0 = \frac{\partial \|\nu_0\|}{\partial \psi_m} = 4\nu_m \left[ \left( \sum_{k \neq m} \nu_k \sin 2\psi_k \right) \cos 2\psi_m - \left( \sum_{k \neq m} \nu_k \cos 2\psi_k \right) \sin 2\psi_m \right].$$

The equation above has two solutions  $\psi_m^1$  and  $\psi_m^2$ , which are also candidates for  $\psi_m^*$ .  $\square$

We next consider another special case of  $\mathcal{Q}$ , where

$$f(\mathbf{q}) = \sum_{j=1}^J \delta(\mathbf{q} - \mathbf{q}_j)$$

where  $\{\mathbf{q}_j\}_{j=1}^J$  are  $J$  positions in region  $\mathcal{R}^a$ . This corresponds to the case in which the agent can be in  $J$  different positions. In this case, the performance metric

$$\mathcal{P}^a(\mathcal{R}^a) = \sum_{j=1}^J \mathcal{P}(\mathbf{q}_j) \quad (51)$$

and the node deployment problem becomes

$$\begin{aligned}\mathcal{Q}_{MP} : \min_{\{\mathbf{p}_k\}_{k \in \mathcal{N}_b}} & \sum_{j=1}^J \mathcal{P}(\mathbf{q}_j) \\ \text{subject to } & \mathbf{p}_k \in \mathcal{R}^d, k \in \mathcal{N}_b\end{aligned} \quad (52)$$

where MP denotes the deployment problem for the agent in multiple possible positions.

We continue to assume that anchors are deployed on the boundary of a convex region and the position of anchor  $k$  is parametrized by the angle from an interior point of the convex region to anchor  $k$ , denoted by  $\theta_k$ . In this way, we can write  $\mathbf{p}_k = \mathbf{h}(\theta_k)$ . Here we do not require the RIIs between anchor  $k$  and  $\{\mathbf{q}_j\}_{j=1}^J$  to be a constant as a function of  $\theta_k$ .

For the case in which the agent can be in multiple positions, Algorithm 3 can be modified to solve  $\mathcal{Q}_{MP}$  and the modified version is given in Algorithm 4. In line 3, the goal is to minimize the average iSPEB  $\mathcal{P}^a(\mathcal{R}^a)$  in (51) over  $\theta_m$ . As  $\mathcal{P}^a(\mathcal{R}^a)$  in (51) is a summation of  $J$  terms, the minimal  $\theta_m^*$  does not admit a simple expression as

$\psi_m^*$  in Algorithm 3. To address this issue, we can consider a uniform grid-based search method by selecting a finite subset of angles within  $[0, 2\pi)$  and minimizing  $\theta_m$  over this subset.

---

**Algorithm 4:** Relocate-MODIFY [108]

---

**Input:**  $\mathcal{V}_I = [\underline{\varphi}_i, \bar{\varphi}_i]$  and RII as a function of the angle  
**Output:** The optimal angle vector

$$\boldsymbol{\theta}^* = [\theta_1^* \theta_2^* \dots \theta_{N_b}^*]^T$$

1: Randomly initialize  $\boldsymbol{\theta} = [\theta_1 \theta_2 \dots \theta_{N_b}]^T$ ,  $m = 1$ ;  
2: **while**  $\boldsymbol{\theta}$  has not converged **do**  
3:     Find the angle  $\theta_m^*$  that minimizes the average iSPEB  $\mathcal{P}^a(\mathcal{R}^a)$  in (51) over  $\theta_m$  while fixing  $\theta_k$ ,  $k \neq m$ ;  
4:      $\theta_m \leftarrow \theta_m^*$ ;  
5:      $m \leftarrow \text{mod}(m + 1, N_b)$ ;  
6: **end while**

---

### C. Cooperative Case

We next consider a special case of  $\mathcal{Q}_C$ , where  $|\mathcal{S}_2| = 1$  and  $f_1(\mathbf{q}) = \delta(\mathbf{q} - \mathbf{p}_1)$ . This corresponds to the case in which there exists only one target agent at position  $\mathbf{p}_1$  in the network. In this case, the performance metric  $\sum_{k \in \mathcal{S}_2} \mathcal{P}_k^a(\mathcal{R}_k^a) = \mathcal{P}(\mathbf{p}_1)$  and the node deployment problem becomes

$$\begin{aligned} \mathcal{Q}_{C-SP} : & \underset{\{\mathbf{p}_j\}_{j \in \mathcal{S}_1}}{\text{minimize}} \quad \mathcal{P}(\mathbf{p}_1) \\ & \text{subject to} \quad \mathbf{p}_j \in \mathcal{R}^d, \quad j \in \mathcal{S}_1 \end{aligned} \quad (53)$$

where C-SP denotes the cooperative deployment problem for the agent in a single position.

Similarly to  $\mathcal{Q}_{SP}$ , the positions of other nodes can then be parametrized by the relative distances and angles with respect to agent 1, i.e.,  $\mathbf{p}_j = \mathbf{p}_1 + d_{1j}[\cos \phi_{1j} \sin \phi_{1j}]^T$ . We can rewrite  $\mathcal{Q}_{C-SP}$  as follows:

$$\begin{aligned} \mathcal{Q}_{C-SP} : & \underset{\{d_{1j}, \phi_{1j}\}_{j \in \mathcal{S}_1}}{\text{minimize}} \quad \mathcal{P}(\mathbf{p}_1) \\ & \text{subject to} \quad \mathbf{p}_1 + d_{1j}[\cos \phi_{1j} \sin \phi_{1j}]^T \in \mathcal{R}^d, \\ & \quad j \in \mathcal{S}_1. \end{aligned} \quad (54)$$

We now rewrite the performance metric iSPEB  $\mathcal{P}(\mathbf{p}_1) = \text{tr}\{\mathbf{J}_e^{-1}(\mathbf{p}_1)\}$  as a function of  $d_{1j}$  and  $\phi_{1j}$ . Note that the assisting agents need to first determine their positions based on range measurements with neighboring anchors. Hence, the EFIM  $\mathbf{J}_e(\mathbf{p})$  has the same expression as  $\mathbf{J}_e^L(\mathbf{p})$  in (30) of Section IV-C, i.e.,

$$\mathbf{J}_e(\mathbf{p}) = \sum_{k \in \mathcal{N}_a} \sum_{j \in \mathcal{N}_b} \lambda_{kj} \mathbf{V}_{kj} + \sum_{j \in \mathcal{S}_1} \lambda_{1j} \mathbf{V}_{1j}.$$

Consequently, the EFIM  $\mathbf{J}_e(\mathbf{p}_1)$  can be written as

$$\mathbf{J}_e(\mathbf{p}_1) = \mathbf{J}_e^A(\mathbf{p}_1) + \sum_{j \in \mathcal{S}_1} \tilde{\lambda}(d_{1j}, \phi_{1j}) \mathbf{J}_r(\phi_{1j})$$

where

$$\tilde{\lambda}(d_{1j}, \phi_{1j}) = \frac{\lambda_{1j}}{1 + \lambda_{1j} \Delta_{1j}}.$$

Recall that  $\Delta_{1j}$  is defined in (31), representing the position uncertainty of agent  $j$  along the direction between agent 1 and agent  $j$ . The values of  $\Delta_{1j}$  and  $\lambda_{1j}$  are assumed to be known for the design of node deployment strategies in this section.

Without loss of optimality, we can solve  $\mathcal{Q}_{C-SP}$  in the following two steps: first determine  $\{d_{1j}\}_{j \in \mathcal{S}_1}$  for a given set  $\{\phi_{1j}\}_{j \in \mathcal{S}_1}$ , and then determine  $\{\phi_{1j}\}_{j \in \mathcal{S}_1}$ . For the first step, note that  $\mathcal{P}(\mathbf{p}_1)$  depends on  $d_{1j}$  only through  $\tilde{\lambda}(d_{1j}, \phi_{1j})$  and that  $\mathcal{P}(\mathbf{p}_1)$  is a decreasing function of  $\tilde{\lambda}(d_{1j}, \phi_{1j})$ . Consequently, for a given  $\{\phi_{1j}\}_{j \in \mathcal{S}_1}$ , the minimization of  $\mathcal{P}(\mathbf{p}_1)$  over  $\{d_{1j}\}_{j \in \mathcal{S}_1}$  becomes

$$\begin{aligned} d_{1j}^*(\phi_{1j}) &:= \arg \min_{\{d_{1j}: \mathbf{p}_j \in \mathcal{R}^d\}} \mathcal{P}(\mathbf{p}_1) \\ &= \arg \max_{\{d_{1j}: \mathbf{p}_j \in \mathcal{R}^d\}} \tilde{\lambda}(d_{1j}, \phi_{1j}). \end{aligned}$$

Since  $\tilde{\lambda}(d_{1j}, \phi_{1j})$  does not rely on  $d_{1k}$  or  $\phi_{1k}$  ( $k \neq j$ ), the optimization above has a single scalar variable and can be solved efficiently using one-dimensional optimization algorithms.

Next we consider the second step, i.e., determining  $\phi_{1j}^*$  for  $j \in \mathcal{S}_1$ . Directly optimizing  $\mathcal{Q}_{C-SP}$  over  $\phi_{1j}$  is difficult since  $\mathcal{P}(\mathbf{p}_1)$  is not a convex function of  $\{\phi_{1j}\}_{j \in \mathcal{S}_1}$ . To address this issue, we introduce a discretization method that can transform  $\mathcal{Q}_{C-SP}$  to a problem with a similar structure to  $\mathcal{P}_k$  in Section III. In particular, we narrow the feasible set of angles to  $M$  possible values. Let  $\underline{\phi}$  and  $\bar{\phi}$  denote the lower and upper constraint of angles based on the feasible set  $\mathcal{R}^d$ . Consider

$$\mathcal{S}_\phi = \{\theta_1, \theta_2, \dots, \theta_M\} \quad (55)$$

where  $\theta_m = \underline{\phi} + m(\bar{\phi} - \underline{\phi})/M$ , in which  $M \in \mathbb{N}^*$ . We assume that the assisting nodes can be deployed only to positions where the corresponding angles belong to  $\mathcal{S}_\phi$ . This corresponds to replacing the constraint (54) with  $\phi_{1j} \in \mathcal{S}_\phi$  in  $\mathcal{Q}_{C-SP}$ . In this way, the original problem  $\mathcal{Q}_{C-SP}$  is relaxed to

$$\begin{aligned} \mathcal{Q}_{C-SP}^D : & \underset{\mathbf{x} \in \mathbb{R}^M}{\text{minimize}} \quad \text{tr} \left\{ \left( \mathbf{J}_e^A(\mathbf{p}_1) + \sum_{m=1}^M x_m \tilde{\lambda}_m \mathbf{J}_r(\theta_m) \right)^{-1} \right\} \\ & \text{subject to} \quad \mathbf{1}^T \mathbf{x} \leq |\mathcal{S}_1| \\ & \quad x_m \in \mathbb{N}, \quad m = 1, 2, \dots, M \end{aligned} \quad (56)$$

where  $\tilde{\lambda}_m = \tilde{\lambda}(d_m, \theta_m)$ , in which  $d_m$  can be determined using the result from the first step, i.e.,

$$d_m = \arg \max_{\{d: \mathbf{p}_1 + d[\cos \theta_m \sin \theta_m]^T \in \mathcal{R}^d\}} \tilde{\lambda}(d, \theta_m). \quad (57)$$

The solution of  $\mathcal{Q}_{C-SP}^D$  can be used for deploying assisting agents: for  $m = 1, 2, \dots, M$ ,  $x_m$  assisting nodes are placed in the position that corresponds to  $\theta_m$  and  $d_m$ . In fact, we can observe that by discretizing the angles, the deployment problem is converted into a node prioritization problem with a discrete-level of resources.

---

**Algorithm 5:** Node Deployment in Cooperative Networks
 

---

**Input:**  $\mathcal{R}^d$ ,  $|\mathcal{S}_1|$ , function  $\tilde{\lambda}(\cdot, \cdot)$ , and  $J_e^A(p_1)$

**Output:**  $d_{1k}$  and  $\phi_{1k}$ ,  $k \in \mathcal{S}_1$

- 1: Determine  $\mathcal{S}_\phi$  in (55);
  - 2: For  $\theta_m \in \mathcal{S}_\phi$ ,  $m = 1, 2, \dots, M$ , determine  $d_m$  according to (57);
  - 3: Find the optimal solution  $x^*$  of  $\mathcal{Q}_{C-SP}^R$ ;
  - 4: Find a solution  $x$  of  $\mathcal{Q}_{C-SP}^D$  as  $x = x_I + y^*$  based on  $x^*$ ;
  - 5: For  $m = 1, 2, \dots, M$ , deploy  $x_m$  nodes to the position that corresponds to  $\theta_m$  and  $d_m$ , i.e.,  $p_1 + d_m [\cos \theta_m \sin \theta_m]^T$ .
- 

The program  $\mathcal{Q}_{C-SP}^D$  is an integer optimization problem, which is generally difficult to solve. Here we relax  $\mathcal{Q}_{C-SP}^D$  by replacing (56) with  $x \succcurlyeq 0$  and let  $\mathcal{Q}_{C-SP}^R$  denote this relaxed problem. As the performance metric of  $\mathcal{Q}_{C-SP}^R$  has a similar structure with  $\mathcal{P}_k$ , we can solve  $\mathcal{Q}_{C-SP}^R$  using the methods introduced in Section III. Let  $x^*$  denote the solution of the relaxed problem  $\mathcal{Q}_{C-SP}^R$ . There are several ways to use  $x^*$  for generating a solution of  $\mathcal{Q}_{C-SP}^D$  and we describe here a simple one. Rewrite  $x^* = x_I + x_F$ , where  $x_I$  and  $x_F$  denote the vectors consisting of integer parts and fractional parts of  $x^*$ , respectively. Consider a vector  $y^* \in \mathbb{R}^M$  as follows:

$$y_k^* = \begin{cases} 1, & [x_F]_k \text{ is one of the } m^* \text{ largest elements in } x_F \\ 0, & \text{otherwise} \end{cases}$$

where  $m^* = |\mathcal{S}_1| - 1^T x_I$ . In this way, we find a feasible solution of  $\mathcal{Q}_{C-SP}^D$  as  $x_I + y^*$ . Algorithm 5 gives details on how to solve  $\mathcal{Q}_{C-SP}$ .

## VII. PERFORMANCE EVALUATION

This section illustrates the performance of network operation strategies for different settings. Recall that for a given instantiation of channel parameters and node positions, the performance metric in Section II-C is considered to be a deterministic quantity. This implies that the values of the performance metric vary with these conditions. To understand the behavior of the network operation strategies, we will analyze the localization performance using the cumulative distribution function (CDF) of a position error metric over many instantiations of channels and node positions. To this end, a synchronous 2-D network is considered. In Sections VII-A and VII-B, 36 anchors are deployed on a regular  $6 \times 6$  lattice with 100-m separation between two neighboring anchors. Therefore, the convex hull of these 36 anchors is a square region of 500 m by 500 m. Agents are randomly deployed in this region. An orthogonal frequency-division multiplexing (OFDM) radio technology at the physical layer is considered for the range measurements. The carrier frequency is  $f_c = 2$  GHz, the bandwidth is 10 MHz, and the subcarrier spacing is 15 kHz. The transmitting signal has a duration of 66.67  $\mu$ s [158].

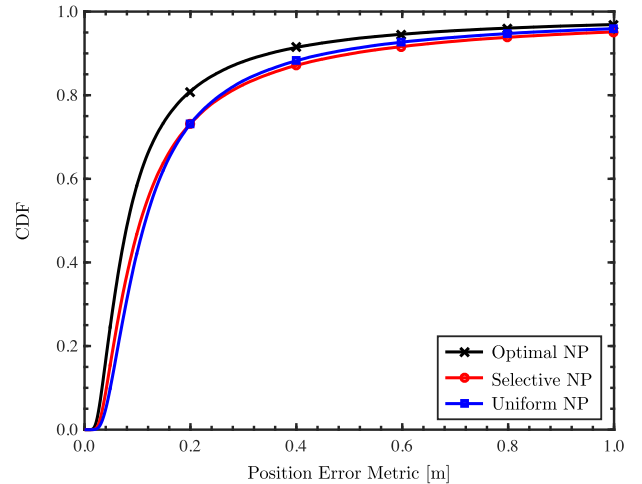


**Fig. 9.** CDF of the root iSPEB for different node prioritization strategies. A non-cooperative network with perfectly known parameters is considered.

---

The noise power spectral density is  $-169$  dBm/Hz, or equivalently, the noise figure is equal to 5 dB.

The RIIs between anchors and agents are determined as follows. For anchor  $k$ , the LOS/non-LOS (NLOS) state is generated for agents considering the Urban Micro scenario [159], with spatial consistency of LOS/NLOS states among agents accounted for according to the approach in [160]. Let  $\mathcal{N}_{LOS,k}$  denote the set of agents that have LOS states with anchor  $k$ . For channels between anchor  $k$  and agents in  $\mathcal{N}_{LOS,k}$ , delays and amplitudes are generated using QuaDRiGa [161] by setting anchor  $k$  as the transmitter and the agents in  $\mathcal{N}_{LOS,k}$  as the receivers with the scenario given by the Urban Micro B1 model. The RIIs between anchor  $k$  and agent  $j \in \mathcal{N}_{LOS,k}$  are then calculated based on [72], whereas the RIIs between anchor  $k$  and agent  $j \in \mathcal{N}_a \setminus \mathcal{N}_{LOS,k}$  are set to 0 [72]. Thus, for a particular anchor, the spatial consistency of channel fading among the agents are accounted for. The RIIs among agents are determined in the same way by first generating LOS/NLOS states as well as the delay and amplitudes, and then performing the calculation of the RII according to [73].

In the following sections, the CDF of the position error is evaluated as the empirical probability (i.e., the fractions of instantiations over many channel conditions and node positions) that the position error metric is less than or equal to the abscissa. We consider the position error metric to be either the root iSPEB, the root normalized nSPEB or the worst-case root iSPEB depending on the scenario of interest.<sup>8</sup>

<sup>8</sup>Since the iSPEB is a lower bound on the MSE achieved by any localization approach, the CDF of the root iSPEB is a universal upper bound on the CDF of the root MSE. Moreover, in scenarios where the iSPEB provides a tight bound on the MSE of a specific localization approach, the CDF of the root iSPEB serves as a tight approximation for the CDF of the root MSE.

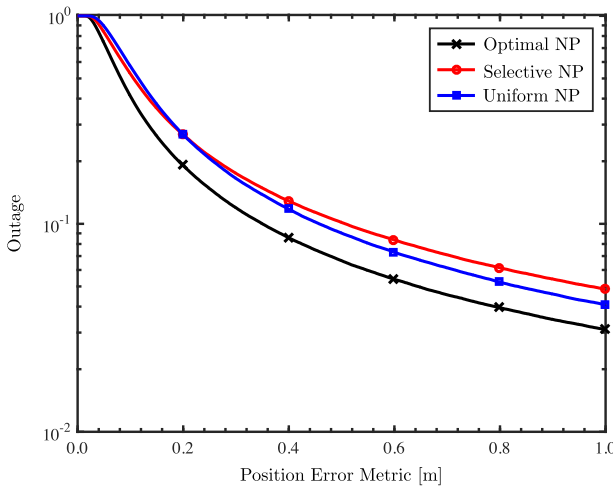


**Fig. 10.** Outage of the root iSPEB for different node prioritization strategies. A non-cooperative network with perfectly known parameters is considered.

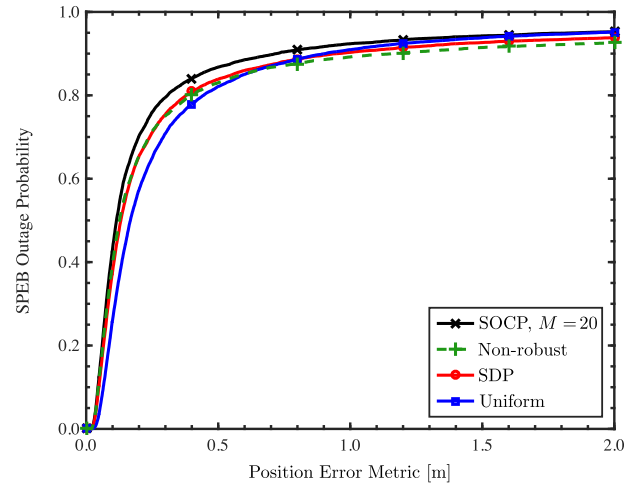


**Fig. 11.** CDF of the worst-case root iSPEB for different node prioritization strategies with  $\epsilon = 0.1$ . In the SOCP strategy, the parameter  $M = 20$ . A non-cooperative network with uncertainty in parameters is considered.

## A. Node Prioritization

We first evaluate the performance gain of the node prioritization strategies in a non-cooperative network with perfectly known parameters such as RIIs and angles. We deploy  $N_a = 1$  agent uniformly. The position error is evaluated in situations where the agent has LOS states to at least two anchors.<sup>9</sup>

In this section, consider that the NPV is based on power. The total available power is 1 mW. We compare three node prioritization strategies:

- uniform—the available power is equally divided among all anchors that have LOS states to the agent;
- selective—three anchors are selected based on the quality of the inter-node measurement and the available transmitting power is equally divided among these three anchors;
- optimal—the available power is allocated according to the optimal NPV in Section III-C.

The uniform strategy serves as a baseline for evaluating the performance of the node prioritization strategies.

Fig. 9 shows the performance of the optimal, the selective, and the uniform node prioritization strategies, where the benefit of optimized (selective and optimal) node prioritization strategies is evident. For example, the median position error (50th percentile) for the optimal strategy is 0.082 m, whereas it is 0.106 and 0.115 m for the selective and uniform strategies, respectively. This corresponds to position error increases of 29% and 40%, respectively, for the selective and uniform strategies over the optimal strategy. Another metric of interest is the 95th percentile mark, which is used to evaluate the essentially maximum error of a deployed system [31]. From Fig. 9 we note that in 95% of cases the optimal strategy has a position error less than or equal to 0.644 m, whereas the selective

and uniform strategies have errors of 0.971 and 0.834 m, respectively. Here, the selective and uniform strategies have position error increases of 51% and 30%, respectively, over the optimal strategy.

Note that the performance of the network operation strategies can also be presented in terms of the position error outage.<sup>10</sup> Fig. 10 shows the performance of the node prioritization strategies. For a target position error of 0.5 m, it can be seen that the uniform, selective, and optimal strategies result in outages of 9.0%, 10.2%, and 6.6%, respectively. This corresponds to outage increases of 55% and 36%, respectively, for the selective and uniform strategies over the optimal strategy. Since the CDF and the outage can be equivalently evaluated, we will present the performance of the network operation strategies only in terms of the CDF for brevity in the rest of this section.

We next evaluate the performance gain of the node prioritization strategies in a non-cooperative network with uncertainty in parameters. In this scenario, we again consider  $N_a = 1$  agent, with the total available power equal to 1 mW. The position error is evaluated in situations where the agent has LOS states to at least two anchors. The true position of the agent can be anywhere in the circle centered at its nominal position with radius of 10 m. Therefore, the maximum uncertainty in  $\phi_{kj}$  is  $\arcsin(10/d_{kj})$ . We require that the distance between the agent and any anchor to be at least 11 m so that the anchors are not in the agent's uncertainty region. Let  $\epsilon = 0.1$  denote the normalized uncertainty set size. The true value of  $\xi_{kj}$  is uniformly selected between  $(1 - \epsilon)\hat{\xi}_{kj}$  and  $(1 + \epsilon)\hat{\xi}_{kj}$ , where  $\hat{\xi}_{kj}$  denotes the nominal value of the ranging quality. In addition to the uniform strategy

<sup>10</sup>The outage is a well-known concept in wireless communications [162]–[164]. In the context of location-aware networks, the outage is similarly defined as the empirical probability that the position error metric is greater than the abscissa.

<sup>9</sup>These situations occur in more than 92% of the total instantiations.

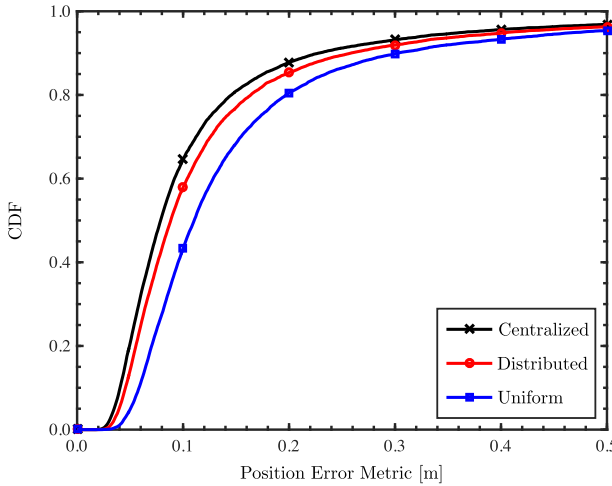


**Fig. 12.** CDF of the root normalized nSPEB (i.e.,  $\sqrt{P(p; x)/N_a}$ ) for different node prioritization strategies. A cooperative network with perfectly known parameters is considered.

serving as the baseline, we introduce three other node prioritization strategies for comparison:

- SDP—the available transmitting power is allocated according to the solution of the SDP-based formulation in Section III-D;
- SOCOP—the available transmitting power is allocated according to the solution of the SOCP-based formulation in Section III-D with  $M = 20$  in  $\mathcal{P}_{R,k}^M$ ;
- non-robust—the available transmitting power is allocated according to the NPV obtained in Section III-C based on nominal parameters. See also Section II-B for a description of the non-robust method.

Fig. 11 shows the performance of the non-robust, SOCP, SDP, and uniform node prioritization strategies with  $\epsilon = 0.1$ . Recall that the worst-case iSPEB given in (25) is the maximum iSPEB over the uncertainty in  $\phi_{kj}$  and  $\xi_{kj}$ . Here, the benefit of the robust and optimized (SOCP and SDP) node prioritization strategies is evident from the figure. For example, the median position errors for the SOCP, non-robust, and SDP strategies are 0.114, 0.126, and 0.131 m, respectively, whereas it is 0.167 m for the uniform strategy. This corresponds to position error increases of 46%, 33%, and 27%, respectively, for the uniform strategy over the SOCP, non-robust, and SDP strategies. At the 95th percentile, the SOCP, uniform, and SDP strategies have position errors of 1.861, 1.931, and 3.028 m, respectively, whereas it is 6.036 m for the non-robust strategy. This corresponds to position error increases of 99%, 213%, and 224%, respectively, for the non-robust strategy over the SDP, uniform, and SOCP strategies. Thus, in contrast to the median performance, the non-robust strategy performs the worst among all the strategies at the 95th percentile.

We next evaluate the performance gain of the node prioritization strategies in a cooperative network with perfectly known parameters. We randomly deploy  $N_a = 3$  agents. The first agent is uniformly deployed in the square

region of 500 m by 500 m, whereas the second and third agents are uniformly deployed in a circle centered at the first agent with radius of 50 m. The position error is evaluated in situations where each agent has LOS states to at least two anchors. For each agent, the total available power for ranging to the anchors is 0.5 mW, whereas the total available power for ranging to the agents is 0.5 mW. We compare three node prioritization strategies:

- uniform—the available transmitting power is equally divided among all nodes (including anchors and other agents) that have LOS states to the agent;
- centralized—the available transmitting power is allocated according to the solution of the SDP-based formulation in Section IV-B;
- distributed—the available transmitting power is allocated according to the solution of the SOCP-based formulation in Section IV-C.

The uniform strategy serves as a baseline for evaluating the performance of the node prioritization strategies.

Fig. 12 shows the performance of the centralized, distributed, and uniform node prioritization strategies, where the benefit of optimized (centralized and distributed) node prioritization strategies is evident. For example, the median errors for the centralized and distributed strategies are 0.078 and 0.088 m, respectively, whereas it is 0.111 m for the uniform strategy. This corresponds to position error increases of 42% and 26% for the uniform strategy over the centralized and distributed ones. In 95% of cases, the centralized and distributed strategies have position errors less than or equal to 0.366 and 0.407 m, respectively, whereas the uniform strategy has an error of 0.476 m. The uniform strategy has position error increases of 30% and 17% over the centralized and distributed ones. Note that the centralized and distributed strategies demonstrate similar performance, and thus the proposed distributed strategy achieves a nearoptimal performance.<sup>11</sup>

## B. Node Activation

We next evaluate the performance gain of the node activation strategies in cooperative localization and navigation networks. We randomly deploy a group of  $N_a = 4$  agents in an area of 50 m by 50 m, and the group of agents moves together along a circular trajectory centered at [250 m, 250 m] with radius 150 m. The total available power is set to be  $N_a$  mW at each instant. Moreover, in this section, we set the standard deviation of the intra-node measurement noise  $\sigma_m = 0.05$  m and assume that the noise is independent over different time slots for simplicity.<sup>12</sup> We first compare two node activation strategies, where the total

<sup>11</sup>Recall that the centralized strategy provides the optimal performance as it is based on the SDP formulation.

<sup>12</sup>Note that the noise in the intra-node measurement is correlated over time if accelerometer measurements are considered. For this scenario, one can augment the state vector to include both the velocity and acceleration [74] and the optimal node activation strategy can then be developed based on the augmented state model. For simplicity, we consider a model where the noise is independent over time.

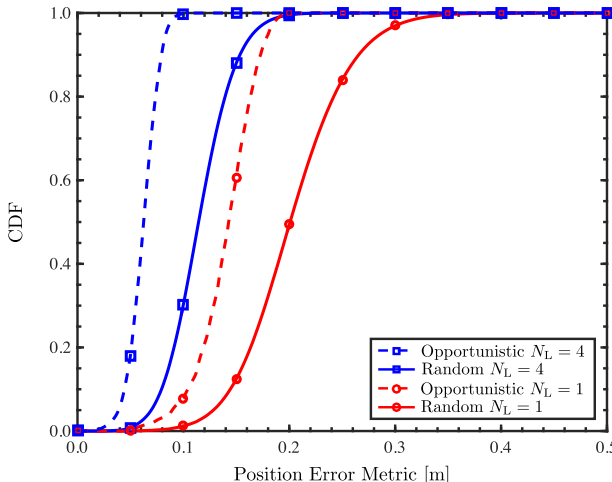


**Fig. 13.** CDF of the root iSPEB for different node activation strategies. The number of inter-node measurements used are  $N_L = 1$  and 4. A cooperative network is considered.

power is equally divided over  $N_L$  inter-node measurements at each instant.

- Opportunistic activation—For each of the  $N_L$  measurements, the agent that can maximally reduce the network localization error is activated and the activated agent chooses the best neighbor for making an inter-node measurement. This process is repeated in a sequential manner until  $N_L$  measurement pairs are determined.
- Random activation—For each of the  $N_L$  measurements, an agent is activated randomly and the activated agent chooses a random neighbor that has an LOS state for making an inter-node measurement. This process is repeated in a sequential manner until  $N_L$  measurement pairs are determined.

The random strategy serves as a baseline for evaluating the performance of the node activation strategies.

Fig. 13 shows the performance of the opportunistic and random node activation strategies for different numbers of inter-node measurements. Note that the opportunistic node activation strategy outperforms the random activation strategy, since the opportunistic node activation strategy always selects the most critical agents to make inter-node measurements. Here, the median position errors are 0.063 and 0.114 m for the opportunistic and random activation strategies with four inter-node measurements, respectively. This corresponds to a position error increase of 81% for the random strategy over the opportunistic strategy. Likewise, with four inter-node measurements, it is 0.083 and 0.166 m for the opportunistic and random activation strategies, respectively, at the 95th percentile, which gives a 100% increase in the position error.

Furthermore, both strategies using four inter-node measurements outperform the corresponding strategies using one inter-node measurement as expected. Comparing the opportunistic activation strategies with the random activation strategies, the former ones have steeper rates of

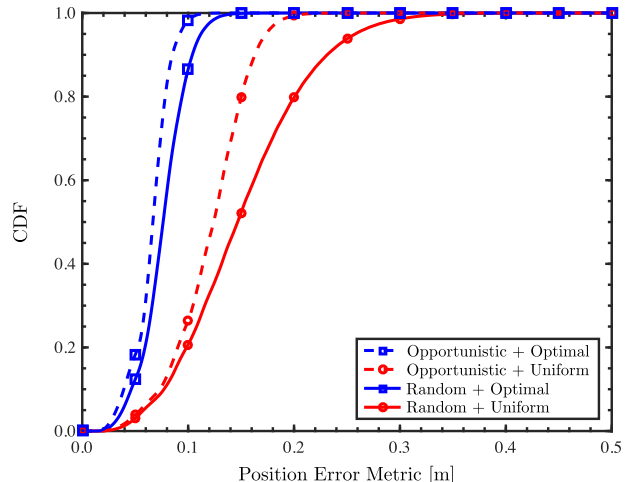


**Fig. 14.** CDF of the root iSPEB for different combinations of node activation and node prioritization strategies. A cooperative network is considered.

increase in the CDF corresponding to achieving lower position errors for both one and four inter-node measurements. This is because the opportunistic activation aims at maximally reducing the nSPEB by selecting an appropriate agent, thus preventing individual agents from accumulating large localization errors. These results show that the optimized (opportunistic) node activation can significantly reduce the localization error compared to random node activation.

Next we consider a joint design of the node activation combined with the node prioritization strategies developed described in Sections III and IV. Note that in this case, the number of inter-node measurements depends on the outcome of the node prioritization strategy. The total available power is again set to be  $N_a$  mW, and four different combinations of node activation and node prioritization strategies are considered as follows.

- Opportunistic activation + optimal prioritization—The agent that can maximally reduce the network localization error based on the optimal node prioritization is activated, and the activated agent uses the transmitting power according to the optimal NPV for making inter-node measurements with its neighbors.
- Opportunistic activation + uniform prioritization—The agent that can maximally reduce the network localization error based on the uniform prioritization is activated, and the activated agent uses equal transmitting power for making inter-node measurements with its neighbors that have LOS states.
- Random activation + optimal prioritization—An agent is activated randomly, and the activated agent uses the transmitting power according to the optimal NPV for making inter-node measurements with its neighbors.
- Random activation + uniform prioritization—An agent is activated randomly, and the activated agent

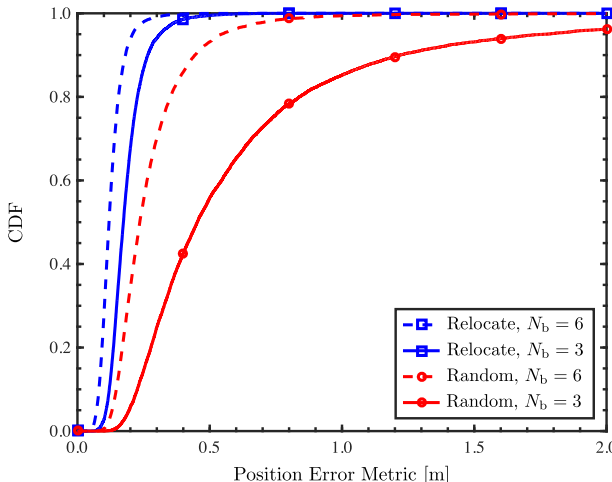


**Fig. 15.** CDF of the root iSPEB for different node deployment strategies. The number of anchors are  $N_b = 6$  and 3. A non-cooperative network is considered.

uses equal transmitting power for making inter-node measurements with its neighbors that have LOS states.

Fig. 14 shows the performance of different combinations of node activation and node prioritization strategies. First, similarly to the previous scenario, one can observe that the opportunistic activation strategy outperforms the random activation strategy. Second, under the same node activation strategy, the performance with optimal node prioritization is better than that with uniform prioritization. This is because for any given activated agent, the power is more efficiently used according to the optimal NPV. Therefore, joint node activation and node prioritization can achieve a twofold performance gain. As an example, take the median position error of 0.147 m obtained by random activation + uniform prioritization as a baseline. The median position error is 0.067 m from opportunistic activation + optimal prioritization, while it is 0.076 and 0.124 m for optimized prioritization only and activation only, respectively. This corresponds to position error increases of 119%, 93%, and 19% for the baseline over the optimized strategies. Likewise, in 95% of cases, the position error is less than or equal to 0.092, 0.112, 0.174, and 0.258 m, respectively, for the four combinations of strategies.

### C. Node Deployment

We now evaluate the performance gain of the node deployment strategies in a non-cooperative network. Recall that in non-cooperative networks, only anchors are deployed to improve the localization accuracy of agents. As in Section VI-B, we consider a scenario in which there is only one agent, and the RII  $\nu_k$  is a piecewise constant function of the angle  $\psi_k$ . Recall that  $[0, 2\pi)$  is divided into  $I$  intervals denoted by  $\mathcal{V}_i$ 's. We assume that  $\mathcal{V}_i = [2\pi(i-1)/I, 2\pi i/I)$ ,  $i = 1, 2, \dots, I$  with  $I = 5$  and that in each  $\mathcal{V}_i$ , the RII is generated independently for the

anchor-to-agent distance equal to 300 m and the total transmitting power for each agent is equal to 1 mW. Only the LOS states are accounted for. We compare two node deployment strategies:

- random: anchors are deployed randomly where the angle  $\psi_k$  is generated from a uniform distribution in  $[0, 2\pi)$ ;

- Relocate: anchors are deployed based on Algorithm 3. The random strategy serves as a baseline for evaluating the performance of the node deployment strategies.

Fig. 15 shows the performance of the Relocate and random node deployment strategies for different numbers of anchors, where the benefit of the optimized (Relocate) node deployment strategy is evident. As an example for  $N_b = 6$  anchors, the median position error for the Relocate strategy is 0.119 m, whereas it is 0.236 m for the random strategy. This corresponds to a position error increase of 98% for the random strategy over the Relocate strategy. For  $N_b = 3$ , the median position error for the Relocate strategy is 0.174 m, whereas it is 0.453 m for the random strategy. This corresponds to a position error increase of 160% for the random strategy over the Relocate strategy. Regarding the 95th percentile, for  $N_b = 6$ , it is 0.208 and 0.544 m for the Relocate and random strategies, respectively. The random strategy has a position error increase of 162% over the Relocate one. At the 95th percentile for  $N_b = 3$ , it is 0.312 and 1.770 m for the Relocate and random strategies, respectively. This corresponds to a position error increase of 467% for the random strategy over the Relocate strategy.

Note that the number of anchors plays a different role in the random and Relocate strategies. For the random strategy, the median of the position error has an increase of 92% for the case with  $N_b = 3$  over the one with  $N_b = 6$ , whereas the increase is only 46% for the Relocate strategy. For the random strategy, the 95th percentile of the position error has an increase of 225% for the case with  $N_b = 3$  over the one with  $N_b = 6$ , whereas the increase is only 50% for the Relocate strategy. The number of anchors affects the performance of the random strategy significantly because more anchors provide not only resource gain (the accuracy improvement due to more measurements) but also diversity gain (the accuracy improvement due to higher chances of forming a desirable geometry with high channel quality). In contrast, the Relocate strategy already accounts for the geometry and channel quality so that the diversity gain is not remarkable, which explains the decreased accuracy improvement due to having more anchors.

We next evaluate the performance gain of node deployment in a cooperative network. Three anchors are placed at the trisection points of the circle centered at the origin with radius 400 m and one of the anchors is placed at [400 m, 0 m]. The feasible region  $\mathcal{R}^d$  is a circle centered at [200 m, 0] with radius 200 m. Six assisting agents are deployed in this region. The target agent is deployed randomly in the region  $([-200 \text{ m}, 200 \text{ m}] \times$

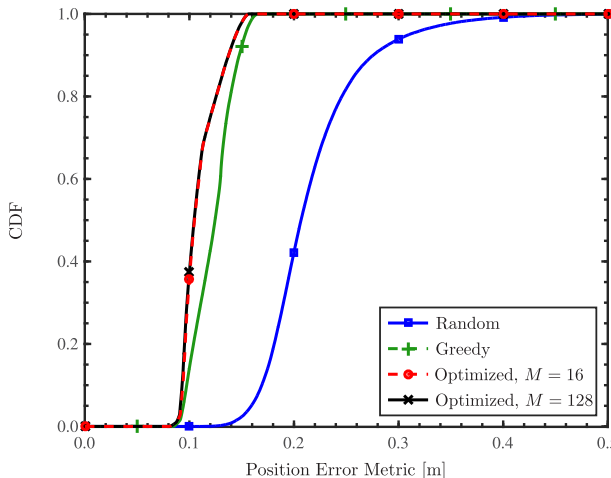


**Fig. 16.** CDF of the target agent's root iSPEB for different node deployment strategies. In the optimized strategy, the parameter  $M = 128$  and 16. A cooperative network is considered.

$[-200 \text{ m}, 200 \text{ m}] \cap (\mathcal{R}^d)^c$ . The total transmitting power for each agent is 1 mW. The shadowing and multipath effects are not considered in this case and only the LOS states are accounted for. We compare three node deployment strategies:

- random—the assisting agents are deployed uniformly in the feasible region  $\mathcal{R}^d$ ;
- greedy—the assisting nodes are deployed sequentially at the positions in the feasible region  $\mathcal{R}^d$  for minimizing the iSPEB;
- optimized—the nodes are deployed in the feasible region based on Algorithm 5, with different values of  $M$  as described in (55).

The random strategy serves as a baseline for evaluating the performance of the node deployment strategies.

Fig. 16 shows the performance of the optimized (with  $M = 128$  and  $M = 16$ ), greedy, and random node deployment strategies, where the benefit of the optimized and greedy node deployment strategies is evident. For example, the median position error for the optimized strategy (both  $M = 16$  and  $M = 128$ ) is 0.105 m, whereas it is 0.125 and 0.207 m for the greedy and random strategies, respectively. This corresponds to position error increases of 97% and 66%, respectively, for the random strategy over the optimized and greedy ones. At the 95th percentile, the optimized strategy has a position error of 0.145 m, whereas the greedy and random strategies have errors of 0.153 and 0.310 m, respectively. Here, the random strategy has position error increases of 114% and 103% over the optimized and greedy ones, respectively.

Note that the optimized strategy ( $M = 16$  and 128) outperforms the greedy one (16% decrease of the median position error and 5% decrease of the 95th percentile). Moreover, the complexity of the greedy strategy increases linearly with the number of assisting nodes, whereas the optimized strategy depends only on  $M$ . In scenarios with large numbers of assisting nodes, the optimized strategy

has an advantage over the greedy one in terms of computational complexity. Moreover, with the optimized strategy, we observe that the curve corresponding to  $M = 16$  almost overlaps with that corresponding to  $M = 128$ . This result provides insight into the implementation of the optimized strategy: using a small  $M$  results in a strategy with much lower computational complexity yet negligible performance loss compared to one using a larger  $M$ .

### VIII. CONCLUSION

Network operation strategies play a critical role in NLN since they not only affect the network lifetime, but also determine the localization accuracy. In this paper, we have presented a comprehensive tutorial on network operation strategies, in particular node prioritization, node activation, and node deployment. We have studied the structure of the localization performance metric and exploited the insights gained to derive different optimization methods. We have discussed some important aspects resulting from the analysis, including such concepts as cooperation techniques, robustness guarantees, and distributed designs, and we have characterized the performance gain obtained from the network operation.

The benefit of adopting efficient network operation strategies compared to the baseline strategies is evident from the numerical examples. In particular, we have shown the performance improvement for each of the following operation strategies.

- Node prioritization—The penalty for not employing optimization methodologies can be as large as 46% in terms of the median position error metric. In particular, the median position error increase of the uniform strategy is 40% over the optimal strategy in non-cooperative networks; it is 46% over the SOCP strategy with uncertainty in parameters; and it is 26% and 42% over the distributed and centralized strategies, respectively, in cooperative networks.
- Node activation—Random activation has been shown to have a median position error increase of 81% compared to the opportunistic strategy with four inter-node measurements. The joint design of the node activation combined with the node prioritization strategies adds another layer of optimization and gives further improvement in localization accuracy.
- Node deployment—in non-cooperative networks, the random strategy has been shown to have a median position error of up to 160% more than the optimized Relocate strategy, while in cooperative networks, the random strategy has a median position error increase of more than 66% over the optimized and greedy strategies. The optimized strategy has been shown to have a better performance compared to the greedy one with the benefit of being computationally more efficient in scenarios with many assisting agents.

Note that practical imperfections in hardware implementations would degrade the localization accuracy with respect

to that presented in this paper. However, the degradation due to these imperfections would be similar for all the network operation strategies presented, and thus the relative accuracy improvement reported in this paper is expected to still hold. While the performance characterization of various NLN strategies has been exhaustively presented, there are still open challenges to be addressed. For example, the latency of position information is critical, especially in highly dynamic environments. However, fewer analytical methodologies have emerged to evaluate and optimize the latency in localization and navigation networks. Moreover,

location secrecy and privacy are gradually becoming more of a concern for location-based services, but techniques that achieve both high accuracy and high secrecy in NLN through network operation strategies are yet to be developed.  $\square$

## Acknowledgments

The authors would like to thank J. Chen, A. Conti, Z. Liu, and S. Mazuelas for their helpful suggestions and careful reading of the manuscript.

## REFERENCES

- [1] M. Z. Win et al., "Network localization and navigation via cooperation," *IEEE Commun. Mag.*, vol. 49, no. 5, pp. 56–62, May 2011.
- [2] N. Bulusu, J. Heidemann, and D. Estrin, "GPS-less low-cost outdoor localization for very small devices," *IEEE Pers. Commun.*, vol. 7, no. 5, pp. 28–34, Oct. 2000.
- [3] E. Paolini, A. Giorgetti, M. Chiani, R. Minutolo, and M. Montanari, "Localization capability of cooperative anti-intruder radar systems," *EURASIP J. Adv. Signal Process.*, vol. 2008, Apr. 2008, Art. no. 726854.
- [4] S. Gezici et al., "Localization via ultra-wideband radios: A look at positioning aspects for future sensor networks," *IEEE Signal Process. Mag.*, vol. 22, no. 4, pp. 70–84, Jul. 2005.
- [5] B. T. Robinson, "Who goes there?" *IEEE Spectrum*, vol. 40, no. 10, pp. 42–47, Oct. 2003.
- [6] F. Meyer et al., "Message passing algorithms for scalable multitarget tracking," *Proc. IEEE*, vol. 106, no. 2, pp. 221–259, Feb. 2018.
- [7] J. Guivant, E. Nebot, and S. Baiker, "Autonomous navigation and map building using laser range sensors in outdoor applications," *J. Robot. Syst.*, vol. 17, no. 10, pp. 565–583, Oct. 2000.
- [8] S.-H. Lee and C. C. Chung, "Robust multilane on-road vehicle localization for autonomous highway driving vehicles," *IEEE Trans. Control Syst. Technol.*, vol. 25, no. 2, pp. 577–589, Mar. 2017.
- [9] G. Bresson, Z. Alsayed, L. Yu, and S. Glaser, "Simultaneous localization and mapping: A survey of current trends in autonomous driving," *IEEE Trans. Intell. Veh.*, vol. 2, no. 3, pp. 194–220, Sep. 2017.
- [10] K. Witrisal et al., "High-accuracy localization for assisted living: 5G systems will turn multipath channels from foe to friend," *IEEE Signal Process. Mag.*, vol. 33, no. 2, pp. 59–70, Mar. 2016.
- [11] F. Buccafurri, G. Lax, S. Nicolazzo, and A. Nocera, "Robust multilane on-road vehicle localization for autonomous highway driving vehicles," *IEEE Trans. Serv. Comput.*, to be published.
- [12] P. Barsocchi, S. Chessa, F. Furfari, and F. Potortù, "Evaluating ambient assisted living solutions: The localization competition," *IEEE Pervas. Comput.*, vol. 12, no. 4, pp. 72–79, Oct. 2013.
- [13] D. Miorandi, S. Sicari, F. De Pellegrini, and I. Chlamtac, "Internet of Things: Vision, applications and research challenges," *Ad Hoc Netw.*, vol. 10, no. 7, pp. 1497–1516, Sep. 2012.
- [14] S. D'Oro, L. Galluccio, G. Morabito, and S. Palazzo, "Exploiting object group localization in the Internet of Things: Performance analysis," *IEEE Trans. Veh. Technol.*, vol. 64, no. 8, pp. 3645–3656, Aug. 2015.
- [15] D. Zhang, L. T. Yang, M. Chen, S. Zhao, M. Guo, and Y. Zhang, "Real-time locating systems using active RFID for Internet of Things," *IEEE Syst. J.*, vol. 10, no. 3, pp. 1226–1235, Sep. 2016.
- [16] F. Meyer, B. Etzlinger, Z. Liu, F. Hlawatsch, and M. Z. Win, "Scalable cooperative synchronization and navigation for the Internet of Things," *IEEE Internet Things J.*, vol. 5, 2018, to appear.
- [17] R. K. Ganti, F. Ye, and H. Lei, "Mobile crowdsensing: Current state and future challenges," *IEEE Commun. Mag.*, vol. 49, no. 11, pp. 32–39, Nov. 2011.
- [18] G. Cardone et al., "Fostering participation in smart cities: A geo-social crowdsensing platform," *IEEE Commun. Mag.*, vol. 51, no. 6, pp. 112–119, Jun. 2013.
- [19] F. Zabini and A. Conti, "Inhomogeneous Poisson sampling of finite-energy signals with uncertainties in  $\mathbb{R}^d$ ," *IEEE Trans. Signal Process.*, vol. 64, no. 18, pp. 4679–4694, Sep. 2016.
- [20] S. Bartoletti, A. Conti, and M. Z. Win, "Device-free counting via wideband signals," *IEEE J. Sel. Areas Commun.*, vol. 35, no. 5, pp. 1163–1174, May 2017.
- [21] J. Ko, T. Gao, R. Rothman, and A. Terzis, "Wireless sensing systems in clinical environments: Improving the efficiency of the patient monitoring process," *IEEE Eng. Med. Biol. Mag.*, vol. 29, no. 2, pp. 103–109, Mar./Apr. 2010.
- [22] B. de Vos, J. M. Wolterink, P. A. de Jong, T. Leiner, M. A. Viergever, and I. Işgum, "ConvNet-based localization of anatomical structures in 3-D medical images," *IEEE Trans. Med. Imag.*, vol. 36, no. 7, pp. 1470–1481, Jul. 2017.
- [23] M. Pourhomayoun, Z. Jin, and M. L. Fowler, "Accurate localization of in-body medical implants based on spatial sparsity," *IEEE Trans. Biomed. Eng.*, vol. 61, no. 2, pp. 590–597, Feb. 2014.
- [24] J. Warrior, E. McHenry, and K. McGee, "They know where you are [location detection]," *IEEE Spectrum*, vol. 40, no. 7, pp. 20–25, Jul. 2003.
- [25] L.-J. Kau and C.-S. Chen, "A smart phone-based pocket fall accident detection, positioning, and rescue system," *IEEE J. Biomed. Health Inf.*, vol. 19, no. 1, pp. 44–56, Jan. 2015.
- [26] T. Latif, E. Whitmire, T. Novak, and A. Bozkurt, "Sound localization sensors for search and rescue biobots," *IEEE Sensors J.*, vol. 16, no. 10, pp. 3444–3453, May 2016.
- [27] J. J. Spilker, Jr., "GPS signal structure and performance characteristics," *Navigation*, vol. 25, no. 2, pp. 121–146, Aug. 1978.
- [28] B. W. Parkinson, J. J. Spilker, Jr., P. Axelrad, and P. Enge, Eds., *Global Positioning System: Theory and Applications* (Progress in Astronautics and Aeronautics), vol. 1. Washington, DC, USA: AIAA, 1996.
- [29] B. W. Parkinson, J. J. Spilker, Jr., P. Axelrad, and P. Enge, Eds., *Global Positioning System: Theory and Applications* (Progress in Astronautics and Aeronautics), vol. 2. Washington, DC, USA: AIAA, 1996.
- [30] B. W. Parkinson and S. W. Gilbert, "NAVSTAR: Global positioning system—Ten years later," *Proc. IEEE*, vol. 71, no. 10, pp. 1177–1186, Oct. 1983.
- [31] P. Misra, B. P. Burke, and M. M. Pratt, "GPS performance in navigation," *Proc. IEEE*, vol. 87, no. 1, pp. 65–85, Jan. 1999.
- [32] D. Schneider, "New indoor navigation technologies work where GPS can't," *IEEE Spectrum*, Nov. 2013.
- [33] P. Tseng, "Second-order cone programming relaxation of sensor network localization," *SIAM J. Optim.*, vol. 18, no. 1, pp. 156–185, Feb. 2007.
- [34] D. Moore, J. Leonard, D. Rus, and S. Teller, "Robust distributed network localization with noisy range measurements," in *Proc. SenSys*, Baltimore, MD, USA, Nov. 2004, pp. 50–61.
- [35] T. Tirer and A. J. Weiss, "Performance analysis of a high-resolution direct position determination method," *IEEE Trans. Signal Process.*, vol. 65, no. 3, pp. 544–554, Feb. 2017.
- [36] H. Wymeersch, S. Maranò, W. M. Gifford, and M. Z. Win, "A machine learning approach to ranging error mitigation for UWB localization," *IEEE Trans. Commun.*, vol. 60, no. 6, pp. 1719–1728, Jun. 2012.
- [37] L. Geng, M. F. Bugallo, A. Athalye, and P. M. Djurić, "Indoor tracking with RFID systems," *IEEE J. Sel. Topics Signal Process.*, vol. 8, no. 1, pp. 96–105, Feb. 2014.
- [38] A. Conti, M. Guerra, D. Dardari, N. Decarli, and M. Z. Win, "Network experimentation for cooperative localization," *IEEE J. Sel. Areas Commun.*, vol. 30, no. 2, pp. 467–475, Feb. 2012.
- [39] R. Niu, A. Vempaty, and P. K. Varshney, "Received signal strength based localization in wireless sensor networks," *Proc. IEEE*, vol. 106, no. 6, Jun. 2018.
- [40] J. Xu, X. Shen, J. W. Mark, and J. Cai, "Mobile location estimation in CDMA cellular networks by using fuzzy logic," *Wireless Commun. Mobile Comput.*, vol. 7, no. 3, pp. 285–298, Mar. 2007.
- [41] D. Dardari, A. Conti, U. Ferner, A. Giorgetti, and M. Z. Win, "Ranging with ultrawide bandwidth signals in multipath environments," *Proc. IEEE*, vol. 97, no. 2, pp. 404–426, Feb. 2009.
- [42] B. Denis, J.-B. Pierrot, and C. Abou-Rjeily, "Joint distributed synchronization and positioning in UWB ad hoc networks using TOA," *IEEE Trans. Microw. Theory Techn.*, vol. 54, no. 4, pp. 1896–1911, Jun. 2006.
- [43] K. Plarre and P. R. Kumar, "Tracking objects with networked scattered directional sensors," *EURASIP J. Adv. Signal Process.*, vol. 2008, Jan. 2008, Art. no. 74.
- [44] Y. Shen and M. Z. Win, "On the accuracy of localization systems using wideband antenna arrays," *IEEE Trans. Commun.*, vol. 58, no. 1, pp. 270–280, Jan. 2010.
- [45] N. Patwari, J. N. Ash, S. Kyperountas, A. O. Hero, R. L. Moses, and N. S. Correal, "Locating the nodes: Cooperative localization in wireless sensor networks," *IEEE Signal Process. Mag.*, vol. 22, no. 4, pp. 54–69, Jul. 2005.
- [46] Y. Luo and C. L. Law, "Indoor positioning using UWB-IR signals in the presence of dense multipath with path overlapping," *IEEE Trans. Wireless Commun.*, vol. 11, no. 10, pp. 3734–3743, Oct. 2012.
- [47] H. Wymeersch, J. Lien, and M. Z. Win, "Cooperative localization in wireless networks,"

- Proc. IEEE*, vol. 97, no. 2, pp. 427–450, Feb. 2009.
- [48] A. Conti, D. Dardari, M. Guerra, L. Mucci, and M. Z. Win, “Experimental characterization of diversity navigation,” *IEEE Syst. J.*, vol. 8, no. 1, pp. 115–124, Mar. 2014.
- [49] U. A. Khan, S. Kar, and J. M. F. Moura, “Linear theory for self-localization: Convexity, barycentric coordinates, and Cayley–Menger determinants,” *IEEE Access*, vol. 3, pp. 1326–1339, 2015.
- [50] J. J. Caffery and G. L. Stüber, “Overview of radiolocation in CDMA cellular systems,” *IEEE Commun. Mag.*, vol. 36, no. 4, pp. 38–45, Apr. 1998.
- [51] A. H. Sayed, A. Tarighat, and N. Khajehnouri, “Network-based wireless location: Challenges faced in developing techniques for accurate wireless location information,” *IEEE Signal Process. Mag.*, vol. 22, no. 4, pp. 24–40, Jul. 2005.
- [52] S. Mazuelas, A. Conti, J. C. Allen, and M. Z. Win, “Soft range information for network localization,” *IEEE Trans. Signal Process.*, vol. 66, no. 12, pp. 3155–3168, Jun. 2018.
- [53] A. Rabbachin, I. Oppermann, and B. Denis, “GML ToA estimation based on low complexity UWB energy detection,” in *Proc. PIMRC*, Helsinki, Finland, Sep. 2006, pp. 1–5.
- [54] S. Venkatesh and R. M. Buehrer, “NLOS mitigation using linear programming in ultrawideband location-aware networks,” *IEEE Trans. Veh. Technol.*, vol. 56, no. 5, pp. 3182–3198, Sep. 2007.
- [55] S. Bartoletti, W. Dai, A. Conti, and M. Z. Win, “A mathematical model for wideband ranging,” *IEEE J. Sel. Topics Signal Process.*, vol. 9, no. 2, pp. 216–228, Mar. 2015.
- [56] K. Liu, X. Liu, and X. Li, “Guogou: Enabling fine-grained smartphone localization via acoustic anchors,” *IEEE Trans. Mobile Comput.*, vol. 15, no. 5, pp. 1144–1156, May 2016.
- [57] Z. Liu, W. Dai, and M. Z. Win, “Mercury: An infrastructure-free system for network localization and navigation,” *IEEE Trans. Mobile Comput.*, vol. 17, no. 5, pp. 1119–1133, May 2018.
- [58] J. Prieto, S. Mazuelas, and M. Z. Win, “Context-aided inertial navigation via belief condensation,” *IEEE Trans. Signal Process.*, vol. 64, no. 12, pp. 3250–3261, Jun. 2016.
- [59] P. D. Groves, *Principles of GNSS, Inertial, and Multisensor Integrated Navigation Systems*. Norwood, MA, USA: Artech House, 2008.
- [60] A. R. J. Ruiz, F. S. Granja, J. C. Prieto, and J. I. G. Rosas, “Accurate pedestrian indoor navigation by tightly coupling foot-mounted IMU and RFID measurements,” *IEEE Trans. Instrum. Meas.*, vol. 61, no. 1, pp. 178–189, Jan. 2012.
- [61] E. Foxlin, “Pedestrian tracking with shoe-mounted inertial sensors,” *IEEE Comput. Graph. Appl.*, vol. 25, no. 6, pp. 38–46, Nov./Dec. 2005.
- [62] W. Chen and X. Meng, “A cooperative localization scheme for Zigbee-based wireless sensor networks,” in *Proc. IEEE Int. Conf. Netw.*, Singapore, Sep. 2006, pp. 1–5.
- [63] U. A. Khan, S. Kar, and J. M. F. Moura, “Distributed sensor localization in random environments using minimal number of anchor nodes,” *IEEE Trans. Signal Process.*, vol. 57, no. 5, pp. 2000–2016, May 2009.
- [64] U. A. Khan, S. Kar, and J. M. F. Moura, “DILAND: An algorithm for distributed sensor localization with noisy distance measurements,” *IEEE Trans. Signal Process.*, vol. 58, no. 3, pp. 1940–1947, Mar. 2010.
- [65] J. P. Beaudeau, M. F. Bugallo, and P. M. Djurić, “RSSI-based multi-target tracking by cooperative agents using fusion of cross-target information,” *IEEE Trans. Signal Process.*, vol. 63, no. 19, pp. 5033–5044, Oct. 2015.
- [66] S. Safavi and U. A. Khan, “An opportunistic linear-convex algorithm for localization in mobile robot networks,” *IEEE Trans. Robot.*, vol. 33, no. 4, pp. 875–888, Aug. 2017.
- [67] S. Safavi and U. A. Khan, “Localization in mobile networks via virtual convex hulls,” *IEEE Trans. Signal Inf. Process. Netw.*, vol. 4, no. 1, pp. 188–201, Mar. 2018.
- [68] N. Alsindi and K. Pahlavan, “Cooperative localization bounds for indoor ultra-wideband wireless sensor networks,” *EURASIP J. Adv. Signal Process.*, vol. 8, no. 2, pp. 1–13, Jan. 2008.
- [69] C. Savarese, J. M. Rabaey, and J. Beutel, “Locationing in distributed ad-hoc wireless sensor networks,” in *Proc. IEEE Int. Conf. Acoust. Speech Signal Process.*, vol. 4, May 2001, pp. 2037–2040.
- [70] X. Tan and J. Li, “Cooperative positioning in underwater sensor networks,” *IEEE Trans. Signal Process.*, vol. 58, no. 11, pp. 5860–5871, Nov. 2010.
- [71] R. M. Vaghefi, M. R. Gholami, R. M. Buehrer, and E. G. Strömbäck, “Cooperative received signal strength-based sensor localization with unknown transmit powers,” *IEEE Trans. Signal Process.*, vol. 61, no. 6, pp. 1389–1403, Mar. 2013.
- [72] Y. Shen and M. Z. Win, “Fundamental limits of wideband localization—Part I: A general framework,” *IEEE Trans. Inf. Theory*, vol. 56, no. 10, pp. 4956–4980, Oct. 2010.
- [73] Y. Shen, H. Wymeersch, and M. Z. Win, “Fundamental limits of wideband localization—Part II: Cooperative networks,” *IEEE Trans. Inf. Theory*, vol. 56, no. 10, pp. 4981–5000, Oct. 2010.
- [74] Y. Shen, S. Mazuelas, and M. Z. Win, “Network navigation: Theory and interpretation,” *IEEE J. Sel. Areas Commun.*, vol. 30, no. 9, pp. 1823–1834, Oct. 2012.
- [75] M. Z. Win, Y. Shen, and W. Dai, “A theoretical foundation of network localization and navigation,” *Proc. IEEE*, vol. 106, no. 7, pp. 1136–1165, Jul. 2018.
- [76] H. Chen, G. Wang, Z. Wang, H. C. So, and H. V. Poor, “Non-line-of-sight node localization based on semi-definite programming in wireless sensor networks,” *IEEE Trans. Wireless Commun.*, vol. 11, no. 1, pp. 108–116, Jan. 2018.
- [77] M. I. Skolnik, *Introduction to Radar Systems*, 3rd ed. New York, NY, USA: McGraw-Hill, 2002.
- [78] S. Bartoletti, A. Giorgetti, M. Z. Win, and A. Conti, “Blind selection of representative observations for sensor radar networks,” *IEEE Trans. Veh. Technol.*, vol. 64, no. 4, pp. 1388–1400, Apr. 2015.
- [79] F. Meshkati, H. V. Poor, and S. C. Schwartz, “Energy-efficient resource allocation in wireless networks,” *IEEE Signal Process. Mag.*, vol. 24, no. 3, pp. 58–68, May 2007.
- [80] E. Maşazade, R. Niu, P. K. Varshney, and M. Keskinoz, “Energy aware iterative source localization for wireless sensor networks,” *IEEE Trans. Signal Process.*, vol. 58, no. 9, pp. 4824–4835, Sep. 2010.
- [81] H. Godrich, A. M. Haimovich, and R. S. Blum, “Target localization accuracy gain in MIMO radar-based systems,” *IEEE Trans. Inf. Theory*, vol. 56, no. 6, pp. 2783–2803, Jun. 2010.
- [82] T. Wang, G. Leus, and L. Huang, “Ranging energy optimization for robust sensor positioning based on semidefinite programming,” *IEEE Trans. Signal Process.*, vol. 57, no. 12, pp. 4777–4787, Dec. 2009.
- [83] H. Godrich, A. P. Petropulu, and H. V. Poor, “Power allocation strategies for target localization in distributed multiple-radar architectures,” *IEEE Trans. Signal Process.*, vol. 59, no. 7, pp. 3226–3240, Jul. 2011.
- [84] W. Dai, Y. Shen, and M. Z. Win, “Distributed power allocation for cooperative wireless network localization,” *IEEE J. Sel. Areas Commun.*, vol. 33, no. 1, pp. 28–40, Jan. 2015.
- [85] W. Dai, Y. Shen, and M. Z. Win, “Energy-efficient network navigation algorithms,” *IEEE J. Sel. Areas Commun.*, vol. 33, no. 7, pp. 1418–1430, Jul. 2015.
- [86] X. Shen and P. K. Varshney, “Sensor selection based on generalized information gain for target tracking in large sensor networks,” *IEEE Trans. Signal Process.*, vol. 62, no. 2, pp. 363–375, Jan. 2014.
- [87] T. Zhang, A. F. Molisch, Y. Shen, Q. Zhang, H. Feng, and M. Z. Win, “Joint power and bandwidth allocation in wireless cooperative localization networks,” *IEEE Trans. Wireless Commun.*, vol. 15, no. 10, pp. 6527–6540, Oct. 2016.
- [88] J. Li, T. Zhang, A. F. Molisch, and Q. Zhang, “Power allocation in asynchronous location-aware sensor networks,” in *Proc. IEEE Int. Conf. Commun.*, Kuala Lumpur, Malaysia, May 2016, pp. 1–6.
- [89] J. Chen, W. Dai, Y. Shen, V. K. N. Lau, and M. Z. Win, “Power management for cooperative localization: A game theoretical approach,” *IEEE Trans. Signal Process.*, vol. 64, no. 24, pp. 6517–6532, Dec. 2016.
- [90] J. Chen, W. Dai, Y. Shen, V. K. N. Lau, and M. Z. Win, “Resource management games for distributed network localization,” *IEEE J. Sel. Areas Commun.*, vol. 35, no. 2, pp. 317–329, Feb. 2017.
- [91] A. I. Mourikis and S. I. Roumeliotis, “Performance analysis of multirobot cooperative localization,” *IEEE Trans. Robot.*, vol. 22, no. 4, pp. 666–681, Aug. 2006.
- [92] J. Gribben, A. Boukerche, and R. W. N. Pazzi, “Scheduling for scalable energy-efficient localization in mobile ad hoc networks,” in *Proc. IEEE Conf. Sensor Ad Hoc Commun. Netw.*, Boston, MA, USA, Jun. 2010, pp. 1–9.
- [93] G. E. Garcia, L. S. Muppireddy, and H. Wymeersch, “On the trade-off between accuracy and delay in cooperative UWB navigation,” in *Proc. IEEE Wireless Commun. Netw. Conf. (WCNC)*, Apr. 2013, pp. 1603–1608.
- [94] S. Dwivedi, D. Zachariah, A. De Angelis, and P. Händel, “Cooperative decentralized localization using scheduled wireless transmissions,” *IEEE Commun. Lett.*, vol. 17, no. 6, pp. 1240–1243, Jun. 2013.
- [95] T. Wang, Y. Shen, A. Conti, and M. Z. Win, “Analysis of network navigation with scheduling strategies,” in *Proc. IEEE Int. Conf. Commun.*, London, U.K., Jun. 2015, pp. 3562–3566.
- [96] T. Wang, Y. Shen, A. Conti, and M. Z. Win, “Network navigation with scheduling: Error evolution,” *IEEE Trans. Inf. Theory*, vol. 63, no. 11, pp. 7509–7534, Nov. 2017.
- [97] L. Shi, M. Epstein, B. Sinopoli, and R. M. Murray, “Effective sensor scheduling schemes in a sensor network by employing feedback in the communication loop,” in *Proc. IEEE Int. Conf. Control Appl.*, Singapore, Oct. 2007, pp. 1006–1011.
- [98] T. Wang, Y. Shen, and M. Z. Win, “A general analytical framework of scheduling algorithms for network navigation,” in *Proc. IEEE Int. Conf. Commun.*, Sydney, NSW, Australia, Jun. 2014, pp. 4583–4588.
- [99] Z. Zhao, R. Zhang, X. Cheng, L. Yang, and B. Jiao, “Network formation games for the link selection of cooperative localization in wireless networks,” in *Proc. IEEE Int. Conf. Commun.*, Sydney, NSW, Australia, Jun. 2014, pp. 4577–4582.
- [100] T. Wang, A. Conti, and M. Z. Win, “On the design of scheduling algorithms for wireless navigation networks,” in *Proc. IEEE Global Telecomm. Conf.*, Washington, DC, USA, Dec. 2016, pp. 1–6.
- [101] J. S. Abel, “Optimal sensor placement for passive source localization,” in *Proc. IEEE Int. Conf. Acoust. Speech Signal Process.*, Albuquerque, NM, USA, Apr. 1990, pp. 2927–2930.
- [102] H. Zhang, “Two-dimensional optimal sensor placement,” *IEEE Trans. Syst. Man Cybern.*, vol. 25, no. 5, pp. 781–792, May 1995.
- [103] J. B. McKay and M. Pachter, “Geometry optimization for GPS navigation,” in *Proc. IEEE Conf. Decision Control*, San Diego, CA, USA, Dec. 1997, pp. 4695–4699.
- [104] T. Hegazy and G. Vachtsevanos, “Sensor placement for isotropic source localization,” in *Proc. 2nd Int. Workshop Inf. Process. Sensor Netw.*, Palo Alto, CA, USA, Apr. 2003, pp. 432–441.

- [105] G. Han, C. Zhang, L. Shu, and J. J. Rodrigues, "Impacts of deployment strategies on localization performance in underwater acoustic sensor networks," *IEEE Trans. Ind. Electron.*, vol. 62, no. 3, pp. 1725–1733, Mar. 2015.
- [106] A. Sinha, T. Kirubarajan, and Y. Bar-Shalom, "Optimal cooperative placement of GMTI UAVs for ground target tracking," in *Proc. IEEE Aerosp. Conf.*, Big Sky, MT, USA, Mar. 2004.
- [107] D. B. Jourdan and N. Roy, "Optimal sensor placement for target localization," in *Proc. IEEE/ION Conf. Position, Location, Navigat. (PLANS)*, San Diego, CA, USA, Apr. 2006.
- [108] D. B. Jourdan and N. Roy, "Optimal sensor placement for agent localization," *ACM Trans. Sensor Netw.*, vol. 4, no. 3, pp. 13:1–13:40, May 2008.
- [109] Y. Shen and M. Z. Win, "Energy efficient location-aware networks," in *Proc. IEEE Int. Conf. Commun.*, Beijing, China, May 2008, pp. 2995–3001.
- [110] S. Mazuelas, R. M. Lorenzo, A. Bahillo, P. Fernandez, J. Prieto, and E. J. Abril, "Topology assessment provided by weighted barycentric parameters in harsh environment wireless location systems," *IEEE Trans. Signal Process.*, vol. 58, no. 7, pp. 3842–3857, Jul. 2010.
- [111] J. Zhou, J. Shi, and X. Qu, "Landmark placement for wireless localization in rectangular-shaped industrial facilities," *IEEE Trans. Veh. Technol.*, vol. 59, no. 6, pp. 3081–3090, Jul. 2010.
- [112] A. N. Bishop, B. Fidan, B. D. O. Anderson, K. Dogancay, and P. N. Pathirana, "Optimality analysis of sensor-target localization geometries," *Automatica*, vol. 46, no. 3, pp. 479–492, Mar. 2010.
- [113] S. Martínez and F. Bullo, "Optimal sensor placement and motion coordination for target tracking," *Automatica*, vol. 42, no. 4, pp. 661–668, Apr. 2006.
- [114] W. Meng, L. Xie, and W. Xiao, "Optimality analysis of sensor-source geometries in heterogeneous sensor networks," *IEEE Trans. Wireless Commun.*, vol. 12, no. 4, pp. 1958–1967, Apr. 2013.
- [115] Z. Ma and K. C. Ho, "A study on the effects of sensor position error and the placement of calibration emitter for source localization," *IEEE Trans. Wireless Commun.*, vol. 13, no. 10, pp. 5440–5452, Oct. 2014.
- [116] Z. Liu, W. Dai, and M. Z. Win, "Node placement for localization networks," in *Proc. IEEE Int. Conf. Commun.*, Paris, France, May 2017, pp. 1–6.
- [117] B. Teague, Z. Liu, F. Meyer, and M. Z. Win, "Peregrine: 3-D network localization and navigation," in *Proc. IEEE Latin-Amer. Conf. Commun.*, Guatemala City, Guatemala, Nov. 2017, pp. 1–6.
- [118] F. P. Kelly, A. K. Maulloo, and D. K. H. Tan, "Rate control for communication networks: Shadow prices, proportional fairness and stability," *J. Oper. Res. Soc.*, vol. 49, no. 3, pp. 237–252, Mar. 1998.
- [119] Z.-Q. Luo and W. Yu, "An introduction to convex optimization for communications and signal processing," *IEEE J. Sel. Areas Commun.*, vol. 24, no. 8, pp. 1426–1438, Aug. 2006.
- [120] G. J. Foschini, "Private conversation," AT&T Labs-Res., Middletown, NJ, USA, Tech. Rep., May 2001.
- [121] L. A. Shepp, "Private conversation," AT&T Labs-Res., Middletown, NJ, USA, Tech. Rep., Mar. 2001.
- [122] D. Bertsekas and R. Gallager, *Data Networks*, 2nd ed. Englewood Cliffs, NJ, USA: Prentice-Hall, 1992.
- [123] L. Tassiulas and A. Ephremides, "Stability properties of constrained queueing systems and scheduling policies for maximum throughput in multihop radio networks," *IEEE Trans. Autom. Control*, vol. 37, no. 12, pp. 1936–1948, Dec. 1992.
- [124] M. J. Neely, E. Modiano, and C. E. Rohrs, "Dynamic power allocation and routing for time-varying wireless networks," *IEEE J. Sel. Areas Commun.*, vol. 23, no. 1, pp. 89–103, Jan. 2005.
- [125] L. Georgiadis, M. J. Neely, and L. Tassiulas, *Resource Allocation and Cross-Layer Control in Wireless Networks*. Hanover, MA, USA: NOW, 2006.
- [126] M. J. Neely, "Order optimal delay for opportunistic scheduling in multi-user wireless uplinks and downlinks," *IEEE/ACM Trans. Netw.*, vol. 16, no. 5, pp. 1188–1199, Oct. 2008.
- [127] S. Hanly and R. Mathar, "On the optimal base-station density for CDMA cellular networks," *IEEE Trans. Commun.*, vol. 50, no. 8, pp. 1274–1281, Aug. 2002.
- [128] F. Richter, A. J. Fehske, and G. P. Fettweis, "Energy efficiency aspects of base station deployment strategies for cellular networks," in *Proc. IEEE Semiannu. Veh. Technol. Conf.*, Anchorage, AK, USA, Sep. 2009, pp. 1–5.
- [129] F. Richter and G. Fettweis, "Base station placement based on force fields," in *Proc. IEEE Semiannu. Veh. Technol. Conf.*, Yokohama, Japan, May 2012, pp. 1–5.
- [130] A. N. D'Andrea, U. Mengali, and R. Reggiannini, "The modified Cramér–Rao bound and its application to synchronization problems," *IEEE Trans. Commun.*, vol. 42, no. 234, pp. 1391–1399, Feb./Apr. 1994.
- [131] P. Tichavský, C. H. Muravchik, and A. Nehorai, "Posterior Cramér–Rao bounds for discrete-time nonlinear filtering," *IEEE Trans. Signal Process.*, vol. 46, no. 5, pp. 1386–1396, May 1998.
- [132] A. Catovic and Z. Sahinoglu, "The Cramer–Rao bounds of hybrid TOA/RSS and TDOA/RSS location estimation schemes," *IEEE Commun. Lett.*, vol. 8, no. 10, pp. 626–628, Oct. 2004.
- [133] C. Chang and A. Sahai, "Cramér–Rao-type bounds for localization," *EURASIP J. Appl. Signal Process.*, vol. 2006, Dec. 2006, Art. no. 94287.
- [134] L. Mailaender, "On the geolocation bounds for round-trip time-of-arrival and all non-line-of-sight channels," *EURASIP J. Adv. Signal Process.*, vol. 2008, Dec. 2007, Art. no. 584670.
- [135] Y. Han et al., "Performance limits and geometric properties of array localization," *IEEE Trans. Inf. Theory*, vol. 62, no. 2, pp. 1054–1075, Feb. 2016.
- [136] H. L. Van Trees, *Detection, Estimation and Modulation Theory, Part 1*. New York, NY, USA: Wiley, 1968.
- [137] H. V. Poor, *An Introduction to Signal Detection and Estimation*, 2nd ed. New York, NY, USA: Springer-Verlag, 1994.
- [138] I. Reuven and H. Messer, "A Barankin-type lower bound on the estimation error of a hybrid parameter vector," *IEEE Trans. Inf. Theory*, vol. 43, no. 3, pp. 1084–1093, May 1997.
- [139] S. Joshi and S. Boyd, "Sensor selection via convex optimization," *IEEE Trans. Signal Process.*, vol. 57, no. 2, pp. 451–462, Feb. 2009.
- [140] E. Tzoreff and A. J. Weiss, "Single sensor path design for best emitter localization via convex optimization," *IEEE Trans. Wireless Commun.*, vol. 16, no. 2, pp. 939–951, Feb. 2017.
- [141] E. Tzoreff and A. J. Weiss, "Path design for best emitter location using two mobile sensors," *IEEE Trans. Signal Process.*, vol. 65, no. 19, pp. 5249–5261, Oct. 2017.
- [142] W. W.-L. Li, Y. Shen, Y. J. Zhang, and M. Z. Win, "Robust power allocation for energy-efficient location-aware networks," *IEEE/ACM Trans. Netw.*, vol. 21, no. 6, pp. 1918–1930, Dec. 2013.
- [143] Y. Shen, W. Dai, and M. Z. Win, "Power optimization for network localization," *IEEE/ACM Trans. Netw.*, vol. 22, no. 4, pp. 1337–1350, Aug. 2014.
- [144] Y. Shen, "Network localization and navigation: Theoretical framework, efficient operation, and security assurance," Ph.D. dissertation, Dept. Electr. Eng. Comput. Sci., Massachusetts Inst. Technol., Cambridge, MA, USA, Jun. 2014.
- [145] W. Dai, Y. Shen, and M. Z. Win, "A computational geometry framework for efficient network localization," *IEEE Trans. Inf. Theory*, vol. 64, no. 2, pp. 1317–1339, Feb. 2018.
- [146] S. Boyd and L. Vandenberghe, *Convex Optimization*. Cambridge, U.K.: Cambridge Univ. Press, 2004.
- [147] D. P. Bertsekas, *Convex Optimization Theory*. Belmont, MA, USA: Athena Scientific, 2009.
- [148] D. P. Bertsekas, A. Nedic, and A. E. Ozdaglar, *Convex Analysis and Optimization*. Belmont, MA, USA: Athena Scientific, 2003.
- [149] M. S. Lobo, L. Vandenberghe, S. Boyd, and H. Lebret, "Applications of second-order cone programming," *Linear Algebra Appl.*, vol. 284, nos. 1–3, pp. 193–228, Nov. 1998.
- [150] T. M. Chan, "Optimal output-sensitive convex hull algorithms in two and three dimensions," *Discrete Comput. Geometry*, vol. 16, no. 4, pp. 361–368, Apr. 1996.
- [151] M. de Berg, O. Cheong, M. van Kreveld, and M. Overmars, *Computational Geometry: Algorithms and Applications*. Springer-Verlag, 2008.
- [152] S. Mazuelas, Y. Shen, and M. Z. Win, "Spatio-temporal information coupling in network navigation," *IEEE Trans. Inf. Theory*, to be published.
- [153] M. Z. Win, P. C. Pinto, A. Giorgetti, M. Chiani, and L. A. Shepp, "Error performance of ultrawideband systems in a Poisson field of narrowband interferers," in *Proc. IEEE Int. Symp. Spread Spectr. Techn. Appl.*, Manaus, Brazil, Aug. 2006, pp. 410–416.
- [154] M. Z. Win, "A mathematical model for network interference," in *IEEE Commun. Theory Workshop*, Sedona, AZ, USA, May 2007.
- [155] M. Z. Win, P. C. Pinto, and L. A. Shepp, "A mathematical theory of network interference and its applications," *Proc. IEEE*, vol. 97, no. 2, pp. 205–230, Feb. 2009.
- [156] M. Haenggi, J. G. Andrews, F. Baccelli, O. Dousse, and M. Franceschetti, "Stochastic geometry and random graphs for the analysis and design of wireless networks," *IEEE J. Sel. Areas Commun.*, vol. 27, no. 7, pp. 1029–1046, Sep. 2009.
- [157] H. ElSawy, A. Sultan-Salem, M. S. Alouini, and M. Z. Win, "Modeling and analysis of cellular networks using stochastic geometry: A tutorial," *IEEE Commun. Surveys Tuts.*, vol. 19, no. 1, pp. 167–203, 1st Quart., 2017.
- [158] Technical Specification LTE; Evolved Universal Terrestrial Radio Access (E-UTRA); User Equipment (UE) Radio Transmission and Reception, document 3GPP TS 136.101 V11.2.0 (2012-11), 3rd Generation Partnership Project, Nov. 2012.
- [159] Technical Report LTE; 5G; Study on Channel Model for Frequency Spectrum Above 6 GHz, document 3GPP ETSI TR 138 900 V14.3.1 (2017-08), 3rd Generation Partnership Project, Aug. 2017.
- [160] F. Ademaj, M. K. Müller, S. Schwarz, and M. Rupp, "Modeling of spatially correlated geometry-based stochastic channels," in *Proc. IEEE Semiannu. Veh. Technol. Conf.*, Toronto, ON, Canada, Sep. 2017, pp. 1–6.
- [161] S. Jaeckel, L. Raschkowski, K. Börner, L. Thiele, F. Burkhardt, and E. Eberlein, "QuaDRiGa—Quasi deterministic radio channel generator, user manual and documentation," Fraunhofer Heinrich Hertz Inst., Berlin, Germany, Tech. Rep., 2017.
- [162] A. Conti, M. Z. Win, M. Chiani, and J. H. Winters, "Bit error outage for diversity reception in shadowing environment," *IEEE Commun. Lett.*, vol. 7, no. 1, pp. 15–17, Jan. 2003.
- [163] A. Conti, M. Z. Win, and M. Chiani, "Invertible bounds for M-QAM in Rayleigh fading," *IEEE Trans. Wireless Commun.*, vol. 4, no. 5, pp. 1994–2000, Sep. 2005.
- [164] A. Conti, W. M. Gifford, M. Z. Win, and M. Chiani, "Optimized simple bounds for diversity systems," *IEEE Trans. Commun.*, vol. 57, no. 9, pp. 2674–2685, Sep. 2009.

## ABOUT THE AUTHORS

**Moe Z. Win** (Fellow, IEEE) is a Professor at the Massachusetts Institute of Technology (MIT) and the founding director of the Wireless Information and Network Sciences Laboratory. Prior to joining MIT, he was with AT&T Research Laboratories and NASA Jet Propulsion Laboratory.



His research encompasses fundamental theories, algorithm design, and network experimentation for a broad range of realworld problems. His current research topics include network localization and navigation, network interference exploitation, and quantum information science. He has served the IEEE Communications Society as an elected Member-at-Large on the Board of Governors, as elected Chair of the Radio Communications Committee, and as an IEEE Distinguished Lecturer. Over the last two decades, he held various editorial positions for IEEE journals and organized numerous international conferences. Currently, he is serving on the SIAM Diversity Advisory Committee.

Dr. Win is an elected Fellow of the American Association for the Advancement of Science (AAAS) and the Institution of Engineering and Technology (IET). He was honored with two IEEE Technical Field Awards: the IEEE Kiyo Tomiyasu Award (2011) and the IEEE Eric E. Sumner Award (2006, jointly with R. A. Scholtz). Together with students and colleagues, his papers have received numerous awards. Other recognitions include the IEEE Communications Society Edwin H. Armstrong AchievementAward (2016), the International Prize for Communications Cristoforo Colombo (2013), the Copernicus Fellowship (2011) and the *Laurea Honoris Causa* (2008) from the Università degli Studi di Ferrara, and the U.S. Presidential Early Career Award for Scientists and Engineers (2004). He is an ISI Highly Cited Researcher.

**Yuan Shen** (Member, IEEE) received the B.E. degree (with highest honor) in electronic engineering from Tsinghua University, Beijing, China, in 2005 and the S.M. and Ph.D. degrees in electrical engineering and computer science from the Massachusetts Institute of Technology (MIT), Cambridge, MA, USA, in 2008 and 2014, respectively.



He is an Associate Professor at the Department of Electronic Engineering, Tsinghua University. Prior to that, he was a Research Assistant and then Postdoctoral Associate at the Wireless Information and Network Sciences Laboratory, MIT, in 2005–2014. He was with the Hewlett-Packard Labs in winter 2009 and the Corporate R&D at Qualcomm Inc. in summer 2008. His research interests include statistical inference, network science, communication theory, information theory, and optimization. His current research focuses on network localization and navigation, inference techniques, resource allocation, and intrinsic wireless secrecy.

Prof. Shen was a recipient of the Qiu Shi Outstanding Young Scholar Award (2015), the China's Youth 1000-Talent Program (2014), the Marconi Society Paul Baran Young Scholar Award (2010), and the MIT Walter A. Rosenblith Presidential Fellowship (2005). His papers received the IEEE Communications Society Fred W. Ellersick Prize (2012) and three Best Paper Awards from IEEE international conferences. He is an elected Vice Chair (2017–2018) and Secretary (2015–2016) for the IEEE ComSoc Radio Communications Committee. He serves as TPC symposium Co-Chair for IEEE Globecom (2018 and 2016), the European Signal Processing Conference (EUSIPCO 2016), and the IEEE ICC Advanced Network Localization and Navigation (ANLN) Workshop (2016, 2017, and 2018). He also serves as Editor for the IEEE TRANSACTIONS ON WIRELESS COMMUNICATIONS (since 2018), IEEE COMMUNICATIONS LETTERS (since 2015), and IEEE CHINA COMMUNICATIONS (since 2017), and served as Guest Editor for the *International Journal of Distributed Sensor Networks* (in 2015).

**Wenhan Dai** (Student Member, IEEE) received the B.S. degrees in electronic engineering and in mathematics from Tsinghua University, Beijing, China, in 2011 and the S.M. degree in aeronautics and astronautics from the Massachusetts Institute of Technology (MIT), Cambridge, MA, USA, in 2014, where he is currently working toward the Ph.D. degree at the Wireless Information and Network Sciences Laboratory.



His research interests include communication theory and stochastic optimization with application to wireless communication and network localization. His current research focuses on efficient network localization, cooperative network operation, and ultrawideband communication.

Mr. Dai was honored by the Marconi Society with the Paul Baran Young Scholar Award (2017). He received the Marconi-BISITE Best Paper Award from the IEEE ICUWB (2017), the Chinese Government Award for Outstanding Student Abroad (2016), the first prize of the IEEE Communications Society Student Competition (2016), and the Student Paper Award (first place) from the IEEE CWIT (2015). He was recognized as the exemplary reviewer of IEEE COMMUNICATIONS LETTERS (2014).

**George Chrisikos** (Fellow, IEEE) is responsible for advanced technology development at Qualcomm Inc., and has been working in the research, design, and development of communication systems and algorithms for wireless and mobile applications. Previously, he was the Engineering Director and Systems Product-Line Manager at Applied Wave Research (AWR) Inc., where he was responsible for architecting and leading the development of a design automation technology product that gained widespread adoption by the wireless communication industry worldwide. Earlier, he was responsible for the design of CDMA and WLAN semiconductor chipsets for startup companies, and advanced satellite systems for commercial and government sectors at The Aerospace Corporation.



Dr. Chrisikos was selected as an IEEE Distinguished Lecturer and his work has resulted in over 115 granted and pending U.S. and international patents. He has been an invited speaker and delivered keynotes at various corporations and conferences worldwide, published numerous papers in international journals and conferences, and contributed to textbooks. He has received a number of accolades, including the IEEE Kiyo Tomiyasu Award and the Aerospace Corporate Achievement Award. He serves on the Advisory Board of the USC Department of Electrical Engineering, as Editor of the IEEE SIGNAL PROCESSING MAGAZINE, and on the Advisory Board of the IEEE COMMUNICATIONS LETTERS. He was named a Guest Editor of IEEE Proceedings and Journals, and served on the executive committees of IEEE conferences.

He received the Ph.D. degree in electrical engineering from the University of Southern California (USC), Los Angeles, CA, USA, under the USC Dean's Doctoral Merit Fellowship. He received the M.S. and B.S. degrees in electrical engineering as a Presidential Scholar. He graduated *summa cum laude* with distinction and was the Valedictorian of his class.

**H. Vincent Poor** (Fellow, IEEE) received the Ph.D. degree in electrical engineering and computer science from Princeton University, Princeton, NJ, USA, in 1977.

From 1977 until 1990, he was on the faculty of the University of Illinois at Urbana-Champaign, Urbana, IL, USA. Since 1990, he has been on the faculty at Princeton University, where he is currently the Michael Henry Strater University Professor of Electrical Engineering. During 2006–2016, he served as Dean of Princeton's School of Engineering and Applied Science. He has also held visiting appointments at several other universities, including most recently at Berkeley and Cambridge. His research interests are in the areas of information theory and signal processing, and their applications in wireless networks, energy systems, and related fields. Among his publications in these areas is the recent book *Information Theoretic Security and Privacy of Information Systems* (Cambridge, U.K.: Cambridge Univ. Press, 2017).

Dr. Poor is a member of the National Academy of Engineering and the National Academy of Sciences, and is a foreign member of the Chinese Academy of Sciences, the Royal Society, and other national and international academies. Recent recognition of his work includes the 2017 IEEE Alexander Graham Bell Medal, Honorary Professorships at Peking University and Tsinghua University, both conferred in 2017, and a D.Sc. *honoris causa* from Syracuse University also awarded in 2017.

